1989

Dynamic and photometric evolutionary models of tidal tails and ripples

John F. Wallin
Iowa State University

INFORMATION TO USERS

The most advanced technology has been used to photograph and reproduce this manuscript from the microfilm master. UMI films the text directly from the original or copy submitted. Thus, some thesis and dissertation copies are in typewriter face, while others may be from any type of computer printer.

The quality of this reproduction is dependent upon the quality of the copy submitted. Broken or indistinct print, colored or poor quality illustrations and photographs, print bleedthrough, substandard margins, and improper alignment can adversely affect reproduction.

In the unlikely event that the author did not send UMI a complete manuscript and there are missing pages, these will be noted. Also, if unauthorized copyright material had to be removed, a note will indicate the deletion.

Oversize materials (e.g., maps, drawings, charts) are reproduced by sectioning the original, beginning at the upper left-hand corner and continuing from left to right in equal sections with small overlaps. Each original is also photographed in one exposure and is included in reduced form at the back of the book. These are also available as one exposure on a standard 35mm slide or as a 17" x 23" black and white photographic print for an additional charge.

Photographs included in the original manuscript have been reproduced xerographically in this copy. Higher quality 6" x 9" black and white photographic prints are available for any photographs or illustrations appearing in this copy for an additional charge. Contact UMI directly to order.

UMI

University Microfilms International
A Bell & Howell Information Company
300 North Zeeb Road, Ann Arbor, MI 48106-1346 USA
313/761-4700 800/521-0600

Order Number 9003576

Dynamic and photometric evolutionary models of tidal tails and ripples

Wallin, John F., Ph.D.

Iowa State University, 1989

U·M·I
300 N. Zeeb Rd.
Ann Arbor, MI 48106

Dynamic and photometric evolutionary models of tidal tails and ripples

by

John F. Wallin

A Dissertation Submitted to the

Graduate Faculty in Partial Fulfillment of the

Requirements for the Degree of

DOCTOR OF PHILOSOPHY

Department: Physics

Major: Astrophysics

Approved:

Signature was redacted for privacy.

In Charge of Major Work

Signature was redacted for privacy.

For the Major Department

Signature was redacted for privacy.

For the Graduate College

Iowa State University

Ames, Iowa

1989

TABLE OF CONTENTS

FOREWARD

"If we indulge in fanciful imagination and build worlds of our own, we must not wonder at our going wide from the path of truth and nature.... On the other hand, if we add observation to observation, without attempting to draw not only certain conclusions, but also conjectural views from them, we offend against the very end for which only observations ought to be made."

-William Herschel

"There are times, when all the world's asleep,
These questions run too deep, for such a simple man.
Won't you please, please tell me what to learn,
I know it sounds absurd, please tell me who I am."

-Supertramp,'The Logical Song"

GENERAL INTRODUCTION

I. PREFACE

This dissertation is a theoretical investigation into the outer regions of morphologically peculiar galaxies. Even though the category of study is peculiar galaxies, these systems are not extremely rare. From the survey of Arp and Madore (1986), it has been estimated that about 6% of the galaxies in the southern sky are peculiar and more than 30% of those are interacting with at least one other galaxy. In this work, two specific types of tidal or collisional phenomena are examined: the star formation in tidal tails and the dynamical development of ripples in early-type disks. Both dynamical and photometric models are presented. The basic mechanism for the formation of tidal tails has been known since the early 1970s, so the present investigation is focused on detailed modeling of density enhancements which are presumed to drive an enhanced star formation rate. The photometric consequences of this type of interaction are also explored. The mechanisms for the formation of ripples and shells around early-type galaxies are apparently more complex and are not as well understood. These are critically examined below and a new mechanism for the formation of these features is studied numerically.

II. EXPLANATION OF DISSERTATION FORMAT

This dissertation is divided into six sections. The Introduction outlines the background and reviews the literature which provides the basis for these investigations. The next chapter presents the investigations into the star formation in tidal tails and bridges followed by a section on the dynamical models of the formation of ripples around early-type disk galaxies. The work on the formation of ripples around early-type disk galaxies was done in conjunction with Curtis Struck-Marcell and appeared in the *Astronomical Journal* (Wallin and Struck-Marcell 1988). These chapters are written in journal format and should stand as self-contained works. The final section of the dissertation is a summary of the conclusions found in this research along with suggested areas for future work. Two appendices have been written to explain the restricted three-body code and the broad-band photometric code used in this investigation. Copies of the numerical codes used in the dynamical simulations are included in the final appendix.

III. TIDAL TAILS OF INTERACTING DISK GALAXIES

A. Summary of Dynamical Models

Since the early 1970s, a basic understanding of the dynamical and photometric processes in morphologically peculiar galaxies has been developed through the use of numerical models. The dynamical modeling of tidal tails and bridges by Toomre and Toomre (1972) matched the appearance of interacting galaxies with simple dynamical models. The available amount of observational data for these systems has also dramatically increased during the past two decades. Some of these dynamical models have been tested using photometric and spectroscopic measurements of observed systems (van der Hulst 1979). Observed global colors have been modeled using photometric codes (cf. Larson and Tinsley 1978, Struck-Marcell and Tinsley 1978).

As noted by Bruzual (1981), the study of galactic evolution has generally been divided into two separate areas, photometric evolution and dynamical evolution. It has long been known that these two areas are actually linked because of the connection between the star formation rate and the tidal and collisional interaction of galaxies. Even though there is clear connection between star formation and interaction (Larson and Tinsley 1978, Kennicutt et al. 1987, Bushouse 1987), it has been difficult to combine photometric and dynamical models because of the problems of deriving a star formation rate from dynamical models.

The use of dynamical models of interacting galaxies as a way of understanding unusual morphologies has been used extensively since Toomre and Toomre's (1972) revolutionary paper. Although other authors using similar methods investigated the same types of systems as Toomre and Toomre (cf. Eneev, Kozlov, and Sunyaev 1973), none made as many detailed comparisons to observed systems and gained as much attention. Their result that tidal interactions can produce both bridges between interacting galaxies and tidal tails away from the center of mass of the system has offered a solution to one of the greater problems in extragalactic astronomy.

Besides the restricted three-body method of Toomre and Toomre (1972), self-consistent N-body codes have been developed for the modeling of star clusters and galactic interactions. These self-consistent N-body models have not been as extensively used in studying interacting galaxies as they might have been, because of the high computational cost of running them (Aarseth 1972). One area where they have been extensively used for is the modeling of dynamical friction and galaxy mergers. The use of true N-body models allows the simulated interacting galaxy to experience an effective frictional force caused by the perturbed of halo particles during the encounter. This phenomenon has been approximated analytically since the 1940s (Chandrasekhar 1942, 1943), but only has been recently numerically modeled (White 1983, Negroponte and White 1983, Barnes 1988). The effects of dynamical friction

cause the orbit of the perturbing galaxy eventually to merge with the main galaxy. Many elliptical galaxies might be formed from this type of interaction (Schweizer 1980, 1983, 1986). Dynamical friction affects the orbits of interacting galaxies and will eventually cause them to merge. Although dynamical friction can drastically affect the long term evolution of a pair of galaxies, the development of the tidal tail is relatively insensitve to the orbit of the companion galaxy.

A number of hydrodynamical simulations have been used to model the gas distribution of interacting galaxies. The ring galaxy simulations by Appleton and Struck-Marcell (1987b, Struck-Marcell and Appleton 1987) have given some insight into the formation of a inner rings and the development of off-center collisions in these systems. In these simulations, the gravitational and pressure forces are included for symmetric and near symmetric encounters. Pressure forces include the winds from areas with newly formed stars using the cloud-fluid method (Struck-Marcell et al. 1987, Appleton and Struck-Marcell 1987b, Struck-Marcell and Appleton 1987)

Another series of models have been used to investigate the effects of a prograde tidal encounter on the gas density. Noguchi and Ishibashi (1986) have actually calculated the global color change resulting from this type of interaction by using an estimate of the global change in the star formation rate. In that investigation, the gas was treated as a group of massless sticky test

particles. A collision between two particles was treated as a formation of an O-B association which eventually gave up its mass in the form of a supernovae wind. Colors were estimated by assuming the perturbation of the colors was caused by a change in the number of these O-B stars.

B. Photometric Models

Most previous work on the photometric evolution of galaxies has focused primarily on the long term evolutionary effects present in elliptical galaxies (cf. Bruzual 1981, Bruzual 1983, Arimoto and Yoshii 1986, Chokshi and Wright 1987). Only a few authors have examined the effect a burst of star formation has on a spiral galaxy's photometric colors (cf. Struck-Marcell and Tinsley 1978, Larson and Tinsley 1978, Noguchi and Ishibashi 1986) because of the difficulty in examining the past history of star formation in these systems. Elliptical galaxies are much easier systems to model in terms of the star formation rate because of the single burst nature of the star formation history. The photometric evolution of elliptical galaxies can, in principle, be used to determine the distances to clusters and could provide important information about cosmology. Because the color of elliptical galaxies is sensitive to the stellar evolutionary tracks, the metallicity, the redshift and the initial mass function, the process of modeling the photometric evolution of elliptical galaxies is extremely complex and difficult (cf. Bruzual 1983). Because the star formation has essential stopped by the time we observe elliptical galaxies, the changes in the colors of

these galaxies are very subtle and very slow. Although the stellar populations of galaxies are younger at high redshifts, the bluer light emitted at earlier times is more greatly affected by redshift than those nearby. Even correcting for the Hubble expansion, currently there is only tenuous observational evidence for photometric evolution in these systems (Koo 1985, Bruzual 1986).

Most photometric models of spiral galaxies have used a simple exponentially decreasing star formation rate to approximate the global star formation rate (Bruzual 1981, Bruzual 1983, Arimoto and Yoshii 1986, Belfort et al. 1987, Chokshi and Wright 1987). Although these models are very simple to use and seem to work adequately for the global colors, they cannot deal with colors on a level smaller than the entire galaxy since star formation does not take place uniformly over the entire disk.

The optical colors of spiral galaxies are clearly dominated by the effects of star formation. The bluish colors of spiral arms and HII regions clearly outline regions of on-going star formation. The reddish colors of the bulges and globular clusters show the effects a decreasing star formation has on a population's colors. Changes in the metallicity content with time have some effect on the colors also (Arimoto and Yoshii 1986), but the presence of intermediate and high-mass main sequence stars have a greatest effect on the colors of spiral galaxies.

The near-infrared colors of normal spiral and elliptical galaxies are very similar (cf. Frogel 1985, Joy 1986). Numerical models of

the JHK bands have been completed by a several authors (cf. Struck-Marcell and Tinsley 1978, Aaronson et al. 1978) for normal galaxies. Starbursts galaxies deviate from these normal colors in a variety of directions in the JHK plane (Telesco et al. 1985, Joy 1986). In starburst galaxies, the near-infrared colors are affected by extinction, thermal emission from warm dust, and HII continuum emission (Telesco and Gatley 1984). The infrared emission from blue star photospheres is not as important as the secondary emission caused by these stars in dust and HII regions in some galaxies (Joy 1986). In order to numerically model these effects, it would be necessary have a radiative transfer model of the interstellar medium for the galaxies of interest. Deviations from the colors of normal spiral, however, can be used as an indication of a starburst.

C. Observational Measurements of Star Formation

A large number of observational studies have examined the star formation rates of interacting galaxies using a number of different techniques. One technique, which has become very popular since IRAS data has become available, is based on the use of IRAS far-infrared fluxes. The far-infrared flux is defined in the IRAS galaxy catalog as a linear combination of the IRAS 60μm and the 100μm band fluxes. The combination of these two bands gives a reliable estimate of the 80μm flux for a wide variety of infrared spectra. Because of the strong correlation between the far-infrared flux

(FIR) and the infrared spectral index[1], it is possible to relate the infrared flux in a galaxy to its current star formation rate (de Jong et al. 1984).

This correlation has been explained using a two component model for infrared emission in the interstellar medium (cf. de Jong and Brink 1986). The low temperature (30K) cool dust is assumed to cause diffuse galactic cirrus emission similar to our own galaxy, and a hotter (60K) component is believed to result from regions of star formation. Because both components contribute to the far infrared emission of galaxies, a correlation exists between the infrared color temperature and the far infrared flux. Since the dust in galaxies is optically thick in the B band and optically thin in the far-infrared, the B band flux is less sensitive to the current star formation than the FIR flux. The relative amount of star formation can be related to the ratio between the FIR flux and the B band flux.

The use of the FIR flux and the ratio between the FIR flux and the B band flux has been used by a number of authors to calculate the global star formation rate and measure the relative star formation rate in different galaxies (cf. Appleton and Struck-Marcell 1987a, Brink 1986, Persson 1986, de Jong et al. 1984).

---

[1]The spectral index is defined as the ratio of two infrared band fluxes from an object. For extragalactic work, the 60μm and 100μm band fluxes are normally used. Models for far-infrared emission use the 60μm/100μm ratio and the 12μm/25μm ratio to determine the sources of infrared emission.

The conversion between FIR fluxes and the actual star formation rate is dependent on the form of the initial mass function in the high-mass range (Persson 1986).

Another technique used to determine the star formation rate of galaxies uses H-alpha fluxes. The amount of H-alpha flux present is directly related to the amount of ionizing ultraviolet radiation in a region and the number of HII regions. The amount of ultraviolet radiation depends primarily on the number of high mass main sequence stars present. Because high mass stars have relatively short lifetimes, the number of these stars gives good indication of the star formation presently occurring in a region. Once again, the conversion of H-alpha fluxes into the star formation rate is sensitive to the form of the initial mass function at high masses.

Another difficulty of using H-alpha fluxes to measure star formation rate is extinction by dust. In order to accurately measure the actual H-alpha flux, it is necessary to understand the internal extinction of galaxies. IRAS FIR studies do not suffer from this difficulty because of the optically thin conditions present at far-infrared wavelengths in galaxies.

Using the IRAS far-infrared fluxes and H-alpha, a number of studies have been done examining the global star formation rate of interacting disk galaxies. A correlation between interaction and the global star formation rate has been observed by a number of authors using both infrared and H-alpha measurements (cf. Bushouse, 1987, Kennicutt et al. 1987). This correlation has been noted in studies

Kennicutt et al. 1987). This correlation has been noted in studies using both H-alpha measurement and FIR fluxes (Bushouse 1987). Measurements of the star formation rates in the same galaxies using different techniques differ by a factor of about six (Bushouse 1987), but the correlation between interaction and star formation activity exists in both. Studies of the nuclear regions in interacting and normal galaxies have shown a similar correlation between the level of star formation in the inner regions and interaction (Bushouse 1986, Keel et al. 1985). Some of this correlation probably is from nuclear activity rather than an increased star formation rate (Hummel 1980).

Measurements of the amount of CO have also been used as an indicator of the star formation rate. A general correlation between the CO flux in 2.6 mm observations and the far-infrared flux has been found in a sample of about 160 galaxies (Young 1987). Much of the scatter present in this correlation is due to different dust temperatures in the sample of galaxies as measured by the far-infrared color temperature. The azimuthally averaged distribution of CO, H-alpha, and blue light follow similar trends in nearly face-on late spirals, indicting the connection between the amount of CO and the star formation rate (Young 1987). The ratio of the infrared flux to CO flux also give an indication of the efficiency of star formation in galaxies by comparing the number of stars formed compared to the amount of gas forming them (cf. Young et al. 1986).

Even though there is strong observational evidence for enhanced global star formation rates in interacting galaxies, few studies have examined the location of star formation in the outer regions of these galaxies. The emphasis in these studies have been on either the global star formation rates or the star formation rates in the nuclear regions. This bias has a variety of origins.

For observational programs which have used the FIR fluxes to measure the star formation rate, the primary problems have been resolution, low signal level and confusion with foreground sources. The low resolution of the IRAS satellite[2] has made the detection of anything besides the global properties of most galaxies impossible. The relatively high signal in the inner regions also makes it difficult to find the lower signal level expected in the outer levels of interacting galaxies because of hysteresis losses. The presences of infrared cirrus in our galaxy also makes it difficult to determine if extended emission is from extragalactic sources or simply from the dust in our own galaxy.

A study of H-alpha fluxes in the tidal features of interacting galaxies has not been completed for a statistical sample of galaxies. The reasons why this type of study has not been done is not obvious. The most likely reason is the relatively low surface brightness levels in the outer regions of galaxies compared to the nuclear regions

[2]The resolution of IRAS is approximately 4 minutes of arc at 100μm (IRAS Catalog and Atlases Volume 1 : Explanatory Supplement 1988).

and inner disk regions. The amount of surface brightness in a typical disk decreases exponentially with radius (Freeman 1970) and the amount of HI gas decreases approximately as 1/r for most galaxies (Quirk 1972, Kennicutt 1989, Struck-Marcell 1989), so the amount of star formation in the outer disk would be expected to be lower than the inner regions.

A lower rate of star formation does not mean that star formation is not currently taking place. In a recent study of the outer regions of galaxies using multi-color CCD photometry (Schombert et al. 1989), the broad-band photometric colors of tidal features in interacting galaxies were compared to their inner regions. The colors of the tidal tails and plumes in this study were found to be bluer in B-V and V-r[3]on average than the main galaxies of the sample. The effect is even stronger for the tidal bridges in the study.

Two possible explanations were suggested for these data: dereddening or an increased rate of star formation. The colors of any spiral galaxy have some internal reddening present. The dust in the spirals preferentially absorbs blue light and passes red light, causing a reddening of the observed colors. If the amount of dust were larger in the main galaxy than in the tidal features, the colors of the inner regions would be redder than the colors of the tidal features. However, the very blue absolute colors of some of the tidal

[3]The photometric system used in this study combined the Johnson B and V filters with the Gunn r and i filters.

features suggests that not all cases can be explained by this hypothesis. For the tidal tails, the B-V color ranged from 0.25 to 0.73. Along with the blue colors, a knotty appearance in some tidal tails and plume indicates that star formation is taking place in at least some of this sample.

D. Models of Star Formation and Photometric Evolution in Tidal Tails

As a step towards understanding the blue colors of the tidal tails and plumes, a simple model for enhanced star formation the outer regions of interacting galaxies was developed. A restricted three-body code was used to model the changes in density in comoving regions during the interaction.

In these simple dynamical models, the local density history is followed for regions which eventually become part of the tidal tail. A density enhancement is formed from the dynamically driven waves created in the tail during the interaction. The effects of this density increase by a simple power law (Schmidt 1959). The photometric consequences of this star formation history are examined using numerical models. Although the hydrodynamical and self-gravitational forces were not included in this study, it is first-order attempt to understand the star formation processes in the outer regions of interacting galaxies.

IV. RIPPLES[4] IN THE OUTER REGIONS OF DISK GALAXIES

A. Overview

The existence of ripples in the outer regions of galaxies has been known since at least the 1960s (cf. Arp 1966). These ripples typically have outer radii of a few hundred kpc and are positioned symmetrically about the center of early-type galaxies (Kundt and Krause 1985). Concentric shells of low surface brightness surrounding early-type galaxies have been studied both observationally and theoretically by a number of authors.

A catalog of shell galaxies has been compiled for the southern hemisphere by Malin and Carter (1983). In this study, it was found that about 16% of the isolated elliptical galaxies in the southern hemisphere listed in the Second Reference Catalog of Bright Galaxies (de Vaucouleurs et al. 1976) have visible shells on the ESO southern sky survey. Other studies by Schweizer and Seitzer (1988)

---

[4]The terms "ripple" and "shell" refer to the same phenomena. Originally the features were considered to be three-dimensional in nature and named shells. The term ripple has been suggested by Schweizer and Seitzer (1988) as a better alternative since it refers to the photometric appearance without a direct dynamical interpretation. The term "shell" will be reserved for the studies done before Schweizer and Seitzer (1988).

have shown that ripples exist around early-type disk galaxies in addition to ellipticals.

B. Models of the Formation of Ripples

A number of mechanisms have been proposed for the formation of these shells around elliptical galaxies. A model by Fabian et al. (1980) used star formation in a galactic wind interacting with the intergalactic medium to form shells. Kundt and Krause (1985) have proposed a variation of this model which has the wind created by an active galactic nuclei. In these models, material is collected in areas which are shocked as a result of this wind interacting with the intergalactic medium. The shells formed with this mechanism would have to be very young since the shells formed would dissipate in a free-fall timescale.

Another class of models has been proposed by Schweizer (1980) and numerically modeled by Quinn (1984) and Hernquist and Quinn (1987, 1988a, 1988b). In these models, the shells are created by the merging of a small disk-type galaxy into a more massive elliptical. The elliptical galaxy tidally destroys the disk and leaves the debris in concentric shell-like structures.

A variation of this model was suggested which uses mass transfer from a tidally interacting disk to form shells (Schweizer and Seitzer 1988, Hernquist and Quinn 1988a. Schweizer 1986). In this model, the companion's disk is not destroyed in the interaction. Some of the outer layers of the disk are tidally stripped in a close

encounter with the elliptical. This stripped material forms the shells around the early-type galaxy.

In both the accretion and the mass transfer models, the material which forms the shells was originally part of another galaxy. Because random motion in the orbits tends to smooth the distribution of the stars, the sharpness of the structures formed is related to how dynamically cold[5] the galaxy was initially. Because most of the shells observed are quite sharp, the galaxies which formed them must have come from dynamically cold galaxies.

C. Observation of Ripples in External Galaxies

In order to test the different models for the formation of ripples, multicolor CCD observations of shell galaxies were conducted by a number of authors (cf. Carter et al. 1982, Fort et al. 1986). By observing the colors of the shells, it is possible to learn something about the age of the material in the ripples and the conditions which formed the ripples. The colors of observed ripples were typically found to be about B-V = 0.7. This color is typical of the disk of a spiral galaxy, hence the material might have been stripped from a spiral.

---

[5]The term "dynamically cold" implies there is a relatively small amount of random motion present in the orbits of particles compared to their regular circular orbital motion. Elliptical galaxies are considered to be dynamically hot and disk galaxies are dynamically cold.

The formation of stars in the shells seems to be ruled out by these observations, since it is too red for a population of young stars. On the other hand, because of the significant fraction of blue light it is unlikely that the material in the shells was formed at the same time as the very red elliptical galaxies at the center of the shells. The merger hypothesis fits the observations for most of the shell galaxies which have been photometrically observed.

One exception to this agreement between the Quinn models and the observations might be Arp 227. Multicolor photometric measurements of this galaxy found that the ripples have a color of about B-V= 0.9 (Schombert and Wallin 1987). This color is consistent to the inner regions of the system (B-V=0.96, ibid.) and is inconsistent with the colors of the outer regions of the interacting spiral companion (B-V=0.65, Longo and de Vaucouleurs 1983).

In addition, the central galaxy of the Arp 227 system is an S0, not an elliptical. Since it is an S0, a warm disk exists in the galaxy in addition to a large bulge. If this galaxy is a typical S0, however, it is dynamically cold enough for tidal features to form. Because the Arp 227 system has a nearby spiral galaxy apparently interacting with the SO, it is possible that a direct collision is responsible for the formation of ripples in this case instead of mass transfer or a merger.

Even though the colors measured for Arp 227 are red compared to the average, there is some evidence that this system is not unique. Schweizer and Seitzer (1988) suggest that about 30% of the galaxies in the Malin and Carter catalog of shell galaxies are S0's rather than ellipticals. In addition, 48 out of 137 galaxies in this catalog are interacting with at least one close companion. The combination of an S0 central galaxy and a tidally interacting companion suggest that a tidal[6] origin of shells in some systems is possible.

D. A Collisional Model for Ripple Formation

From the observational data on Arp 227 and the examination of similar systems, we proposed and tested a new collisional model for the creation of ripples. In these models, a companion galaxy passes through the disk of an S0 causing oscillations in the outer disk. These oscillations eventually form ripple-like features in the outer regions of the disk. Since the material is from the S0, the colors of the ripples are consistent with the inner disk and not necessarily with those of the companion. A study of the formation of these features is presented in the third chapter along with some insight into the some of the conditions needed to produce these features.

---

[6]The term "tidal" will be used to refer to all interactions which do not involve mass transfer.

V. REFERENCES

Aaronson, M., Frogel, J. A., and Persson, S. E. (1978) *Ap. J.* **220**, 98.

Aarseth, S. J. (1972) in *Gravitational N-Body Problem*, ed. M. Lecar (Dordrecht : D. Reidel), p. 29.

Appleton, P. N. and Struck-Marcell, C. (1987a) *Ap. J.* **312**, 566.

Appleton, P. N. and Struck-Marcell, C. (1987b) *Ap. J.* **318**, 103.

Arimoto, N. and Yoshii, Y. (1986) *Astron. Astrophys.* **164**, 260.

Arp, H. C. (1966). *Atlas of Peculiar Galaxies* (Pasadena : California Institute of Technology).

Arp, H. C. and Madore, B. (1986) *A Catalog of Southern Peculiar Galaxies and Associations* (New York : Cambridge University Press).

Barnes, J. E. (1988) *Ap. J.* **331**, 699.

Belfort, P., Mochkovitch, R. and Dennefeld, M. (1987) *Astron. Astrophys.* **176**, 1.

Brink, K. (1986) in "Spectral Evolution of Galaxies", eds. C. Chiosi and A. Renzini (Dordrecht : D. Reidel), p. 127.

Bruzual, G. A.(1981) *Spectral Evolution of Galaxies*, Ph. D. Thesis, University of California, Berkeley.

Bruzual, G. A. (1983) *Ap. J.* **273**, 105.

Bruzual, G. A. (1986) in *Spectral Evolution of Galaxies*, eds. C. Chiosi and A. Renzini (Dordrecht : D. Reidel), p. 263.

Bushouse, H. A. (1986) *A. J.* **91**(2), 255.

Bushouse, H. A. (1987) *Ap. J.* **320**, 49.

Carter, D., Allen, D.A., and Malin, D.F. (1982). *Nature* **295**, 126.

Chandrasekhar, S. (1942) *Principles of Stellar Dynamics* (Chicago : The University of Chicago).

Chandrasekhar, S. (1943) *Reviews of Modern Physics*, **15**, No. 1.

Chokshi, A. and Wright, E. L. (1987) *Ap. J.* **319**, 44.

de Jong, T. and Brink, K. (1986), in *Star Formation in Galaxies*, ed. C. J. Lonsdale Persson (Washington : NASA Conference Publications CP-2466), p. 323.

de Jong, T., Clegg, P. E., Soifer, B. T., Rowain-Robinson, M., Habing, H. J., Houck, J. R., Aumann, H. H., and Raimond, E. (1984) *Ap. J.* **278**, L67.

de Vaucouleurs, G., de Vaucouleurs, A., and Corwin, H. G. (1976). *Second Reference Catalogue of Bright Galaxies* (Austin : University of Texas Press).

Eneev, T. M., Kozlov, N. N., and Sunyaev, R. A. (1973) *Astron. Astrophys.* **22**, 41.

Fabian, A. C., Nulsen, P. E. J., and Stewart, G. C. (1980). *Nature* **287**, 613.

Fort, B. P., Prieur, J.-L., Carter, D., Meatheringham, S. J., and Vigroux, L. (1986). *Ap. J.* **306**, 110.

Freeman, K. C. (1970) *Ap. J.* **160**, 811.

Frogel, J. A. (1985) *Ap. J.* **298**, 528.

Hernquist, L., and Quinn, P. (1987). *Ap. J.* **312**, 1.

Hernquist, L., and Quinn, P. (1988a). *Ap. J.* **331**, 682.

Hernquist; L., and Quinn, P. (1988b). "Formation of Shell Galaxies II: Nonspherical Potentials" to appear in *Ap. J.*

Hummel, E. (1980) *Astron. Astrophys.* **89**, L1.

IRAS Catalog and Atlases. Volume 1 : Explanatory Supplement (1988) eds. C. A. Beichman, G. Neugebauer, H. J. Habing, P. E. Clegg, and T. J. Chester (Washington : NASA).

Joy, M. (1986) *A Multicolor Infrared Study of Interacting Galaxies*, Ph. D. Thesis, University of Texas.

Keel, W. C., Kennicutt, R. C., Jr., Hummel, E., and van der Hulst, J. M. (1985) *Ap. J.* **90**, 708.

Kennicutt, R. C., Jr. (1989) "The Star Formation Law in Galactic Disks" to appear in *Ap. J.*

Kennicutt, R. C., Jr., Keel, W. C., van der Hulst, J. M., Hummel, E., and Roettiger, K. A. (1987) *A. J.* **93**, 1011.

Koo, D. C. (1985) *A. J.* **90**(3), 418.

Kundt, W. and Krause, M. (1985). *Astron. Astrophys.* **142**, 150.

Larson, R. B. and Tinsley, B. M. (1978) *Ap. J.* **219**, 46.

Longo, G., and de Vaucouleurs, A. (1983). *Univ. Tex. Monogr. Astron.* No. 3.

Malin, D. F., and Carter, D. (1983). *Ap. J.* **274**, 534.Struck-Marcell, C., Scalo, J. M.,·and Appleton, P. N. (1987), in Star Formation in Galaxies, ed. C. J. Lonsdale Persson (NASA Conference Publications CP-2466 :Washington), p. 197.\

Negroponte, J. and White, S. D. M. (1983) *M. N. R. A. S.* **199**, 169.

Noguchi, M. and Ishibashi, S. (1986) *M. N. R. A. S.* **219**, 305.

Persson, C. J. (1986) *Nearly Normal Galaxies*, ed. Faber, S. M. (New York : Springer-Verlag), p. 36.

Quinn, P. (1984). *Ap. J.* **274**, 596.

Quirk, W. J. (1972) *Ap. J.* **196**, L9.

Schmidt, M. (1959) *Ap. J.* **129**, 243.

Schombert, J. M. and Wallin, J. F. (1987). *A. J.* **94**, 300.

Schombert, J. M., Wallin, J. F., and Struck-Marcell, C. (1989) to be submitted to *A. J.*

Schweizer, F. (1978) in *Structure and Properties of Nearby Galaxies*, eds. E. Berkhuijsen and R, Wielebinski (Dordrecht : D. Reidel), p. 279.

Schweizer, F. (1980) *Ap. J.* **237**, 303.

Schweizer, F. (1983) in *Internal Kinematics and Dynamics of Galaxies*, ed. Athanassoula, E. (Dordrecht : D. Reidel), p. 319.

Schweizer, F. (1986) *Science* **231**, 193.

Schweizer, F. and Seitzer, P. (1988). *Ap. J.* **328**, 88.

Struck-Marcell, C. (1989) *Radial Gas Profiles in Diffusive Galaxy Disks*, to be submitted to *Ap. J.*

Struck-Marcell, C. and Appleton, P. N. (1987) *Ap. J.* **323**, 480.

Struck-Marcell, C., Scalo, J. M., and Appleton, P. N. (1987), in *Star Formation in Galaxies*, eds. C. J. Lonsdale Persson (NASA Conference Publications CP-2466 :Washington), p. 197.

Struck-Marcell, C. and Tinsley, B. M. (1978) *Ap. J.* **221**, 562.

Telesco, C. M. and Gatley, I. (1984) *Ap. J.* **235**, 392.

Telesco, C. M., Decher, R., and Gatley, I. (1985) *Ap. J.* **299**, 896.

Toomre, A. and Toomre, J. (1972) *Ap. J.* **178**, 623.

van der Hulst, J. M. (1979) *Astron. Astrophys.* **71**, 131.

White, S. D. M. (1983) in *Internal Kinematics and Dynamics of Galaxies*, ed. Athanassoula, E. (Dordrecht : D. Reidel), p. 337.

Wallin, J. F. and Struck-Marcell, C. (1988) *A. J.* **94**, 300.

Young, J. S. (1987), in *Star Formation in Galaxies*, ed. C. J. Lonsdale Persson (Washington : NASA Conference Publications CP-2466), p. 197.

Young, J. S., Scholerb, F. P., Kenney, J., and Lord, S. D. (1986) *Ap. J.* **304**, 443.

DYNAMICAL AND PHOTOMETRIC MODELS OF STAR FORMATION IN TIDAL TAILS

ABSTRACT

An investigation into the causes of star formation in tidal tails has been conducted using a restricted three-body dynamical model in conjunction with a broad-band photometric code. The test particles are initially placed in circular orbits around a softened point mass and then perturbed by a companion passing in a parabolic orbit (Toomre and Toomre 1972, Eneev et al. 1973). During the passage, the density evolution of the galaxy is examined both in regions within the disk and in selected comoving regions in the tidal features. Even without the inclusion of self-gravity and hydrodynamics, regions of compression form inside the disk and along the tidal tail and tidal bridge causing local density increases of up to 500%. The density changes found from these models and the mechanisms which lead to them are discussed.

The effects these changes have on the colors of the tidal features are examined with a broad-band photometric code. A spiral galaxy population is synthesized and the effects of modest changes in the star formation rate are explored. Assuming the density changes are related to the star formation rate via a Schmidt (1959) law allows us to calculated limits on the density changes needed to make detectable changes in the colors. Density changes similar to those found in the dynamical models will cause detectable changes in the colors of a stellar population.

From these models, it is determined that the blue colors and knotty features observed in the tidal features of some galaxies result from increased rates of star formation induced by tidally produced density increases. Limitations of this model are discussed along with photometric models based on the density evolution in the tails.

I. INTRODUCTION

The existence of tidal tails and bridges in morphologically peculiar galaxies has been known for at least 20 years (Arp 1966). Since their discovery, there has been growing observational evidence from the measurements of broad-band photometric colors that on-going star formation occurs in some of these tidal tails and some evidence that relatively high star formation rates occur in the tidal features in some selected systems (Schweizer 1978, Schombert et al. 1989). Knotty features in some of the tails also suggest on-going star formation occurs in some of these systems (Arp 1966, Arp and Madore 1987). Even though a basic dynamical understanding of the formation of these features has been available since the early 1970s (Toomre and Toomre 1972, Eneev et al. 1973), our understanding of the star formation processes in tidal tails is very incomplete. Previous modeling of the photometric evolution of normal and interacting galaxies (cf. Larson and Tinsley 1978, Struck-Marcell and Tinsley 1978, Bruzual 1981) has focused on the global galaxy colors rather than the spatial variations within the interacting systems. However, with the advent of CCD surface photometry, a great deal of data are becoming available on these spatial variations. In this paper, a simple dynamical model of the local density evolution is used to understand the changes in the star formation rate that occur in the tidal tails of interacting galaxies.

The local photometric consequences from these density changes are also calculated using a broad-band photometric code.

Many observational investigations have linked enhanced global and nuclear activity in the radio continuum, (Hummel 1981, Condon et al. 1982), far-infrared (Bushouse 1987), near-infrared (Telesco et al. 1985), and optical (Larson and Tinsley 1978, Keel et al. 1985) to interactions. Measurements of global colors and comparisons to photometric models indicate a correlation between enhanced star formation and interactions between galaxies (Larson and Tinsley 1978, Struck-Marcell and Tinsley 1978). It has been noted by Sanders et al. (1987) that the fraction of galaxies which are interacting increases monotonically with IRAS brightness for luminosities greater than $3x10^{10}$ L_0 (Soifer et al. 1987). A correlation between high infrared flux and interacting galaxies has also been noted by Bushouse (1987) and Telesco et al. (1988). Near-infrared (Telesco et al. 1985), radio continuum (Condon et al. 1982, Sramek and Weedman 1986) and H-alpha fluxes (Kennicutt et al. 1987, Bushouse 1986, 1987) also indicate possible increased rates of star formation in some interacting galaxies. The infrared luminosity, radio continuum fluxes, and the H-alpha fluxes of some interacting galaxies are affected by nuclear activity (Bushouse 1986, Keel et al. 1985, Hummel 1981), but in some cases it seems clear that increased star formation rates in the disk are responsible for higher spectral luminosities (Bushouse 1987, Kennicutt et al. 1987, Condon et al. 1982, Sramek and Weedman 1986).

The optical CCD photometry by Schombert et al. (1989) shows that the colors of extended tidal features in interacting galaxies are bluer in both B-V and V-Gunn r on the average than the colors of the main galaxies in the sample. The colors seen in the tidal tails ranged between a B-V of 0.25 and 0.73. The colors of tidal bridges were found to be even bluer on average than the tidal tails. Some of these blue colors might be explained by a smaller amount of interstellar dust in the outer regions of these galaxies, but the bluest colors of the sample probably have resulted from a recent increase in the star formation rate.

In this work, we use a restricted three-body code to follow the local comoving density by defining a region around one of the test particles and counting the number of particles within this comoving region as the simulation progresses. A detailed discussion of the method and the limitations are presented in the Dynamical Methods section of this paper.

In regions which become part of the tidal tail, the comoving density increases by a factor of between two and five in low inclination orbits over a variety of mass ratios and impact parameters for the companion galaxy. This density increase is caused by a twisting of the tidal tails combined with the formation of orbital caustics on the outside edge of the tidal tail. With moderate and high inclination orbits, the twisting becomes three-dimensional and does not lead to much compression.

A relationship between the density increase and the star formation rate was suggested by Schmidt (1959). The Schmidt law is given by

$$SFR = K \rho^n \qquad (1)$$

where K is a constant, ρ is the density, and n is constrained to be between one and two. This relationship implies that a change in the star formation rate by a factor between 2 and 25 might accompany the density changes of between 2 and 5 which occur for a relatively short time. A broad-band photometric code was developed to model the color changes caused by a varying star formation rate. In the photometric models, the star formation history is constructed uses an exponentially decreasing star formation rate until near the end of the simulation, when a constant star formation rate is turned on. The photometric models presented show that detectable color changes will occur if the star formation rate is changed by a factor greater than five. A larger change would cause the system to behave like to a single burst during its early evolutionary stages. A discussion about the physical inputs used for these models is included in the Photometric Models section of this paper.

This paper is divided into four major sections. Following the Introduction, the dynamical models of compression in tidal tails are discussed. Photometric models are then presented to relate the changes in density to changes in the photometric color. A Conclusion section is included to summarize the results from the dynamical and photometric models.

II. DYNAMICAL MODELS

A. Methods

Dynamical models of interacting galaxies using numerical simulations have been used to study interacting and merging galaxies by a number of authors (Toomre and Toomre 1972, Lynds and Toomre 1976, Negroponte and White 1983, Hernquist and Quinn 1987, Barnes 1988, Noguchi and Ishibashi 1986, Noguchi 1987). Many of these simulations focused on investigating the formation of ellipticals through mergers (White 1983, Hernquist and Quinn 1987, Barnes 1988). To understand the formation of tidal features, restricted three-body codes have been used to reproduce the morphologies of tails (Toomre and Toomre 1972), rings (Lynds and Toomre 1976), shells (e.g. Hernquist and Quinn 1987), and ripples (Wallin and Struck-Marcell 1988). For the simulations of the density evolution of tidal tails, a similar method is used here.

In the dynamical simulations presented here, test particles are initially placed in a disk in circular orbits around a softened point mass. The companion galaxy is represented by a second softened point mass. Softened point masses are used in these simulations for several reasons. They approximate the mass distribution found in external disk galaxies with rotation curves. It is also simple to compute the force from a softened point mass and numerical instabilities in the integration routines are eliminated. The free

parameters in these simulations are the mass of the companion galaxy, the distance of closest approach, the inclination and argument of perigee of the companion's orbit, the softening lengths of the two galaxies, and the initial radial distribution of the test particles in the main galaxy.

The gravitational constant, along with the mass and outer disk radius of the main galaxy, are defined as unity in these simulations. The argument of perigee is set to zero and the companion galaxy is assumed to be in a parabolic orbit with t=0 corresponding to the periapse. The softening length for the main and companion galaxy is set to 0.1 disk radii. Distances and masses will be expressed in terms of disk radii and galactic masses respectively. The time unit is derived from Kepler's third law. In terms of physical units, a mass of one is defined as 10^{11} solar masses, a radius of one is defined as 15 kpc, giving a unit time of 82.6 Myr.

The integration method used for these simulations was a fourth order Runge-Kutta routine with a fixed time-step. The time-step used was chosen from a series of stability tests on this code detailed elsewhere (Wallin 1989). In these tests, a companion galaxy was placed in an orbit which brought it close to the disk of the main galaxy. After the encounter, the simulation was reversed and the particles were integrated toward their initial positions. The rms postional deviation of the particles and the maximum deflection for a single particle were calculated for a variety of time-steps.

The density history in selected comoving regions is followed through the interaction. This density history is related to the star formation history of the local regions in the galaxy. These comoving regions are initially placed in circular orbits around the main galaxy at a distance of one disk radius. Test particles are placed in a 1/r distribution from a radius of 0.1 to 1.1 disk radii, similar to the HI gas distribution found in the disks of normal galaxies (Quirk 1972, Struck-Marcell 1989, Kennicutt 1989). The regions are then moved as ordinary test particles in the interaction. The density is calculated by counting the number of test particles contained in a box 0.1 disk radii on a side which is centered on the selected test particle at each time-step. Using approximately 10,000 particles in the disk, an average box contains 31 particles before the interaction. Since the particle density decreases as 1/r, the 50 boxes which are followed during the simulation initially have a density of approximately 12 particles per box at their initial radii of 1.0 disk radius. Although the relatively small number of particles limits the density increase detectable, the large number of regions followed allows a reasonable amount of spatial resolution. This spatial resolution is needed to follow the propagation of density waves. Because of the low number of particles in a single box, only density changes greater than a factor of two above the initial density will be considered reliable in these simulations.

It is important to note that the effects of gas pressure and self-gravity of the disk were not included explicitly in these simulations.

After trajectory crossing occurs in the test particles, it is unlikely that the results of these simulations are valid. Because self-gravity would trigger further collapse in regions of high density, these simulations can only be used to find out where compression initially takes place and roughly how much compression would be expected from the perturbations caused by the tidal interaction alone.

Before trajectory crossings occur in the simulations, the hydrodynamical forces on the tidal tail are likely less important than self-gravitational forces if the gas is considered to be isothermal. The isothermal approximation can be used since interstellar HI is generally optically thin to Hα and the cooling time for collisions will likely be relatively short compared to the collisional timescale of interstellar gas clouds. If the density increases to the point where the interstellar medium becomes optically thick, it is likely that star formation will be taking place.

B. Results

To aid in understanding the star formation history of interacting galaxies, the morphological development of tidal features formed in prograde tidal encounters will be discussed. Although many of the results presented in this section are similar to those presented by Toomre and Toomre (1972), it is important to re-examine and expand these results to understand the connections between the tidal interactions and the compressions which lead to star formation in interacting galaxies.

After the review of the global dynamical evolution, the density history for regions which form the tidal features will be presented. The mechanisms which cause these density changes will be explored, as will the possible effects on the star formation history. The effects of different masses, inclinations, and impact parameters of the companion galaxy on the density history of regions which become part of the tidal tails will be discussed, followed by a summary of dynamical results from these models.

1. Morphology

The morphological development of a typical dynamical run is shown in Figure 1. In this simulation, a companion of equal mass to the main galaxy passes in a zero inclination prograde parabolic orbit with a minimum approach distance of 1.6 disk radii. No distortion of this disk is visible at the start of the simulation. Particles are initially in placed in counter-clockwise circular orbits around the main galaxy with the companion out of the frame at the extreme right.

At approximately t=-1.2, a bulge in the disk extending toward the companion develops. At approximately t=-0.8, the particles pinch together as they approach the companion. This bulge eventually lengthens to become the tidal bridge. At the same time, a caustic forms along the leading edge of this bulge and bends into the disk. A caustic is formally defined by the behavior of the second and higher order derivatives in the displacement function, but can be thought of as regions of high density caused by the crossing of

be thought of as regions of high density caused by the crossing of particle trajectories. This caustic divides the disk roughly between the particles which develop into the tidal tail and those which stay associated with the disk.

At t=-0.2, the tidal tail begins to separate from the disk. A second caustic develops at approximately t=+0.2 on the leading edge of the tidal tail. The tidal tail then begins to compress and decrease in width at the base. At about t=+1.0, the particles at the base of the tail overtake the leading edge of the tail and cross the lower caustic. This crossing of particles from the back to the front of the caustic has the appearance of a twist in the tidal tail. This twist propagates along the tidal tail toward its tip. Since the simulation presented in this discussion is two-dimensional, the twisting causes compression and rarefaction in the tidal tail. After the twist has passed a point on the tidal tail, the sharpness of the tidal feature decreases and the density is lowered.

Another effect seen in the simulations is the compression of the disk. After being perturbed by the companion, the orbits of the particles change from circular to elliptical. Since the majority of the particles have periapses which are closer than their initial radii, the density in the disk increases as the volume of the disk decreases. This increase in density might be partially responsible for the higher star formation rates seen in the disks of interacting galaxies (Bushouse 1987).

2. Local Density Enhancements

a. The Tidal Tail

For low inclination orbits, particles which form the tail have density histories which depend on their location relative to the caustics. A typical density history for particles which start outside the first caustic is shown in Figure 2. The density of this region undergoes little change until it passes through the second caustic. As this happens, the density increases by a factor of 50% to 400%, depending on how close to the end of the tidal tail the region is located. From the Schmidt law, the star formation after this twist would be increased to between 5 and 16 times the star formation rate before the collision in the inner tail. It should be noted that the density history after the twist is likely to be unreliable since the effects of self-gravity and hydrodynamics will become more important during a compression.

If the star formation rate follows the density history even after the compression, the decrease in the density seen in Figure 2 after t=1.5 might cause a cutoff in the star formation in this region. A modified version of the Schmidt law has been proposed that follows the form of equation (1) above a critical density (Kennicutt 1989). Belows this critical density, the star formation stops. The rarefaction seen after the initial compression may be sufficient to stop the star formation.

The twisting of the tidal tail is equivalent to a density wave moving along the tail's surface for low inclination orbits. As the wave propagates through a region, the local density along the tail increases. Figure 3 shows the density enhancement for particles at different positions along the tail. As the twist propagates outward, the local density enhancement caused by the twist decreases. This decrease in amplitude is caused primarily by the lower number of particles tidally displaced to the larger radii since the displacement of a particle depends on its initial azimuth and radii.

The particles which start inside the first caustic show a density history similar to that shown in Figure 4. Near the time of closest approach of the companion, the regions have an extended period where the density is three to five times greater than the initial density of the disk. A rarefaction then occurs for about two time-steps. A second compression occurs as the particle passes through the second caustic. This density enhancement from the disk would increase the star formation rate in these regions just before they are separated from the disk. The reliability of the second compression is uncertain because self-gravity and hydrodynamical forces have been neglected. Because the enhanced star formation would have occurred about 100 Myr before the encounter, the

population of stars formed in the disk and displaced to the tidal tail would be relatively young with ages of about 100 Myr[1].

It is important to note that the initial disk compression occurs in all simulations with inclinations between 0 and 90 degrees, although these regions of compression seem to remain generally near the base of the tail. A discussion of how inclination affects these models is included below.

b. Tidal Bridges

A typical density history for a region which forms the tidal bridge is shown in Figure 5. A sharp compression occurs slightly before the time of the companion's closest approach as the particle passes through the first caustic. The sharpness is caused by the high velocity and the direction of its motion of the region relative to the nearly stationary tidal bridge. This region is moving almost perpendicular to the caustic when the compression takes place and is being strongly perturbed by the companion galaxy. Because of the high velocity relative to the other particles in the bridge, it is very likely the gas will be strongly shocked in this region. After cooling takes place, this density increase is likely to lead to a period of new star formation.

---

[1]The exact age of the stars formed in this encounter will depend on the masses and orbits of the main and companion galaxies.

Since the density of tidal bridges is much lower than that of tidal tails, the star formation in these features will not be as large as those from the tidal tails. Some of the particles in the tidal bridge passed through a high density region in the disk before becoming part of the bridge. The compression in the disk might give an enhanced rate of star formation and a blue color in the bridge, in a manner similar to that illustrated for tails in Figure 4.

3. Parameter Dependencies

a. General Discussion

A grid of models was run to investigate the effects the companion galaxy's mass, periapse distance, and inclination have on the density history of a region in the tidal tail. Table 1 contains a detailed list of the parameters used in these models. The amount of compression and the time of the compression depends on these parameters in the simulation. In all the models, the morphological development proceeds in a manner similar to that described above with the elongation of the disk, development of caustics, separation of the tidal tail, and development of twists.

b. The Companion Galaxy's Mass

To test the effect the companion galaxy's mass has on the density development in tidal tails, the companion's mass was set at 0.25, 0.5, 1.0 and 2.0 times that of the main galaxy. The other initial conditions, including the companion's periapse, the inclination, and the starting times, were held constant in the simulations. Overall, the development of global morphology

simulations. Overall, the development of global morphology proceeds in a very similar manner for all masses tested.

Changes in the mass of the companion galaxy result in changes in the time needed for the development of similar morphological features. An example of this time difference is shown in Figure 6. Four very similar morphologies are shown from runs A, B, C, and D. The frames were taken at the point in the simulation where the tidal tails begin to fold at the base. The time necessary to reach this evolutionary stage increases as the companion galaxy's mass decreases.

The reason for this delay is partially related to the lower orbital speed in the lower mass systems. The companion galaxy was assumed to be in a parabolic orbit in all cases, but the orbital velocity depends on the total mass of the two galaxies. If the companion galaxy is low in mass, the orbital velocity is also low.

Even though the tidal forces on the particles are smaller in the lower mass systems, the lower orbital speed allows additional time to perturb the particles' orbits. The density enhancements which occur from the folding of the tidal tail have amplitudes similar to those with comparable positions in simulations with companions of different masses. The time at which the density increases occur depends on the mass of the companion, but the amplitude of the density increase is only weakly related to the companion's mass. This suggests that the changes in the star formation induced in the

tidal tails during interactions will be similar in galaxies which have different mass ratios between the companion and the main galaxy.

c. Inclination Effects

The effects of an inclined companion orbit are tested in models A, E, F, and G. The inclinations in these models were set to 0, 30, 60 and 90 degrees respectively, while all other parameters were held constant.

The density development along the tail depends strongly on the inclination. Figure 7 shows the density history for particles located along the tail for run E. Regions which are more than half the distance outward along the tail do not have a density enhancement corresponding to the twist in these simulations. As noted by Toomre and Toomre (1972), the twisting of the tail is generally a three-dimensional phenomenon. The inner regions of the tail have a density enhancement because the amount of vertical perturbation depends on the radius. For low inclination orbits, the tidal tail is nearly planar, so the compression takes place throughout the tail. The amount of vertical displacement for these tails is quite small compared to the size of the disk. The tidal tail remains essentially in the galaxy's spin plane rather than in the orbital plane of the companion (Toomre and Toomre 1972). If a small amount of random motion was initially present in the vertical direction, or if a larger box was used to measure the density, the density changes along the tail probably would be very similar for models A, E and F.

Particles which pass through the disk before reaching the tail have similar density enhancements, independent of inclination. As stated above, the amount of axial displacement depends on the radius of the particle's orbit; therefore the disk has roughly the same amount of compression, independent of the inclination of the companion galaxy.

d. The Dependence on the Distance of Minimum Approach

The distance of minimum approach for the companion galaxy was varied in runs A, G, and I. The resulting changes in the tidal tails were very similar to those found by changing the mass of the companion galaxy (see Section i above). As the distance of minimum approach is increased, the perturbing force of the companion galaxy decreases. The orbital speed of the companion galaxy also decreases with the larger radii, so the amount of time available for perturbing the test particles increases. Since the interaction happens more slowly, the features formed are more coherent, causing the tails to be narrower and the density enhancements to be stronger. The time necessary to form the tidal features is greater for the simulations with larger periapses because of the lower force from and lower orbital speed of the companion.

e. The Shape of the Potential

The effects different gravitational potentials have on the development of tidal features have not presented in the grid of models in Table 1. Because the tidal features form from material in

inner disk will only weakly affect the development of the tidal tails and bridges. The non-spherical components of the mass distribution inside the particle radii perturb the orbits of the particles by providing torque. Since the bulges are nearly spherically symmetric and disks are nearly axially symmetric, these effects are generally quite small.

The distribution of matter in the halo, however, affects the development of the tidal features more directly. Particles at slightly different initial radii will have a lower difference in their orbital velocities in a system with an extended mass distribution. The differences in the orbital velocities of the particles are partially responsible for the development of the tidal features. Preliminary models indicate extending the mass distribution causes the formation of these features to be delayed. The propagation of the twist in the tidal tail happens later and propagates more slowly in models with extended halos.

4. Summary

Two mechanisms relating to the star formation in tidal tails are proposed. The first is a wave-driven star formation caused by the twisting compression extending to the outer regions of the tails. The propagating twist mechanism is likely to occur only in systems which undergo low inclination encounters with other galaxies, although it occurs for a wide variety of companion masses and impact parameters. This mechanism causes on-going star formation to occur in the tidal tail after the encounter. The second

formation to occur in the tidal tail after the encounter. The second mechanism involves regions of the compressed disk separating from the disk and joining the tail. The second mechanism works for a wide variety of inclinations since the star formation takes place at smaller radii in the disk. This mechanism will lead to a high star formation rate about 50 to 250 Myr before the formation of the tidal tail is complete.

The tidal bridge would have additional star formation from two mechanisms similar to those proposed for the tidal tails. The first mechanism is a collisional process which occurs as clouds overtake the bridge's trailing edge and will lead to on-going star formation in the bridge. In the second mechanism, clouds from the compressed disk are tidally displaced to the region of the bridge. The star formation for this mechanism will take place approximately 50 to 250 Myr before it reaches the tidal bridge.

One general result seen in these simulations is the compression of the inner disk. Along with the tidal stripping, a compression will occur in the disk, leading to enhanced rates of star formation from the tidal encounter. The amount of compression in the disk depends on the mass, the impact parameter, and, to a lesser extent, the inclination of the companion.

III. PHOTOMETRIC MODELS

A. Methods

Population synthesis has been used since the late 1970s as a method of studying photometric evolution (Tinsley and Gunn 1976, Larson and Tinsley 1978, Struck-Marcell and Tinsley 1978). Many of the photometric studies have worked on reproducing the spectral evolution of elliptical galaxies (Bruzual 1981, 1983, Chokshi and Wright 1987). Codes developed for this purpose have often used spectral synthesis as a method of finding the relatively small evolutionary changes caused by an evolving population. Considerations such as metallicity, redshift, and reddening need to be carefully addressed in order to obtain useful results. In interacting galaxies, the broad-band spectral colors are dominated by changes in the star formation rate. In elliptical galaxies, a simple analytical expression such as a single burst are often used to model the star formation rate. For interacting spiral galaxies, a more complicated star formation rate is necessary to fit the photometric observations.

A broad-band code was developed to understand the effects of a changing star formation rate on the spectral colors. The effects of moderate increases and decreases in the star formation rate on an established stellar population are computed using this program.

In the code, a Tinsley-type initial mass function (IMF) was used for the runs; however, the broad-band spectral colors were found to

be only weakly dependent on the form of the IMF (Tinsley 1980, Renzini and Buzzoni 1986). The sources of the stellar model inputs are detailed in Table 2. The clump giant branch stars are set to a single luminosity and temperature for 100 million years for all masses between 0.8 and 3.0 $M_{\odot}$. The decision to use this approximation was motivated by the weak mass dependence of the clump giant stars and the difficulty of modeling this stage of stellar evolution through the helium flash. The main sequence, giant branch, clump giants and asymptotic giant branch tracks are combined into complete evolutionary histories as a function of mass and time. Additional tracks are calculated from the existing tracks using linear interpolation between equivalent evolutionary points.

The initial mass function and the star formation rate are combined to build a star formation history. The contribution of each mass bin is calculated by combining this star formation history and the stellar evolutionary tracks to form an array of effective temperatures and luminosities. The effective temperatures and luminosities are then converted into broad-band spectral colors by using the tables by Johnson (1966). These tables are used because of the inclusion of the near infrared bands and the generally good agreement between these observationally derived values and those calculated from radiative transfer models (cf. Buser and Kurucz 1978).

No chemical evolution is considered in these models. The evolutionary tracks used for these models were typically close to solar. The metallicities for each model are listed in Table 2. Since a varying star formation rate is being examined, it is expected that the metallicity effects will be less important than changes in the star formation rate. Because no internal reddening from interstellar dust is considered in these models, the changes in the colors rather than the absolute colors will examined.

B. Models

A number of simple models were used to examine the effects a changing star formation has on the broad-band spectral colors. For the initial 15 Gyr, the models have an exponentially decreasing star formation rate of the form

$$R(t) = A\, e^{-t/T} \qquad (2)$$

where T is the e-folding time. The e-folding time for these simulations was set at 8 Gyr. During the first 15 Gyr, the star formation rate follows equation (2) with a constant value for A. After 15 Gyr, A is then changed instantaneously by multiplying by a constant factor. The colors are calculated between 100 Myr before and 500 Myr after the star formation rate is changed. In the models presented here, the star formation rate is changed to 5, 2, 1, 1/2, and 0 times the star formation rate at 15 Gyr.

These values were chosen to investigate how small changes in the star formation rate affect the colors of a stellar system. The enhancements used in these models are generally smaller than the bursts investigated previously (Larson and Tinsley 1978, Struck-Marcell and Tinsley 1978) and give limits on minimum enhancements in the star formation rate that could be detected with broad-band photometry. Decreases in the star formation rate along with increases in the star formation rate are also investigated so the color changes caused by rarefaction in the interstellar medium can be investigated.

Figure 8 shows the B-V color changes which occur from these variations in the star formation rate. The colors of the population are altered nearly simultaneously with the changes in the star formation rate. As the star formation rate is increased, the number of upper main sequence stars increases; the number of red giants remains essentially constant because of its dependence on the past star formation history rather than the current star formation rate. Since upper main sequence stars are highly luminous, short-lived and blue, changing the star formation rate influences the colors almost immediately.

For the models with increased star formation rates, the difference between the modified and the original colors decreases with time as the number of giants begins to slowly increase with the evolution of the upper main sequence stars. If the star formation rate is decreased, the number of upper main sequence

stars decreases, and the number of giants remains roughly constant. During the first 500 Myr after the change in the star formation rate, this decrease in the number of main sequence stars causes the B-V color to move toward the red.

Table 3 summarizes the colors of the populations 50 Myr after the changes in the star formation rate occur. If the star formation rate is increased by a factor of five, the B-V color changes by about 0.2 magnitudes. The V-R color changes by about 0.1 magnitudes for the same change in the star formation rate. The weaker dependence the V-R colors have on the present star formation rate results from the larger amount of R light provided by giants. The changes in the U-B colors are even larger than those of the B-V colors.

The weak dependence the star formation rate has on near-infrared colors is illustrated in Figure 9. The near-infrared colors are virtually independent of the changes in the star formation rate (note the scale). The increase in the number of upper main sequence stars changes the amount of blue light and the bolometric luminosity, but the near infrared spectral energy distribution is not significantly affected in these simulations. The further toward the red we examine the colors, the smaller the differences between the initial and modified star formation rate. It is important to note once again that the effects of dust and ionized gas are not included in these simulations. In HII regions, line emission will affect the visual colors of these systems. Dust clouds will primarily affect the

visual colors of the population by absorption and redistribution to the far infrared.

One rather surprising result is the sensitivity of the blue colors to variations in the star formation rate. In the first 50 Myr after the star formation rate is altered, the color changes noticeably for both the x2 and the x5 model in the U-B and B-V bands. Only about 0.5% of the total population of stars are formed during this time for the x5 model. However, since the blue luminosity of an O star is about 10^5 times that of a main sequence G star, a small change in the number of O stars changes the colors of the population in the U-B and B-V bands. Assuming a Schmidt law relates the star formation rate to the density, we conclude that a temporary density increase or decrease of 200% to 500% would cause detectable changes in the colors of a population.

Although the changes in the blue colors could be detected, the variations in the visual and bolometric magnitude may not be seen. Figure 10 shows the changes in the visual magnitude caused by changes in the star formation rate. As the star formation rate increases, the bolometric and visual magnitudes decrease as additional stars are formed; if the star formation rate decreases, the visual and bolometric magnitude increase as the existing population evolves faster than it is replaced. The V magnitude change seen for these simulations is shown in Table 3. For the first 50 Myr, less than 0.5 magnitudes of variation in the V band magnitude will be seen for all the models tested. A change this small may not

observably affect the surface brightness of a feature. After 500 Myr, the change in the visual becomes close to one magnitude when star formation is terminated. Because of relatively small changes in the visual magnitude in these models result from the changes in the star formation rate, the visual surface brightness of a region is unlikely to provide useful information about the recent star formation history of a selected region in a galaxy.

IV. CONCLUSIONS

From the photometric models presented, it has been shown that a moderate change in the star formation rate can change measurably the colors of a population. The colors of a stellar system are determined by changes in the star formation rate rather than the absolute number of stars present. If the star formation rate increases by more than a factor of five, detectable changes in the U-B and B-V colors of the population should be observable within 50 Myr after the changes in the star formation rate begin. Decreases in the star formation rate by a factor greater than about two will begin to significantly affect the U-B and B-V colors of the population on a slightly longer time-scale. Although these modest changes in the star formation rate measurably affect the colors, the effect on visual and bolometric magnitudes is likely to be more difficult to detect.

From the Schmidt law, a change in the local density of 200% to 500% would be needed to cause these variations in the star formation rate. Two mechanisms for creating density enhancements of this magnitude in tidal tails are seen in they dynamical models of tidal features. The first is caused by the twisting motion as particles from the trailing edge of the tail overtake the leading edge of the tail. The density enhancement propagates as the twist travels toward the tip of the tidal tail. The magnitude of this enhancement decreases as the density of the tail

decreases with larger radii. Because the twisting motion is three-dimensional in general, this mechanism is likely to be applicable only for low inclination encounters. The companion's mass and the companion's impact parameter affect the time, and, to a lesser extent, the sharpness of the twist's compression.

The general compression of the disk also can affect the density history of regions that become part of the tidal tail and the tidal bridge. In prograde collisions, the disk initially shrinks as the orbits of most of the particles are perturbed inward. Some of these regions are later tidally stripped from the disk. These stripped areas seem to be located primarily in regions near the base of the tidal tail and the tidal bridge. This compression is likely to increase the star formation rate about 100 Myr before the region becomes part of the tidal feature.

Collisional encounters between particles in the bridge and those overtaking the bridge suggest that increased rates of star formation in tidal bridges might also occur during the encounter. The dependence on the inclination, the impact parameter, and the mass of the companion are difficult to determine because of the low density and high velocities in these regions.

One final note must be added about the nature of tidal features. Tidal tails exist after dynamical friction has merged galaxies into a common envelope (Toomre and Toomre 1972). NGC 7254, NGC 1316 (i.e., Fornax A), and NGC 7252 are all examples of dynamically evolved systems which show signs of tidal tails (Schweizer 1978,

1983). The models presented here are meant to show the early evolution for the system rather than the entire dynamical history. The increases in the star formation rate in the systems' during the first 10^8 years are likely to be unimportant more than 10^9 years after the tidal features are formed. The tidal tails with red colors might be found in these more highly evolved systems.

These models are intended as guides to the type of phenomena which occur from purely dynamical effects. To further understand the star formation processes in tidal tails, additional models need to be constructed which include the hydrodynamical and the self-gravitational forces.

V. REFERENCES

Arp, H. C. (1966). *Atlas of Peculiar Galaxies* (Pasadena : California Institute of Technology).

Arp, H. C., and Madore, B. F. (1987) *A Catalogue of Southern Peculiar Galaxies and Associations* (Cambridge : University Press).

Barnes, J. E. (1988) *Ap. J.* **331**, 699.

Becker, S. A. (1981) *Ap. J. Suppl.* **45**, 475.

Bruzual, G. A. (1981) *Spectral Evolution of Galaxies*, Ph. D. Thesis, University of California, Berkeley.

Bruzual, G. A. (1983) *Ap. J.* **273**, 105.

Bushouse, H. A. (1986) *A. J.* **91**(2), 255.

Bushouse, H. A. (1987) *Ap. J.* **320**, 49.

Buser, R. and Kurucz, R. L. (1978) *Astron. Astrophys.* **70**, 555.

Chokshi, A. and Wright, E. L. (1987) *Ap. J.* **319**, 44.

Condon, J. J., Condon, M. A., Gisler, G., and Puschell, J. J. (1982) *Ap. J.* **252**, 102.

de Loore, C. de Greve, J. P., Vanbeveren, D. (1978) *Astron. Astrophys. Suppl.* **34**, 363.

Eneev, T. M., Kozlov, N. N., and Sunyaev, R. A. (1973) *Astron. Astrophys.* **22**, 41.

Hernquist, L., and Quinn, P. (1987) *Ap. J.* **312**, 1.

Hummel, E. (1981) *Astron. Astrophys.* **96**, 111.

Johnson, H. L. (1966) *Ann. Rev. Astron. Astrophys.*, **4**, 193.

Keel, W. C., Kennicutt, R. C. Jr., Hummel, E., and van der Hulst, J. M. (1985) *A. J.* **90**, 708.

Kennicutt, R. C. Jr., Keel, W. C., van der Hulst, J. M., Hummel, E., and Roettiger, K. A. (1987) *A. J.* **93**, 1011.

Kennicutt, R. C. Jr. (1989) "The Star Formation Law in Galactic Disks", to appear in A. J.

Larson, R. B. and Tinsley, B. M. (1978) *Ap. J.* **219**, 46.

Lattanzio. J. C. (1986) *Ap. J.* **311**, 708.

Lynds, R., and Toomre, A. (1976) *Ap. J.* **209**, 382.

Negroponte, J. and White, S. D. M. (1983) *M. N. R. A. S.* **199**, 169.

Noguchi, M. (1987) *M. N. R. A. S.* **228**, 635.

Noguchi, M. and Ishibashi, S. (1986) *M. N. R. A. S.* **219**, 305.

Quirk, W. J. (1972) *Ap. J.* **196**, L9.

Renzini, A. and Buzzoni, A. (1986) in *Spectral Evolution of Galaxies*, eds. C. Chiosi and A. Renzini (Dordrect : D. Reidel), p. 195.

Sanders, D. B., Soifer, B. T., Neigebauer, G., Scoville, N. Z., Madore, B. F., Danielson, G. E., Elias, J. H., Matthews, K., Lonsdale Persson, C. J., and Persson, S. E. (1987) in *Star Formation in Galaxies*, ed. C. Persson (Washington : NASA Conference Publications CP-2466), p. 411.

Schmidt, M. (1959) *Ap. J.* **129**, 243.

Schombert, J. M., Wallin, J. F., and Struck-Marcell, C. (1989) to be submitted to *A. J.*

Schweizer, F. (1978) in *Structure and Properties of Nearby Galaxies*, eds. Berkhuijsen, E. M. and Wielebinski, R. (Dordrecht : D. Reidel) p. 279.

Schweizer, F. (1983) *Internal Kinematics and Dynamics of Galaxies*, ed. Athanassoula, E. (Dordrecht : D. Reidel), p. 319.

Seidel, E., Demarque, P., and Weinberg, D. (1987) *Ap. J. Suppl.* **63**, 917.

Soifer, B. T., Houck, J. R., and Neugebauer, G. (1987) *Ann. Rev. Astron. Astrophys.*, **25**, 187.

Sramek, R. A. and Weedman, D. W. (1986) *Ap. J.* **302**, 640.

Struck-Marcell, C. (1989) *Radial Gas Profiles in Diffusive Galaxy Disks*, to be submitted to *Ap. J.*

Struck-Marcell, C. and Tinsley, B. M. (1978) *Ap. J.* **221**, 562.

Telesco, C. M., Decher, R., and Gatley, I. (1985) *Ap. J.* **299**, 896.

Telesco, C. M., Wolstencroft, R. D., and Done, C. (1988) *Ap. J.* **329**, 174.

Tinsley, B. M. (1980) *Fund. Cosmic Phys.* **5**, 287.

Tinsley, B. M. and Gunn, J. E. (1976) *Ap. J.* **203**, 52.

Toomre, A. and Toomre, J. (1972) *Ap. J.* **178**, 623.

VandenBerg, D. A. (1985) *Ap. J. Suppl.* **58**, 711.

VandenBerg, D. A., and Hartwick, D. A., Dawson, P. and Alexander, D. R. (1983) *Ap.J.* **266**, 747.

Wallin, J. F. (1989) *Dynamical and Photometric Evolutionary Models of Tidal Tails and Shells*, Ph.D. Thesis, Iowa State University.

Wallin, J. F. and Struck-Marcell, C. (1988) *A. J.* **96**, 1850.

White, S. D. M. (1983) in *Internal Kinematics and Dynamics of Galaxies*, ed. Athanassoula, E. (Dordrecht : D. Reidel), p. 337.

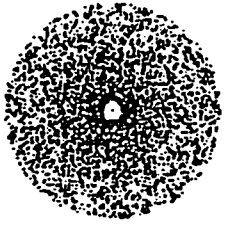

t = -3.0

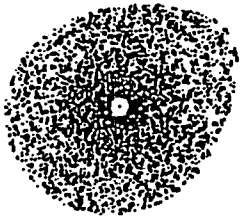

t = -1.4

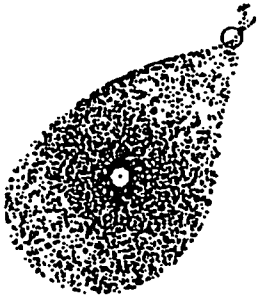

t = -0.8

t = -0.4

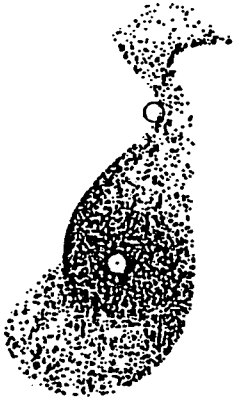

t = -0.2

t = 0.2

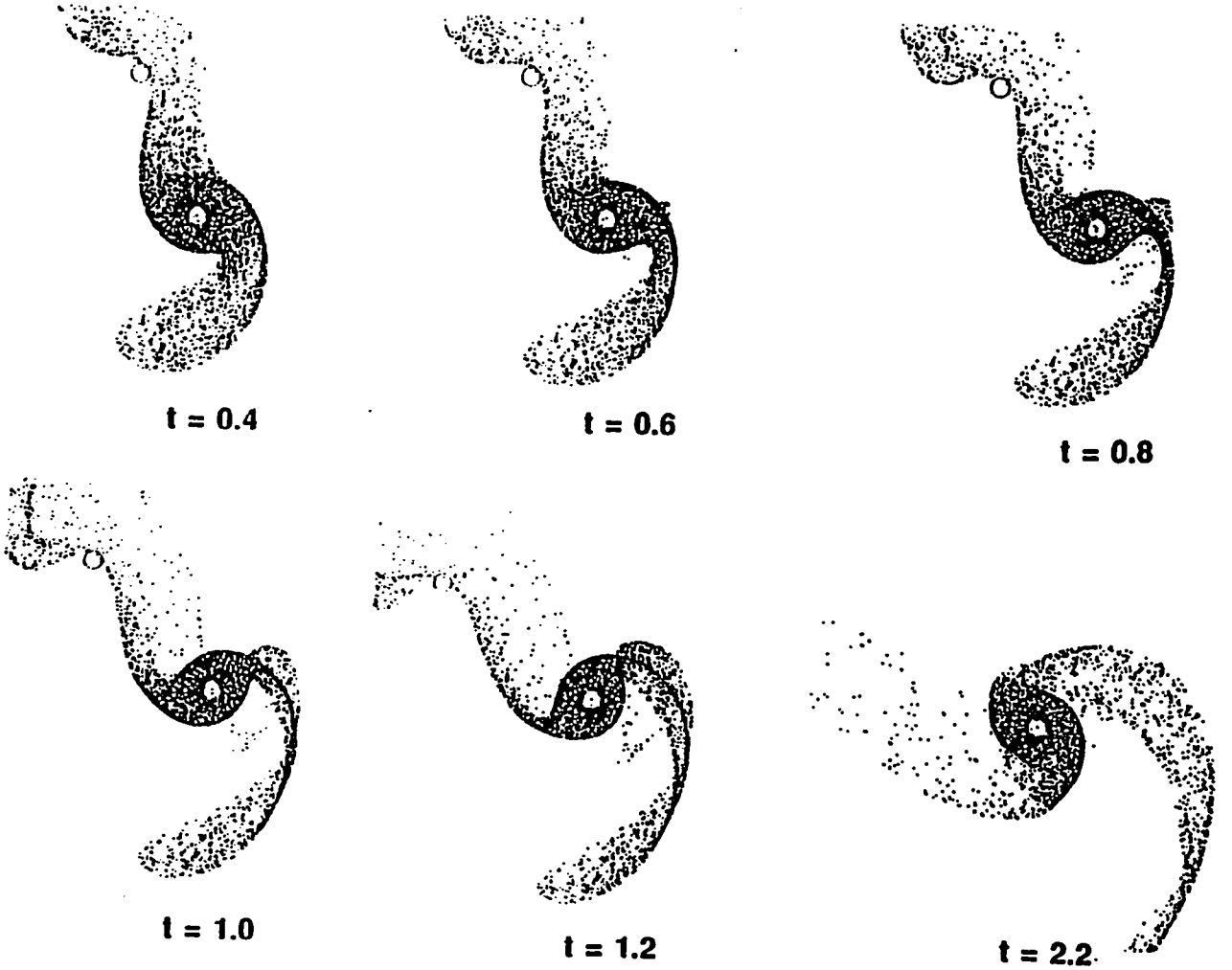

Figure 1 The morphological development of tidal features in a prograde parabolic passage. A time sequence of frames taken from simulation A is shown. The companion galaxy is represented in the frames by the circle. A discussion of the development is conducted in Section III of the text

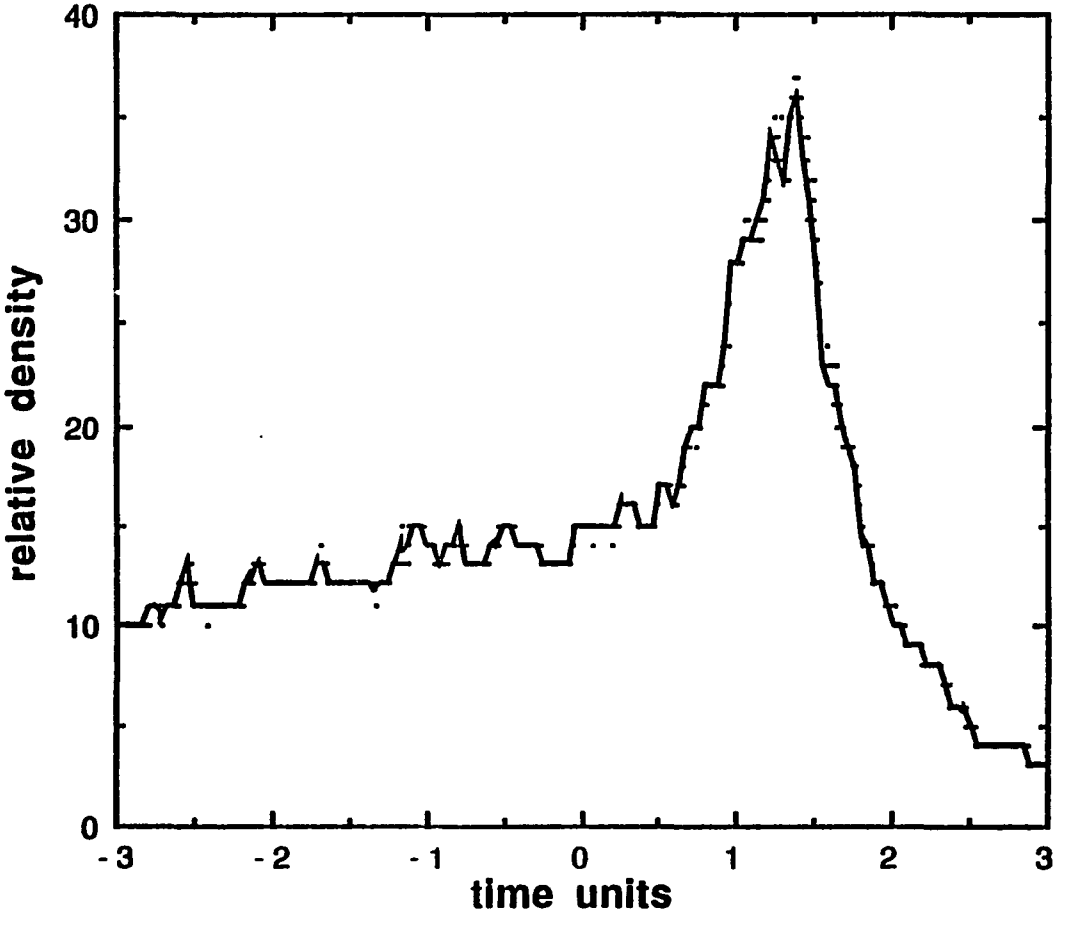

Figure 2. A typical density history for regions in the tail which originated outside the first caustic. This graph shows a typical density history of a region located about one-third of the way between the base to the tip of the tail. The large density increase which occurs at about t=1.5 coincides with the twist passing this point in the tidal tail

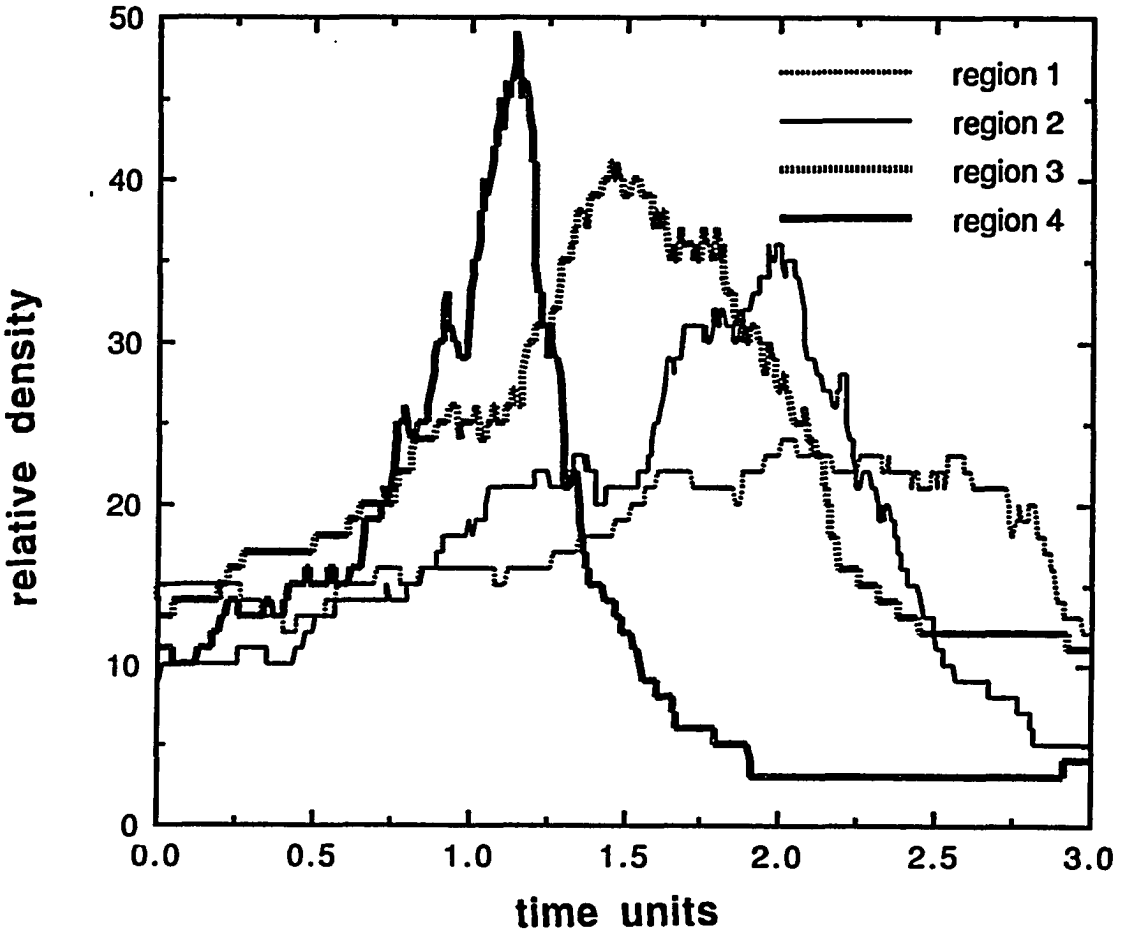

Figure 3. A typical density history for regions at different points along the tidal tail. Region 4 is located the closest to the tail's base and region 1 is located the closest to the tail's tip in the data presented. Regions near the base of the tail experience a larger and earlier density increase than regions located near the tip of the tail

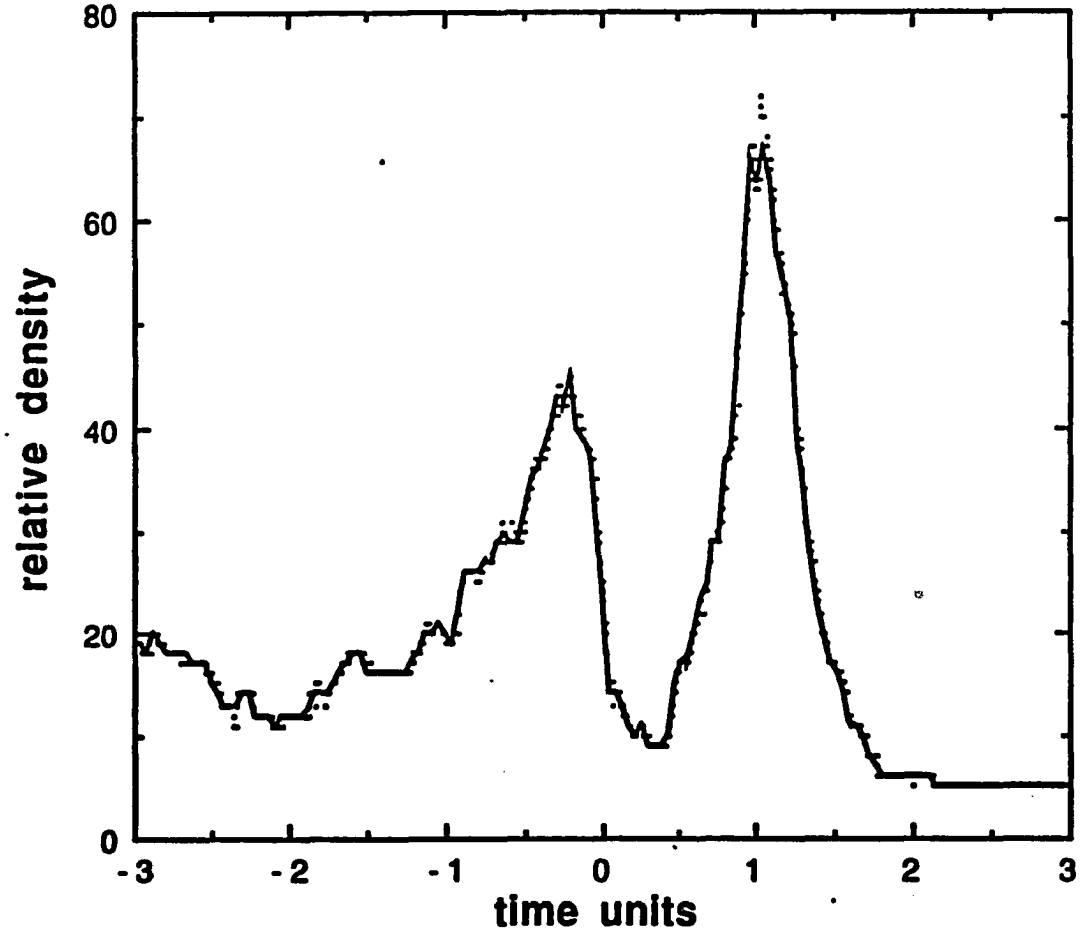

Figure 4. A typical density history for regions in the tidal tail which originated inside the first caustic. Particles that pass through the disk before becoming part of the tidal tail feel a density increase from the general compression of the disk in addition to the compression from the twist in the tail. The first peek corresponds to the disk compression while the second corresponds to the twist

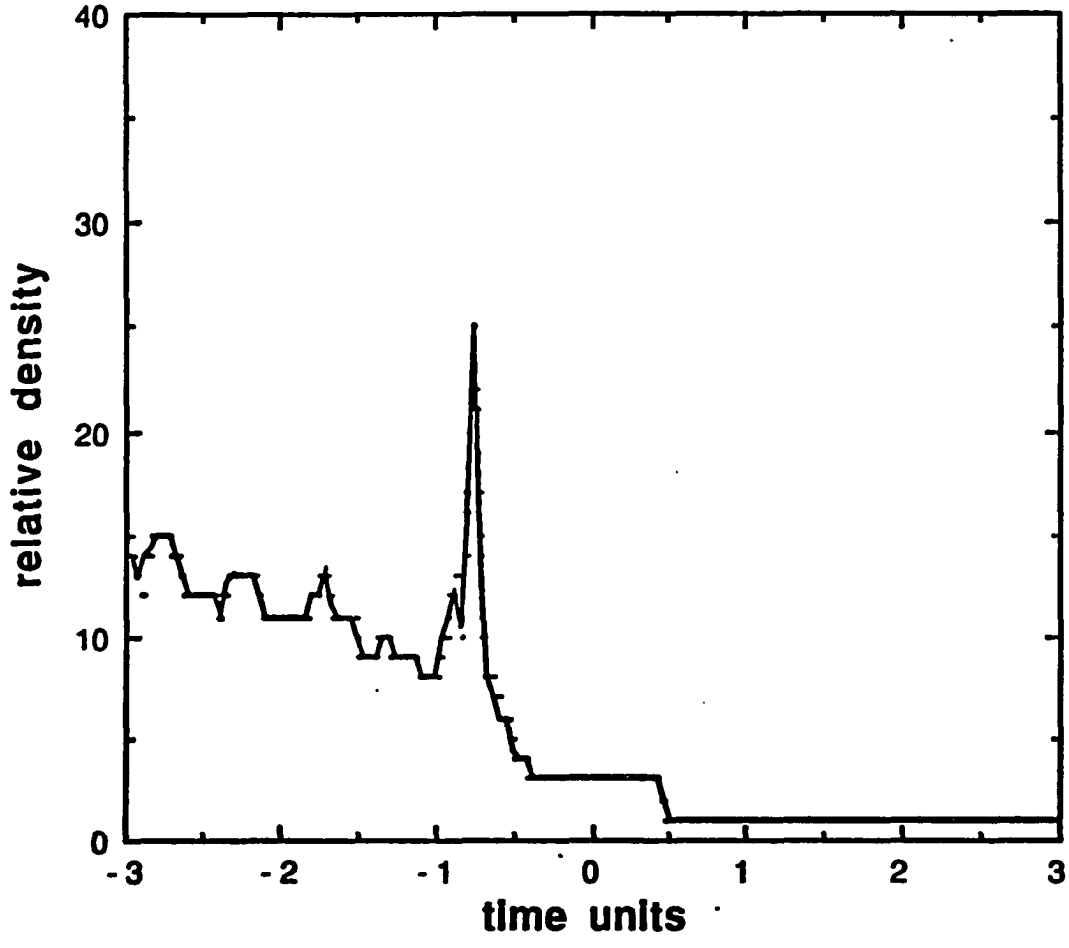

Figure 5. A typical density history for regions which become part of the tidal bridge. The density history for a region that joins the tidal bridge has a sharp increase at the time it encounters the bridge. The region's high velocity combined with its direction of motion cause it a sharply defined density increase during the encounter. If hydrodynamical forces were included, the gas in this region would likely be highly shocked

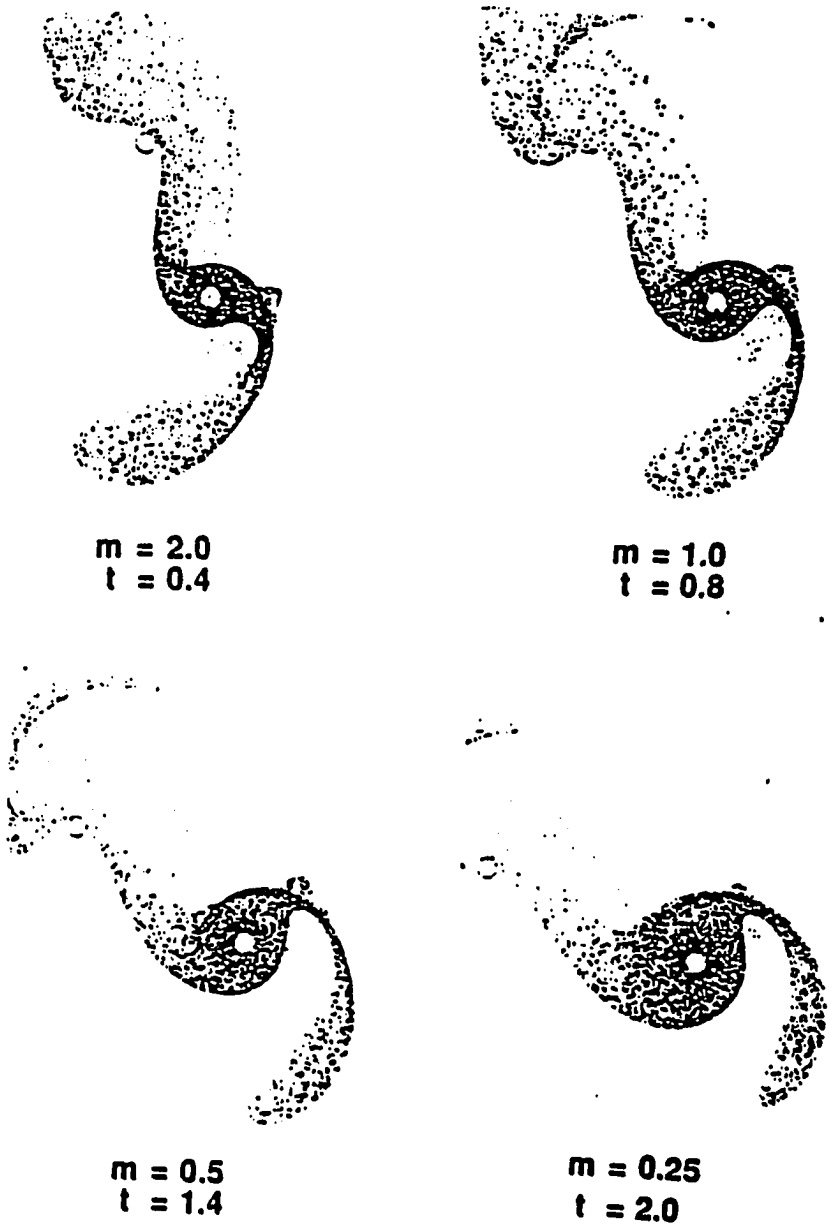

Figure 6. The morphological differences between runs of different masses at similar evolutionary stages. Four different mass companion galaxies were started with identical initial conditions. The frames were taken at the point when tidal tail begins to twist at the base. All the runs pass through similar morphological stages during the simulation

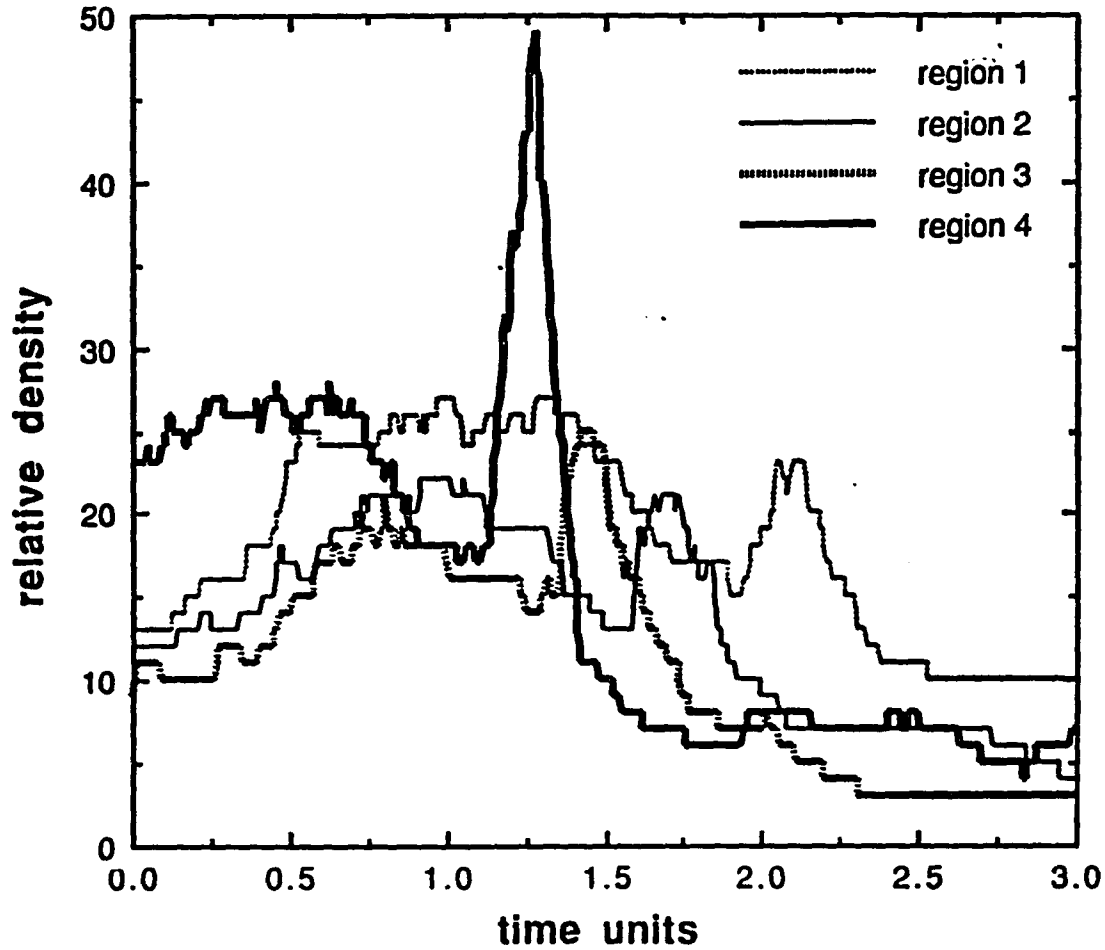

Figure 7. The development for particles along the tail in run E. The regions are in similar positions to those shown in Figure 4. Regions in the outer portion of the tail have no measurable density increase since the thickness of the disk and the tail increase with distance from the disk. It is likely the twisting of the tidal tails influences primarily the inner regions of tidal tail except in low inclination orbits

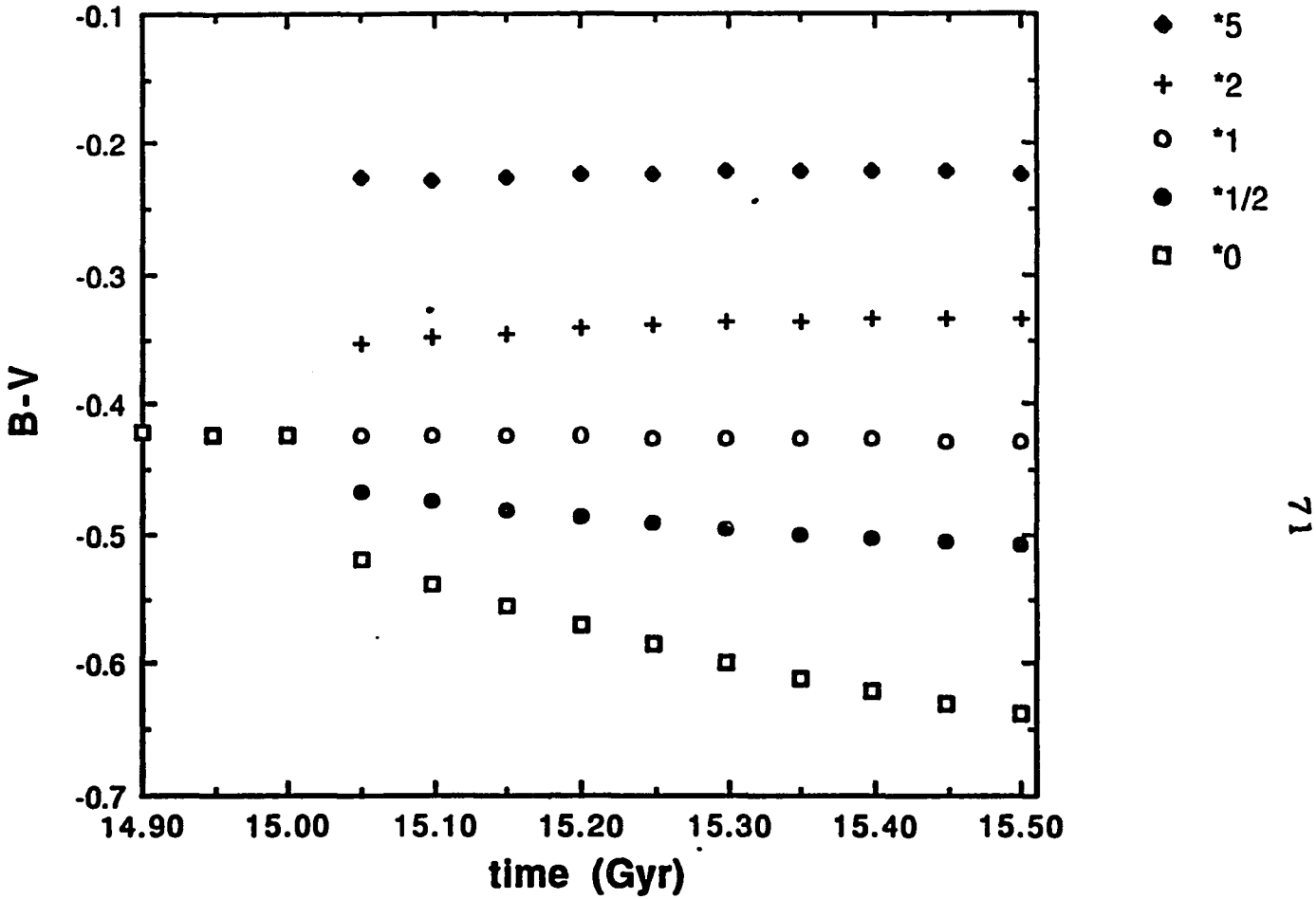

Figure 8. The B-V color changes resulting from the variations in the star formation rate. The star formation rate for the first 15 Gyr of the simulation exponentially decrease with an e-folding time of 8 Gyr. After 15 Gyr, the star formation rate is then multiplied by 5, 2, 1, 1/2, or 0. The B-V colors between 14.9 Gyr and 15.5 Gyr are displayed

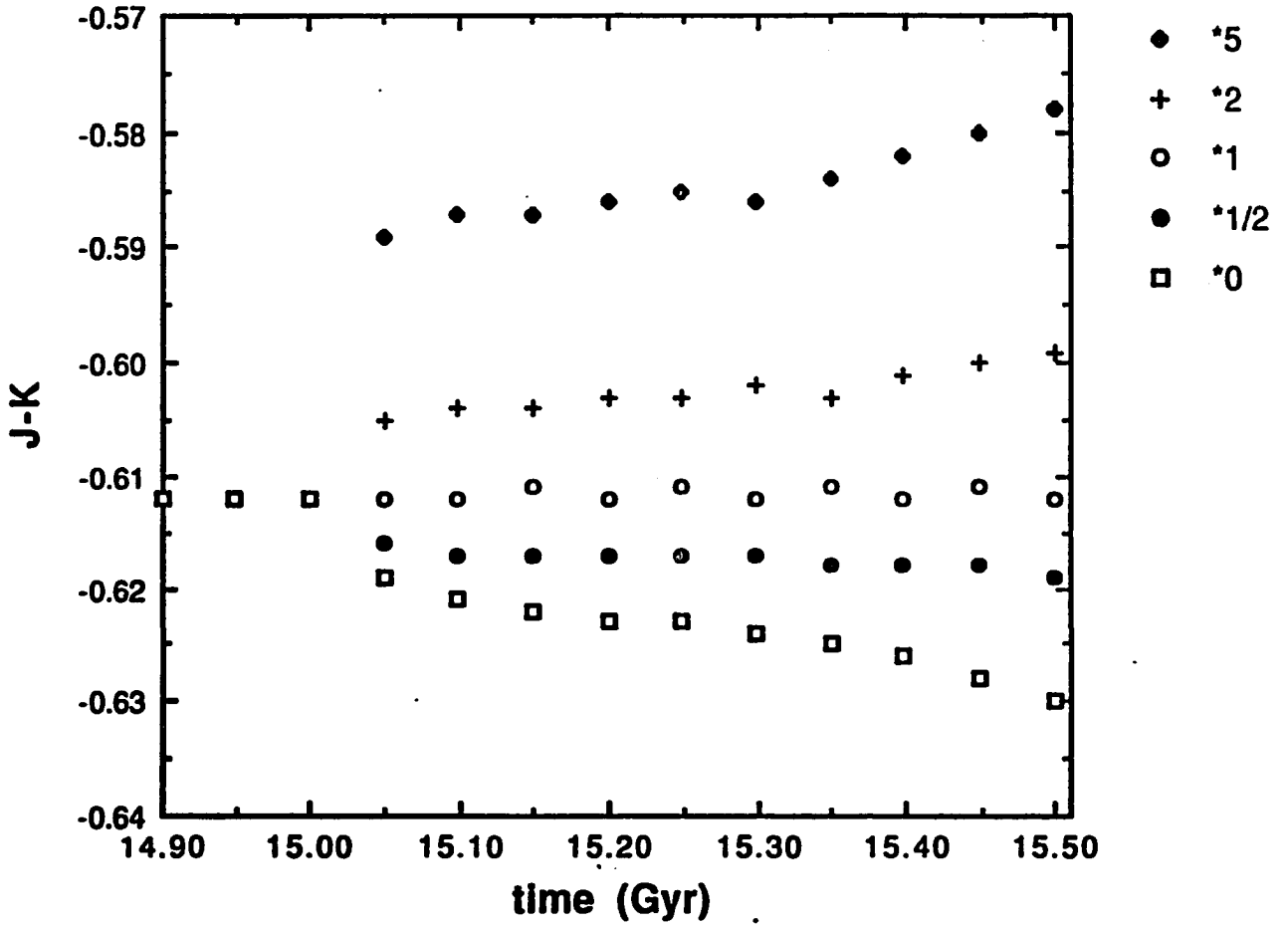

Figure 9. The J-K color changes resulting from the variations in the star formation rate. The star formation rate for the first 15 Gyr of the simulation exponentially decrease with an e-folding time of 8 Gyr. After 15 Gyr, the star formation rate is then multipied by 5, 2, 1, 1/2, or 0. The J-K colors between 14.9 Gyr and 15.5 Gyr are displayed. Little change is seen in the J-K colors for any of the changes in the star formation rate tested

Figure 10. The change in the V magnitude caused by the changes in the star formation rate. The star formation rate for the first 15 Gyr of the simulation exponentially decrease with an e-folding time of 8 Gyr. After 15 Gyr, the star formation rate is then multipied by 5, 2, 1, 1/2, or 0. The V magnitude between 14.9 Gyr and 15.5 Gyr is displayed. The brightness of the population continues to increase for at least the first 500 Myr increases in the star formation rate occur. The brightness also continues to decrease for the first 500 Myr after the star formation rate is decreased

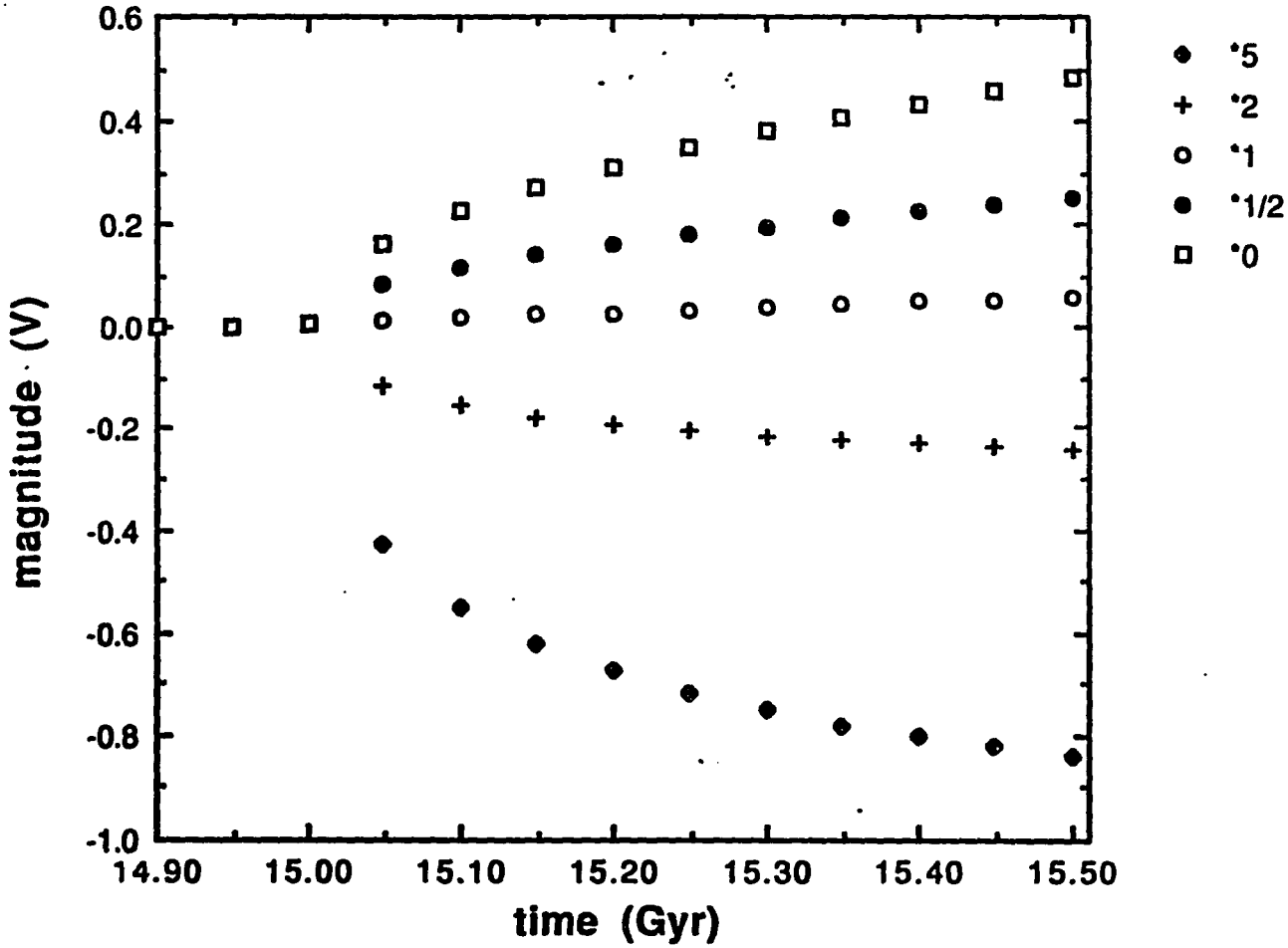
0.6
0.4
0.2
0.0
-0.2
-0.4
-0.6
-0.8
-1.0
magnitude (V)
14.90
15.00
15.10
15.20
15.30
15.40
15.50
time (Gyr)
*5
*2
*1
*1/2
*0

Table 1. A description of the dynamical model parameters used in this study

Model	Inclination	Mass	Impact Parameter
A	0.0	1.00	1.6
B	0.0	0.50	1.6
C	0.0	0.25	1.6
D	0.0	2.00	1.6
E	30.	1.00	1.6
F	60	1.00	1.6
G	90	1.00	1.6
H	0.0	1.00	2.0
I	0.0	1.00	2.5

Table 2 Sources of stellar evolutionary tracks in the photometric evolutionary code

stellar tracks	Z	reference
0.1 - 0.75 M_0 (main sequence)	0.02	VandenBerg, Hartwick, Dawson, and Alexander, 1983
0.7 - 3.0 M_0 (main sequence)	0.0169	VandenBerg, 1985
1.0 - 3.0 M_0 (AGB)	0.02	Lattanzio, 1986
1.0 - 3.0 M_0 (Clump giants)	0.01	Seidel, Demarque, and Weinberg, 1987
3.0 - 11.0 M_0 (main sequence-AGB)	0.02	Becker, 1981
20 .0 - 60.0 M_0	0.03	de Loore, de Greve, Vanbeveren, 1978

Table 3. The colors of the stellar population 50 Myr after the star formation rate is changed

Model[a]	U-B[b]	B-V[c]	V-R[d]	V[e]	F[f]
x5	-0.48	0.22	0.40	-0.44	0.48%
x2	-0.29	0.35	0.47	-0.12	0.19%
x1[g]	-0.15	0.42	0.50	0.00	0.10%
x1/2	-0.05	0.48	0.53	0.07	0.05%
x0[h]	0.09	0.52	0.55	0.15	0.00%

[a]The model name is designated by the change in the star formation rate which occurs at t=15 Gyr.

[b]The U-B color which occurs 50 Myr after the change in the star formation rate,

[c]The B-V color which occurs 50 Myr after the change in the star formation rate.

[d]The V-R color which occurs 50 Myr after the change in the star formation rate.

[e]The change in the visual magnitude which occurs after the change in the star formation rate.

[f]The fraction of stars of the total population formed between 15and 15.05 Gyr for each model.

[g]The star formation rate remains essentially unchanged from the previous time-step.

[h]The star formation cuts off at a time of 15 Gyr,

A COLLISIONAL MODEL FOR THE FORMATION OF RIPPLES IN GAS-POOR DISK GALAXIES

ABSTRACT

The Lynds and Toomre (1976) interpretation of ring galaxies as the natural result of a nearly head-on collision between a disk galaxy and a companion galaxy has become widely accepted. Similarly, Quinn's (1984) interpretation of the shells in elliptical galaxies as the aftermath of the cannibalization of a low-mass companion has been quite successful in accounting for the observations. In this paper we use restricted three-body calculations of high inclination, low impact parameter encounters to argue that the shell-like ripples observed in a number of disk galaxies (c.f. Schweizer and Seitzer 1988) are also collisional artifacts. Specifically, we propose that some of the ripples may be the result of internal oscillations following such an encounter much as in ring galaxies. However, in this case we assume that the target is an early-type disk with a sufficiently low gas fraction that recent star formation does not dominate the appearance of the disturbed disk.

The recent multicolor surface photometry of Schombert and Wallin (1987) indicates that Arp 227 may be an example of this ripple formation process. The appearance of Arp 178 matches the models even more remarkably. A number of the Malin and Carter (1983) shells in disk systems might also be explained by these models. We emphasize that, if correctly interpreted by our models, such systems are in a transient stage of an evolutionary sequence, whose outcome is most probably merger along the lines suggested by the models of Hernquist and Quinn (1987b, 1988).

I. INTRODUCTION

The existence of low surface brightness arcs or "shells" around early-type galaxies has been known for at least 20 years (Arp 1966). In a study of southern shell galaxies (Malin and Carter 1983), it was found that 16% of the isolated southern elliptical galaxies in the Second Reference Catalogue of Bright Galaxies (de Vaucoulers et al. 1976) have visible shells. Thus it can be seen that shell galaxies make up a large subclass of early-type galaxies. Using the data from the Malin and Carter catalog (1983) and the color information available, a number of models have been proposed for the formation of these systems.

One type of model investigated by Fabian et al. (1980) suggests that shells might have been formed in an intergalactic wind interacting with the intergalactic medium. In this model, stars are formed in shells made in the regions of shocked galactic wind material. The colors of the stars would need to be very blue in this case since the stability of the shells would be less than one free fall time. A variation of the galactic winds scenario has been investigated by Kundt and Krause (1985). They propose that active galactic nuclei create a wind which forms gas rich filamentary shells. Stars are formed in these gas shells. Once again, the shells would have to be very blue because of the short dissipation time of the shells.

Another class of models was first proposed by Schweizer (1980) and investigated by Quinn (1984) and Hernquist and Quinn (1986,

1987a, 1987b, 1988) . In these models, a small mass, dynamically cold galaxy encounters a massive elliptical. The elliptical tidally rips apart the disk galaxy and leaves the debris in shell-like structures, destroying the galaxy in the process. The colors of these systems should be approximately the color of the disk galaxy which formed the shells. It should be noted that investigations by Hernquist and Quinn (1988) indicate that spheroidal galaxies can merge with high mass galaxies and form shells also, but the sharpness of the shells is directly related how dynamically cold the merging disk galaxy is.

In a recent paper by Schweizer and Seitzer (1988), a model for ripple formation in galaxies is proposed which uses mass transfer from an interacting companion to form the features. Numerical models of this type have been investigated by Hernquist and Quinn (1988). Since the companion must be a dynamically cold system for mass transfer to form coherent structures, the companion must be a disk system. If the parent galaxy is an elliptical, a color difference should be visible between the body of the parent galaxy and the shells since the star formation took place much later in its evolution. Even if the parent galaxy is an S0, a color difference between the parent galaxy and shells should be detectable unless the merging galaxy is also an S0 or significant changes in the shell colors have taken place due to photometric evolution.

In order to distinguish different dynamical models for the formation of shells, multicolor CCD observations have been

conducted for some of the shell systems. Most of the color studies which have been published (Fort et al. 1986, Pence 1986) indicate the shells of a selected sample of galaxies are composed of bluer material than the parent galaxy. The statistics of this sample are extremely incomplete since currently multicolor observations of the shell-like features are available for only about 5 galaxies. The merger hypothesis seems to get the strongest support from the color observations of Carter et al. (1982) and Forte et al. (1986). The shells had B-V colors of approximately 0.7 which corresponds to the colors of a typical late-type spiral. The colors of the main galaxies have been fairly consistent with those of ellipticals indicating that two types of stellar populations are present.

Recent multicolor CCD observations of Arp 227 (Schombert and Wallin 1987) indicate not all "shells" are composed of a population of stars bluer than the parent galaxy. The differences between Arp 227 and previously studied shell galaxies (cf. Malin and Carter 1983) are:

1. The colors of the "shells" of Arp 227 observed by Schombert and Wallin (B-V= 0.90, V-r = 0.17), are consistent with those of the parent galaxy (B-V=0.96, V-r = 0.20) , and apparently inconsistent with its tidally interacting companion NGC 470 (B-V = 0.75 overall, B-V = 0.68 in the outer regions, Longo and De Vaucouleurs 1983). These data provide some observational evidence that the shell or ripples could have come from the parent galaxy.

2. The brightness profiles of the parent galaxy in Arp 227 indicate it is an S0, not an elliptical. Intensity profiles indicate the presence of an exponential disk in addition to a large bulge. Although a number of cases of shells around early-type disk systems have been found (Malin and Carter 1983, Schweizer and Seitzer 1988), previous multi-color photmetric observations of shell galaxies have been systems with ellipticals surrounded by luminous shells. Because of the more ordered nature of an S0 disk compared to an elliptical, tidal features could be produced which remain coherent for several orbital times. Since the parent galaxy is an S0, the features could be tidal or collisional in nature rather than from a merger.

3. Arp 227 has a tidally distorted companion. About half of the shell galaxies in the Malin and Carter catalog are isolated systems. Out of 137 shell galaxies in the Malin and Carter catalog, 65 are isolated systems, 24 are in loose groups with no close companions, and 48 are in groups with at least one close companion.

4. Some of the "shells" have more symmetric radial brightness profiles than those predicted in merger simulations. Simulations by Hernquist and Quinn (1987b, 1988) have show that the shells have sharp cutoffs on the outer edge. Two of the four shells observed in Arp 227 show a symmetric distribution.

There is evidence which suggests that a number of other galaxies have all or some of the characteristics found in Arp 227. Recent observations by Schweizer and Seitzer (1988) list five more S0 galaxies with "ripples" and suggest that approximately 30% of the galaxies in the Malin and Carter catalog (1983) are not ellipticals, but are actually S0's. This would suggest that about 6% of S0's have ripples. Unfortunately, the colors and brightness profiles of these features are not yet available. In the Malin and Carter catalog (1983), several galaxies, including NGC 1097A, are noted as tidally interacting with their companion. Even though the colors are not available for all these systems, the presence of a tidally interacting companion suggests that the shell-like features surrounding galaxies might result from a tidal or collisional encounter as well as from a merger or galactic wind.

Motivated, in part, by the new observational data available on Arp 227 and the similar morphology of other systems (e.g., Arp 178, Arp 229, and NGC 4382), a new model for the creation of shell-type galaxies is proposed here. In this scenerio, a companion to an S0 travels near the center of the disk in a near vertical passage causing internal oscillations and the formation of ripples in the outer regions of the galaxy. Section II details the numerical method used to investigate these models, Section III explains the effect various orbital parameters have on the formation of ripples, Section IV discusses the features seen in the simulation, and Section V discusses observational tests of the model.

II. NUMERICAL METHOD

In order to investigate this type of encounter, a restricted three-body approach was used to model the system. Similar investigations have been conducted for a wide variety of interacting systems including tails (Toomre and Toomre 1972), rings (Toomre 1978), and shells (Quinn 1984). In this approach, the parent galaxy and the perturbing galaxy are represented by softened point masses and the other particles in the simulation are assumed to have negligible mass. A fourth order Runge-Kutta was used to numerically integrate the equations of motion of the test particles and the companion galaxy. The restricted three-body method can be used to model shell-type galaxies since the region of interest is far from the main concentration of mass in the central regions and the disk self-gravity is unimportant compared to the strong perturbations studied in these simulations.

Despite its limitations, it is apparent that the validity of the restricted three-body approach will be best in the outer regions of the disk where the distance to the center of the system will be the greatest and the mass interior will be the largest.

In our simulations the test particles were initially distributed in uniform annular rings around the nucleus of the parent galaxy. Circular orbital velocities about the nucleus were calculated for the particles and a small random component added. The mass distribution for the parent galaxy and for the perturber were characterized by a softened point mass. The gravitational force and potential are then given by

$$F = \frac{GM}{R^2 + \varepsilon^2} \tag{1}$$

$$V = \left(\frac{GM}{\varepsilon}\right) \arctan\left(\frac{R}{\varepsilon}\right) \tag{2}$$

where ε is the softening length of the potential. The use of a softening length allows a realistic mass distribution to be modeled with a simple one parameter equation. A large softening length corresponds to a extended distribution of matter, while a small softening length characterizes a near point-like distribution. Because of the large bulges characteristically found in S0 galaxies, a softening length for the simulations was typically choosen to be about half the outer radius of the disk. The effects of varying the softening length of the galaxy are detailed in section III.

The units used in the simulation are dimensionless. A radius and mass of one were choosen for the outer radius and mass of the parent galaxy. A velocity of one then corresponds to the orbital velocity of one of the outer particles in the parent galaxy. From the velocity and distance units, a unit interval will correspond to time for an outer particle in the parent galaxy to travel approximately one radian in circular orbit. All times are measured from the time of closest approach of the perturber. For the case of Arp 227, a radius of one corresponds to a distance of about 15 kpc, a unit mass

to about 1 x10^{11} $M_{\odot}$, a unit velocity to about 170 km/s, and a time of one unit to approximately 8 x10^{7}yr.

The simulation is started at a time of -5 or approximately one orbital time of the outer particles before the interaction occurs or approximately 4x10^{8} years before the closest approach. The perturbing particle is described by a mass and softening length. The orbit of the perturber is described by four parameters: the inclination (i), the argument of perigee (w), the distance of closest approach (R_{min}), and the velocity of the perturber at closest approach (V_{min}). The velocity of the perturber is given in terms of the escape velocity of the particle at R_{min}. thus a velocity of one is purely parabolic. In all the simulations presented here, the point of minimum approach is in the plane of the disk, thus the argument of perigee is zero.

The effects of dynamical friction are not included in these simulations since we are interested in a relatively short time following the encounter rather than the longer term dynamical evolution. The effects of dynamical friction would be to increase the interaction time and the consequent disturbance. The added perturbation, however, can be roughly compensated for with a lower orbital velocity. If it were included, the system would almost certainly become a merger remnant eventually and would likely pass through a period of forming Quinn type shells before becoming an ellipical.

The effects of the encounter on the companions are not presented here since the large amplitude, highly position dependent disturbance in the companion is poorly represented by the restricted three-body approximation. In addition, Hernquist and Quinn (1987a) have investigated a wide variety of encounters between ellipticals and low mass companions. The results of their simulations are relevant to this work though some differences should be noted. First of all, the masses of the companions used by Hernquist and Quinn (1987a) was typically 0.02 times the mass of the parent galaxy, while the masses of the companions in the present simulations are typically between 0.1 to 0.2 times that of the parent galaxy. The orbits used by Hernquist and Quinn were initially bound. The orbits used in the present simulations are parabolic and follow the evolution for only about 3 orbital times for the outer particles. In addition, the softening lengths used by Hernquist and Quinn (1987a) were usually smaller than those used here.

Despite these differences, the parameters used in Figure 7 in Hernquist and Quinn (1988) come very close to those of the companion in our calculations at early times after the encounter. In this figure, a companion of 0.1 times the mass of the parent galaxy passes in a bound orbit 7 scale lengths from the center of the main galaxy, which in this case has a large softening length. The orientation of the disk is retrograde to the direction of the orbit.

According to the text, no mass transfer takes place, so no accretion shells are formed in the initial encounter.

III. NUMERICAL RESULTS

A. The Nature of the Ripples

A time sequence for one of the models is shown in Figure 1. In this sample run, the essential features common to all the simulations can be seen. The companion passes through the parent galaxy disk near its center on a nearly vertical trajectory. Radial oscillations are set up in the orbital trajectories of the disk particles which form coherent structures, which persist for several orbital times. The outer regions form ripples in the smooth distribution of the disk, thus shell-like features are created in the brightness profiles. It should be emphasised that the features are not three dimensional in nature. Since the orbital motion of the particles was initially in a plane, the perturbed orbits remain essentially in the same plane. Because of the planar nature of the shells, the ellipticity of the features will depend on the viewing angle. The features found in these simulations are actually density waves in the outer structure of the galaxy's disk rather than three dimensional shells.

Similarities between Arp 178 (Arp 1966) and the frame at time 6 can be seen. The tail-like feature of Arp 178 would be associated with the plume structure visible in this figure. The companion of Arp 178 is a ring galaxy, which has likely passed close to the center of the main galaxy in the system. The later images visible in this time sequence are similar to the ripples seen in Arp 227. The

distortions which develop early in the model disk have wrapped around the galaxy several times, forming the ripple-like features.

These simulations are very similar to those used by Lynds and Toomre (1976) and Toomre (1978) in the formation of ring galaxies. The same types of trajectories were used in Toomre's work with a larger perturber mass and a smaller softening length. The present simulations also follow the evolution of the system for a longer time and have a much higher resolution (i. e., a greater number of test particles) than those published by Toomre. Despite the differences, this model has more in common with the dynamical models typically used for the formation of ring galaxies than previous simulations of shell galaxies by Quinn (1984).

Previous work in the simulation of ring galaxies has emphasized the high star formation rate caused by the shocked gas (Struck-Marcell and Appleton 1987). An encounter with an S0 might not exhibit this same behavior due to the lack of available gas for star formation. Given this lack of gas for star formation, the colors of the ripples should be the same as those of the parent galaxy.

B. Parameter Dependences

The effects on the ripple formation of varying several of the parameters are discussed in this section. In each case, one parameter was varied while the others were held constant. Identical initial conditions for the state of the disk were used. All images were taken at a time of 15 units after the closest approach and are viewed from directly above the disk of the parent galaxy.

1. Companion's Mass

The effects of increasing the companion's mass are shown in Figure 2. The inclination, softening lengths, and impact parameters were held constant as the mass of the companion was varied from 0.05 to 0.80 times the mass of the parent galaxy. At the low end of the mass range, only a slight enlargement of the outer radius of the galaxy is seen. A small tail-like feature is seen extending from the galaxy forming a single shell-like structure along with a number of inner rings. When the mass is between 0.2 to 0.4 times the mass of the parent galaxy, a number of large shell-like features extend from the galaxy. The inner portion of the galaxy remains intact and the outer portion forms ripples. As the mass is increased to 0.8 times the mass of the main galaxy, a large percentage of the particles are captured by the companion and escape the system. A thick tail can be seen extending from the parent galaxy to the upper right corner of the frame toward the companion. In the higher mass simulations, apparent radial features can be seen in the particle distribution. Similar radial features can be seen in the isophotes of Arp 227 (cf. Schweizer and Seitzer 1988).

2. Orbital Inclination

Figure 3 shows the effect of inclination on the disturbed morphology. The inclination was varied from 60 to 120 degrees in 10 degree increments while keeping all other parameters constant. From the figures, it can be seen the exact angle of approach has

little effect on the formation of the shell-like features, at least for impact parameters much less than the softening length.

3. Softening Lengths

The effect of changing softening lengths is shown in Figure 4. Changing the softening length modifies the strength of the potential at short distances for the parent galaxy. For small softening lengths (0.1- 0.3), the particles stay tightly bound to the parent galaxy. As the softening length for the parent galaxy increases, the perturbed particle trajectories experience greater radial excursions. A larger softening length characterizes a more extended distribution of matter causing the potential well to be more flattened and a particle to be less tightly bound than if all the mass was concentrated interior to it. Another noticeable feature in the figure is how the softening length affects the sharpness of the ripples. As the softening length increases and the distribution of particles spreads out over a larger distance, the ripples are smoothed. Because of these effects, a system with an extended bulge would be expected to have smoother features than a one with a small bulge.

4. Impact Parameter

The effects on the system of different impact parameters is illustrated in Figure 5. At low impact parameters, the orbits of all particles are perturbed with approximately the same impulse. This helps the structures formed from encounters of low impact parameters to stay coherent for several orbital times. The structures formed with high impact parameter encounters result in

the particles receiving different perturbations at different azimuths in the disk. This causes the structures which form to dissipate more quickly than those formed in low impact parameter collisions and more complicated wrapping of the particles to occur. In Figure 5, an increasingly complicated pattern can be seen in the outer particles resulting from this effect.

C. Summary

A number of generic features can be seen in the simulations. Ripples in the outer regions of the galaxy form in all of the simulations shown, but are most prominent when the companion mass is in the range 0.1 - 0.5 times the parent galaxy mass. Only the sharpness and their detailed structure is dependent on the encounter parameters. Some of the figures (cf. Figure 5e) have extremely narrow features visible in the shells which are caused by crossing of orbital trajectories. The apparent twisting of the ripples is the result of these orbital crossings. This twisting appears to be a common occurrence in these simulations and recalls the simulations of tail galaxies (Toomre and Toomre 1972, Eneev et al. 1973). Observationally, this apparent twisting will be observed as regions of significately brightened regions in the ripples. In some areas of low surface brightness, the broader features will not be visible and only these higher density areas will be seen.

IV. INTERPRETATION

In the Lynds and Toomre (1976) model galaxy rings are orbit-crossing zones that result from the differential frequencies of the epicyclic oscillations induced by a head-on collision. The outer ring edge is defined by orbit crossings between infalling stars and stars moving out to apoapse. The inner edge is defined by crossings between stars at periapse and trajectories passing out of the ring. The density profile across the ring will appear flat, or double-peaked at the edges, depending on the width of the ring (which depends on the perturbation amplitude) and on the resolution (See Figure 5 of Toomre 1978 and also Struck-Marcell 1988). On the other hand, in the elliptical shell galaxies this orbit-crossing zone encompasses the whole region between the outermost shells, including the elliptical galaxy. The nature of the ripples in the models presented above is more like the rings, but with less symmetry than in classical ring galaxies.

As the models above produce the rings in their central regions, a tidal tail is formed in the outer disk. In these calculations the companion's orbit is parabolic and the target disk and bulge (i.e., the region within a softening length of the center) are assumed to be comparable to or larger than the companion. Roughly speaking, the outer disk sees the encounter as predominantly a tidal interaction, while the inner region reacts more to the direct collision. The result is that collisional rings propagate out into a tidally distorted outer disk. The symmetry of the rings is broken.

The numerical calculations show that the consequences of this include: 1. the rings vary in strength and width as a function of azimuthal angle, 2. spiral wave segments are excited in the inner disk and connect successive rings (as in Toomre's calculations of off-center collisions), and 3. high-order rings eventually overlap. Another interesting point is that the first ring propagates through the whole disk while the tail is forming. This may, in fact, contribute to the tail formation by helping to 'lift' material outward. A phase plane diagram for one of the simulations is presented in Figure 6. The effects of the encounter on the radial structure can be seen. The ripples exhibit similar interleaving in radius to that found in the merger models of Quinn (1984). In the merger simulations by Quinn, the phase wrapping is caused by successive passes of the late-type spiral around the center of the parent elliptical and the motion is predominantly radial. In the present simulations, the phase loops are radial epicyclic motions, plus the radial and angular dependence of the collisional perturbation. This suggests that ripples form within a few orbital times of the particles in the outer regions of the parent disk, which may be significantly shorter than that needed for merger. Thus, it is expected that the ripples will develop and be dissipated over a shorter time scale than the shells formed by mergers.

V. OBSERVATIONAL PREDICTIONS

From the simulations, a number of observational conseqences can be predicted from the models. First of all, the systems which should be investigated are early-type spirals with ripples in their outer disks and a tidally interacting companion. Multicolor photometry should be able to determine if the shells are made of material of similar color to the parent galaxy or from a bluer early-type spiral. Colors can provide a important test of whether the material came from tidal distortion or mass transfer. In these models, the parent galaxy must have a definite disk in order to form these coherent collisional features, thus shell elliptical galaxies are not part of this class. It is therefore important to measure the intensity profiles of the parent galaxies of "shell" galaxies to determine if they are ellipticals or S0.

Testing the hypothesis in systems of two late-type spirals with ripples in their outer regions (i.e. ancient ring galaxies) would be difficult, since the colors of the outer regions will be the same whether there was a merger or a tidal interaction. One possible confirmation of this hypothesis would be the detection of low surface brightness areas between the ripples and the parent galaxy. The models predict the shells are connected with the parent galaxy through low luminosity regions. These areas might be found with deep exposures of CCD's in some of the systems. Deep CCD images might also be able to detect any connections between the companion and the parent galaxies. The detection of possible

optical or neutral hydrogen bridges between the companion and parent galaxy would give additional information to distinguish between collisional or tidal interactions and mass transfer by providing information about the companion's orbit.

Another quantity which can be used to test the relevance of the models is the ellipticity of the ripples. Projection effects will cause the ripples to be elongated with the same ellipticity as the outer regions of the disk. Since the ripples predicted for this model are planar, the resulting projection effects should be easily visible. Because S0 disks are thick, the viewing angle is expected to be constrained since the features must not be hidden by the vertical distribution of the disk.

Another test for this hypothesis is in the intensity profiles of ripples to our models. In our models, the intensity of the ripples is distributed approximately symmetrically about the center line of the ripple, while the merger models predict a sharper cutoff of intensity at the outer region. Thus, brightness profiles would be very useful for distinguishing between the merger and disruption hypotheses and the tidal hypothesis.

Investigations of the tidally interacting companions provide another test of the model. The relative radial velocities will be small since a great deal of energy will probably be dissipated by dynamical friction in the encounter. Deep images of the regions around the companion might show how the outer-most regions of the companion galaxy were affected by the encounter. It is possible

that a tidal bridge might show where the companion galaxy has traveled indicating if it has made a close approach with the center of the parent galaxy. Radio observation of the HI gas distribution might provide crucial information about the dynamics of these systems. The distribution and radial velocities of gas in the companion and the parent galaxy would give important clues about the past history of the system. Observational data and modeling of ring galaxies also provides a link to these systems.

It is important to note one test that cannot be used to distinguish between collisionally induced rings and mass transfer. Schweizer and Seitzer (1988) suggest the interleaving in radius and the direction of wrapping of the shells indicate that the ripples in their sample were produced by mergers or mass transfer, however both of these features are present in the simulations presented here. The interleaving of the shells is visible in Figure 1 and shown in the phase plane diagram in Figure 6. As discussed before, the ripples can exhibit the phase wrapping similar to that in the simulations of Quinn (1984). This phase wrapping characterizes the interleaving in radius.

VI. CONCLUSIONS

From the simulations presented above, it has been shown that ripples occur in disk galaxies for a wide variety of initial condtions. The similarities of this new class of "shells" to ring galaxies is obvious, however, there are a few important distinctions to note.

For example, the current simulation would have virtually no star formation in the parent galaxy due to the encounter. For a galaxy like Arp 227, a low gas mass would make a low rate of star formation occur throughout the galaxy. Since the ripples occur most notably in the outer regions of the galaxy where the density is low, it is possible to have ripples in the outer part of a galaxy which has a greatly enhanced star formation rate in its inner regions. Arp 178, an IRAS source, may be an example. Moreover, the orbital parameters of the perturbing galaxy can vary over a wider range of inclinations and impact parameters than the models for ring galaxies. (cf. Toomre 1978), since the ripples need not be cylindrically symmetric.

A number of observational tests of the hypothesis have been proposed for these systems which should provide a way of distinguishing between the merger models and the tidal models. Further observations of the ellipticity, intensity profiles of the shells and the parent galaxy, multicolor surface brightness maps, along with deep CCD images all provide ways of testing the tidal model on other systems.

However, the most important clues that tidal interactions is responsible for ripple formation may simply be the presence of a disturbed companion and a tidal tail. In the absence of such direct clues, the situation is ambiguous. After all, oscillation ripples and mass transfer are probably just two facets of a merger process. The tidal-collisional model presented here is an early transient stage of the process. The work of Hernquist and Quinn has shown that shells will persist long after the disruption of a small companion. The ripples that result from the merger of a more substantial companion may be a mixture of those produced by internal epicyclic oscillations and those resulting from accretion. Further N-body calculations might allow one to sort the galaxies with ripples and shells into an evolutionary sequence.

VII. REFERENCES

Arp, H. C. (1966). *Atlas of Peculiar Galaxies* (Pasadena : California Institute of Technology).

Carter, D., Allen, D. A., and Malin, D. F. (1982). Nature **295**, 126.

de Vaucoulers, G., de Vaucoulers, A., and Corwind, H. G. (1976). *Second Reference Catalogue of Bright Galaxies* (Austin : University of Texas Press).

Eneev, T. M., Kozlov, N. N., Sunyaev, R. A. (1973). Astron. Astrophys. **22**, 41.

Fabian, A. C., Nulsen, P .E. J., and Stewart, G. C. (1980). Nature **287**, 613.

Fort, B. P., Prieur, J.-L., Carter, D., Meatheringham, S. J., and Vigroux, L. (1986). Ap. J. **306**, 110.

Hernquist, L., and Quinn, P. (1986). Preprint. (Princeton : Institute for Advanced Studies).

Hernquist, L., and Quinn, P. (1987a). Ap. J. **312**, 1.

Hernquist, L., and Quinn, P. (1987b). Preprint. (Princeton : Institute for Advanced Studies).

Hernquist, L., and Quinn, P. (1988). Ap. J. **331**, 682.

Kundt, W. and Krause, M. (1985). Astron. Astrophys. **142**, 150.

Longo, G., and de Vaucouleurs, A. (1983). Univ. Tex. Monogr. Astron. No. 3.

Lynds, R., and Toomre, A. (1976) Ap. J. **209**, 382.

Malin, D. F., and Carter, D. (1980). Nature, **285**, 643.

Malin, D. F., and Carter, D. (1983). Ap. J. **274**, 534.

Pence, W. D. (1986). Ap. J. **310**, 597.

Quinn, P. (1984). Ap. J. **274**, 596.

Schombert, J. M. and Wallin, J. F. (1987). A. J. **94**, 300.

Schweizer, F. (1980) Ap. J. **237**, 303.

Schweizer, F., and Seitzer, P. (1988). Ap. J. **328**, 88.

Struck-Marcell, C. (1989) "Two-Dimensional Caustics in Disturbed Galactic Disks", submitted to Ap. J.

Struck-Marcell, C. and Appleton, P. N. (1987) Ap. J. **323**, 480.

Toomre, A. (1978). *The Large Scale Structure of the Universe, IAU Symp. 79*, eds. Longair, M.S. and Einasto, J. (Dordrect : D. Reidel), p. 109.

Toomre, A., and Toomre, J. (1972). Ap. J. **178**, 623.

Figure 1. Time sequence of a model. The outer ripples develop from a tidally produced protrusion in the outer section of the disk which wraps around the parent galaxy. The companion has a mass of 20% of the parent galaxy and its orbital inclination is 88 degrees with a minimum distance of 0.2 from the center of the parent galaxy. The softening length for the companion is 0.2 and the parent galaxy has a softening length of 0.6

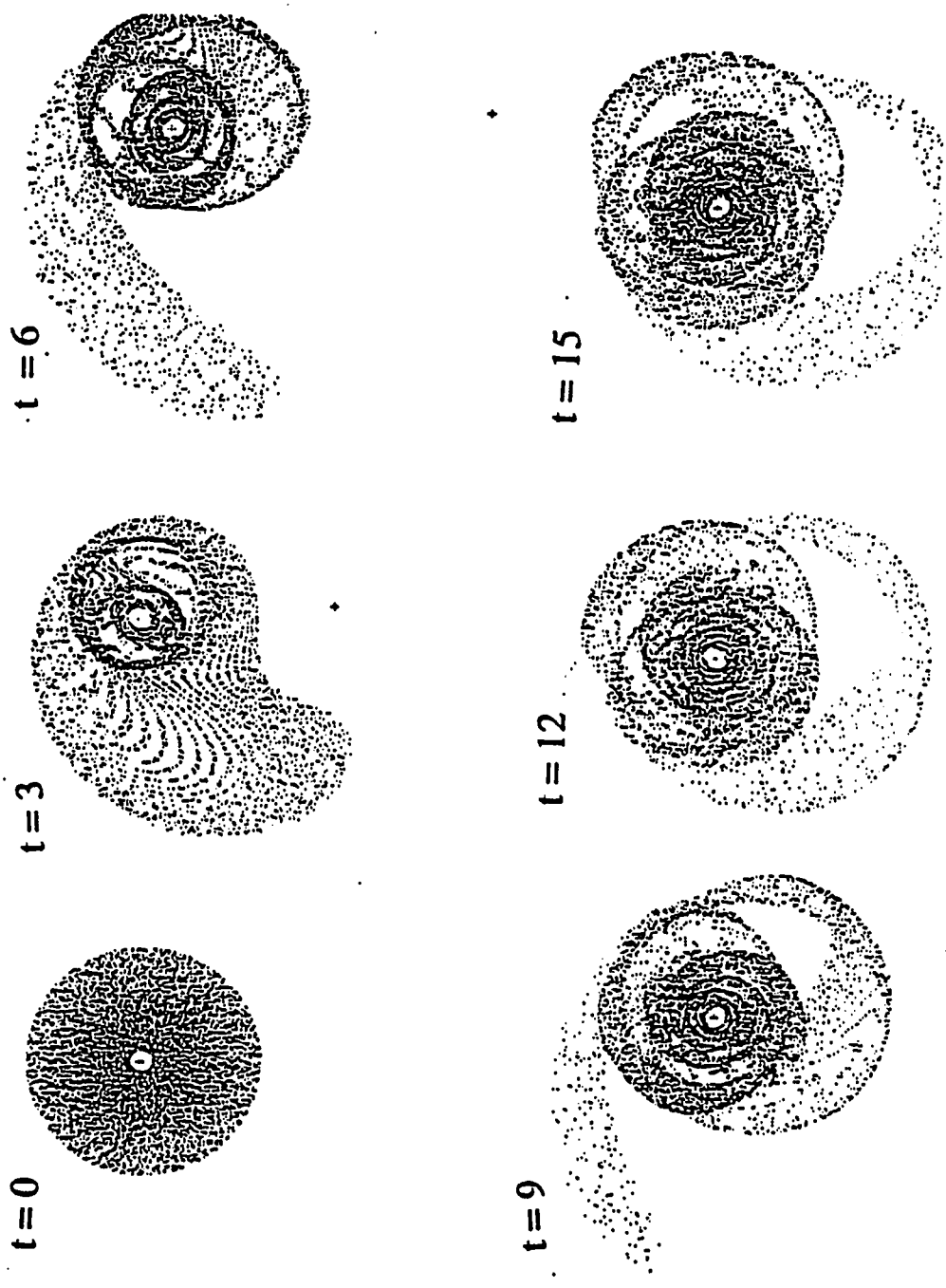
t = 0
t = 3
t = 6
t = 9
t = 12
t = 15

Figure 2. The effect of the companion's mass. As the mass increases, the outer regions of the disk are thrown further from the galaxy causing a more extended final state. Low mass encounters produce primarily a ringing of the galactic disk with little evidence of ripples in the outer disk. In the highter mass encounters, a great deal of mixing is produced in the inner regions with coherent ripple forming on the outer edges. The orbital inclination of the companion is 88 degrees and the companion passes at minimum distance of 0.1 from the center of the parent galaxy. The softening length for the companion is 0.2 and the parent galaxy has a softening length of 0.6. All plots are taken at a time of 15

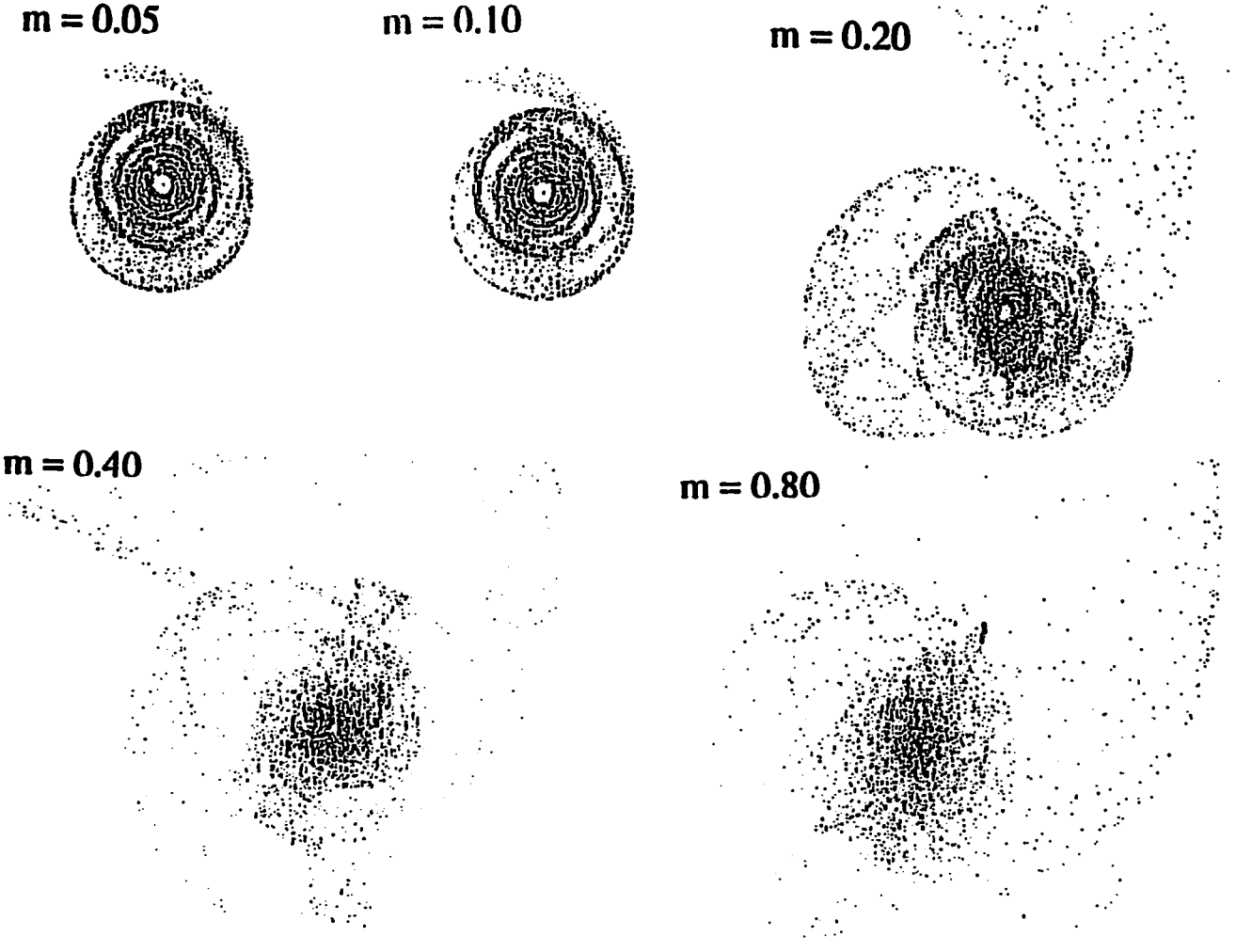
m = 0.05
m = 0.10
m = 0.20
m = 0.40
m = 0.80

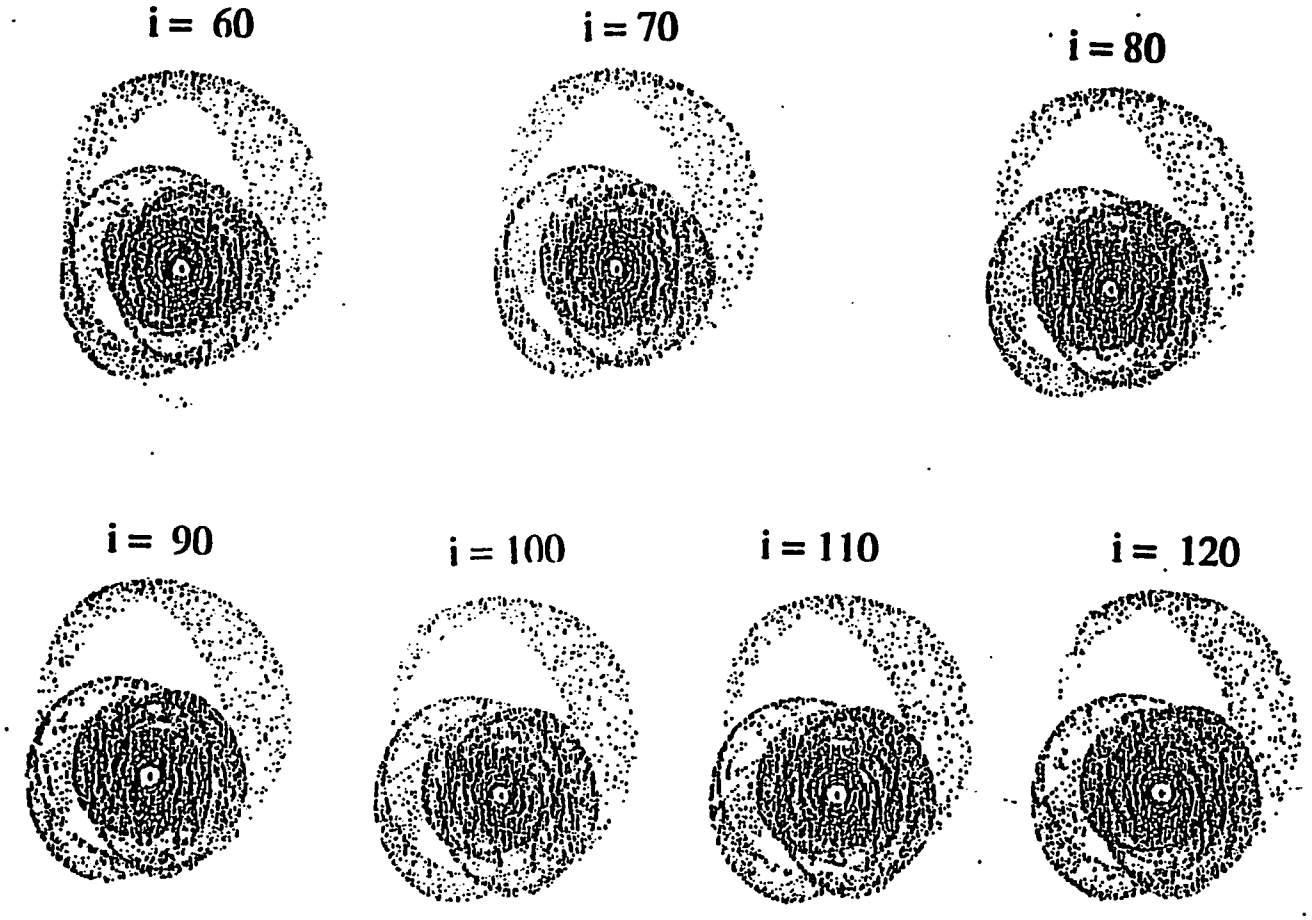

Figure 3. The effect of the companion's inclination. The inclination of the companion's orbit has little effect on the final state of the system. The mass of the companion is 0.1 and the distance of minimum approach is 0.2 from the center of the parent galaxy. The softening length of the companion is 0.2 and the parent galaxy has a softening length of 0.6. All plots are taken at a time of 15

Figure 4. The effect of the softening length of the parent galaxy. With small softening lengths for the parent galaxy, the ripples are sharply defined. With large softening lengths for the parent galaxy, the ripples are more diffuse and the distribution of the ripples is more extended. The companion has a mass of 0.1 and a softening length of 0.2. The orbit has an inclination of 88 degrees and passes at a distance of 0.1 from the center of the parent galaxy. All plots are taken at a time of 15

$\varepsilon = 0.2$

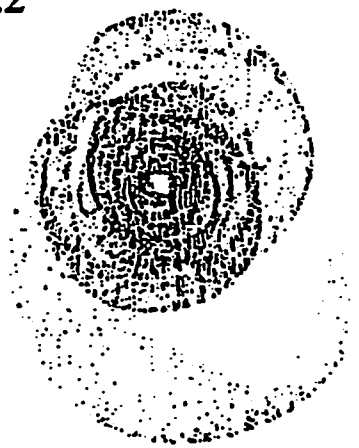

$\varepsilon = 0.4$

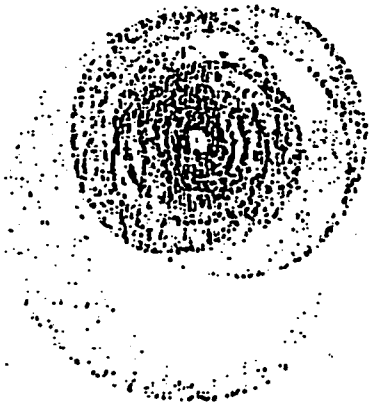

$\varepsilon = 0.6$

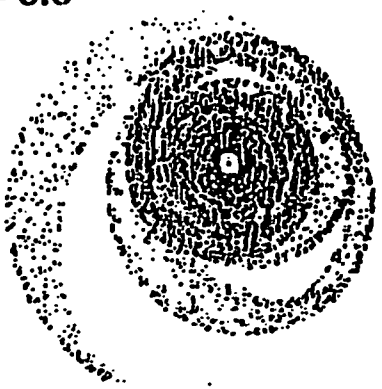

$\varepsilon = 0.8$

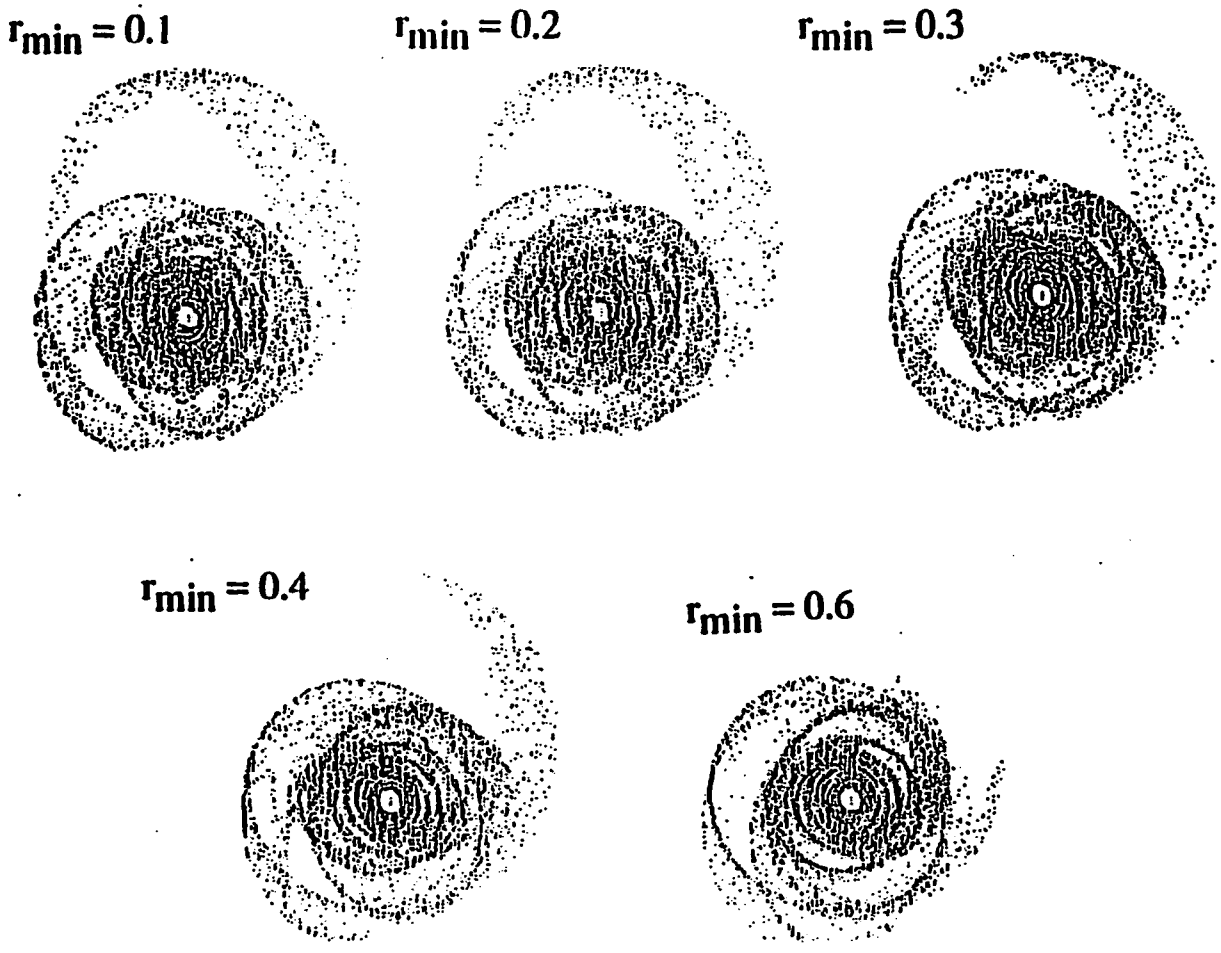

Figure 5. The effect of the impact parameter of the companion galaxy. As the impact parameter increases, the amount of wrapping seen in the outer ripples increases. The companion has a mass of 0.2 and a softening length of 0.2. The orbital inclination was 88 degrees and the softening length for the parent galaxy was 0.6. All plots are at a time of 15

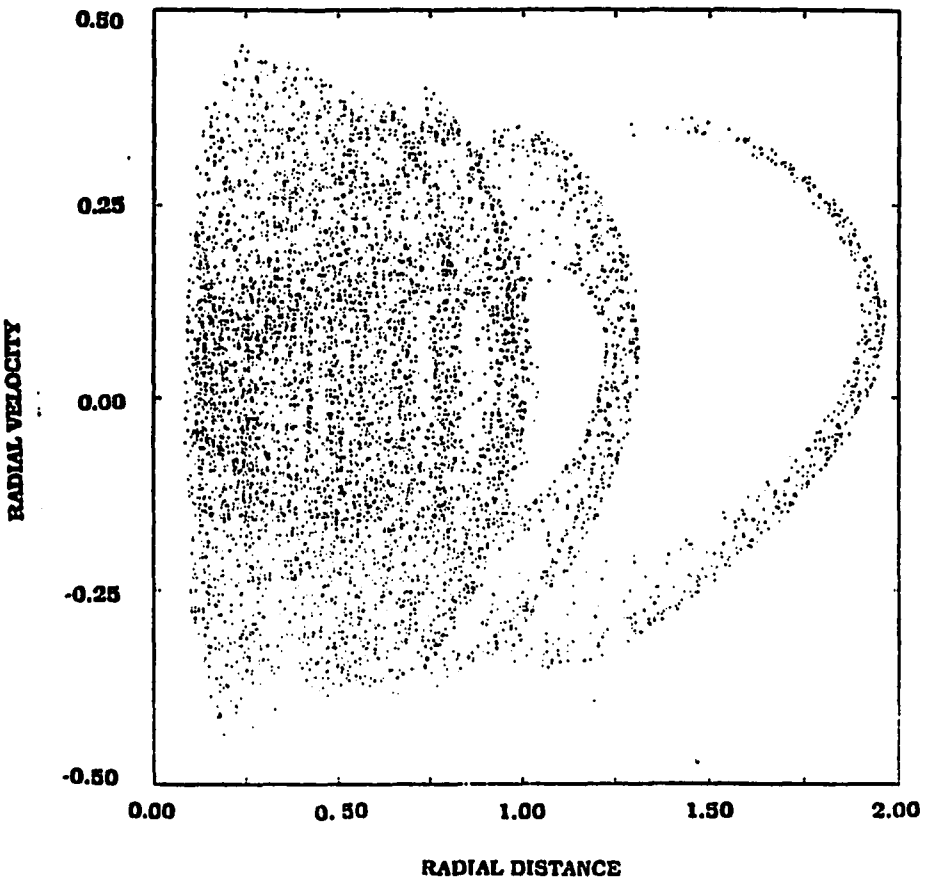

Figure 6. Phase plane diagram for the galaxy. The radial velocity from the center of the parent galaxy is plotted verses the radial distance from the center of the parent galaxy. The structure in this diagram shows the ripples are connected in phase space as well as in physical space. The companion has a mass of 0.2 and a softening length of 0.2. The companion's orbital inclination was 88 degrees and passed at a distance of 0.2 from the center of the parent galaxy. The softening length of the parent galaxy was 0.6. All plots are taken at a time of 15

SUMMARY AND CONCLUSIONS

I. STAR FORMATION IN TIDAL TAILS

From the simulations using a restricted three-body dynamical code and a broad-band photometric evolutionary code, some preliminary conclusions can be drawn about star formation in tidal features in interacting galaxies. The photometric models show that the colors of a stellar population depend strongly on the current star formation rate compared to the previous star formation history. If a population with a star formation history similar to a spiral galaxy has an increase in the star formation rate by a factor of five or more, detectable changes in the B-V color will be seen in less than 50 Myr. A suppression of the star formation rate by a factor of two will affect the B-V colors on a slightly longer time-scale. Using the Schmidt (1959) law, it is estimated that a change in the local density by a factor of two to five could produce detectable color changes.

Several mechanisms are proposed which would produce density enhancements in tidal tails and bridges. For tidal tails, a twisting motion occurs as the particles in the trailing edge of the tail overtake those in the leading edge of the tail. As this twist propagates from the base to the tip, a region of increased density moves along the tail at the point of the twist. From the dynamical models, it appears that this mechanism will occur only in low inclination encounters but for a wide variety of mass ratios and impact parameters for the companion galaxy.

A second mechanism which might affect the star formation history of tidal features is caused by the general compression of the disk during a tidal encounter and the formation of caustics on the outer edge of the disk. Some of the regions become part of the lower portions of the tidal tail after passing through the disk while it is being compressed. This compression might lead to a higher star formation rate about 100 Myr before it becomes part of the tidal feature. This mechanism will affect the density history in portions of both tidal tails and bridges.

A third mechanism is suggested by the trajectory crossings of particles stripped from the disk with the tidal bridge. From the particle trajectories in the simulations, it appears gas clouds would collide with the trailing edge of the tidal bridge. After the energy from the shock is radiated and the region cools, the density might be high enough to cause increased rates of star formation. This mechanism is difficult to examine in these simple dynamical models since the density is low and hydrodynamical forces are important.

II. FUTURE STUDIES OF STAR FORMATION IN TIDAL TAILS

To gain additional insight into the star formation mechanisms in tidal tails, it will be necessary to use a dynamical code which includes hydrodynamical forces. A softened particle hydrodynamics code would be well suited for such an investigation since they can easily deal with hydrodynamical and graviational forces.

By using a combination of hydrodynamical and photometric models, it should be possible to examine how the colors of spiral galaxies are affected by encounters which produce ring galaxy. One-dimensional and two-dimensional hydrodynamical models have been made of ring galaxies (Appleton and Struck-Marcell 1987, Struck-Marcell and Appleton 1987) which could be used to provide the inputs for the photometric evolutionary program.

Including the effects of reddening and absorption by dust in photometric models would greatly aid in understanding the colors in spiral galaxies. Unfortunately, including dust in the simulations cannot be done in a simple or straight-forward manner. The distribution of dust, the distribution of stars, and a model for the redistribution of energy by the dust are all necessary for a model which includes dust in a realistic manner. Although measurements of the redistribution of energy by dust have been made by Johnson (1964) and measurements of the distribution of stars have been made for our galaxy (cf. Binney and Tremaine 1988), the distribution of the dust is more uncertain (Johnson 1964). Until a

better understanding of the distribution of dust is achieved, it is unlikely that including dust in photometric models will be productive.

III. COLLISIONALLY FORMED RIPPLES

Previous theories of the formation of ripples around early-type galaxies have primarily used mass transfer and accretion to form the ripples (cf. Hernquist and Quinn 1987, Schweizer and Seitzer 1988). An alternative theory for the formation of ripples has been presented in which the ripples are formed from radial oscillations of the outer regions in early-type disk galaxies. The formation mechanism is more closely related to models of ring galaxies (Lynds and Toomre 1976) than to the previous models of ripples. This model explains the similarity between the colors of the ripples and the main galaxy of the Arp 227 system. Other systems which have ripples around early-type disks and nearby companions may have also formed their ripples in a similar manner.

Several observational tests are suggested to help resolve when this mechanism is important. Additional measurements of the colors of the ripples found around early-type disks would give information about the uniqueness of the Arp 227 system. Measurements of the intensity profiles of the galaxies at the centers of ripple systems will give information about the number of systems which have both ripples and disks. The location of faint optical or HI bridges between the companion galaxy and the main galaxy could also give additional information about the dynamics of the encounters which formed the ripples. The interleaving of the ripples noted by Schweizer and Seitzer (1988) occurs in both the

collisional models and the accretion models; therefore it cannot be considered a reliable method of determining which mechanism formed the ripples in a given system.

It is likely the accretion, mass transfer, and collisional models are all important at different stages of a merger and can be considered different stages of the same process.

IV. FUTURE STUDIES OF RIPPLE FORMATION

To further understand the formation of ripples, the effects of dynamical friction should be tested in these models. Since the passage of a small galaxy through an early-type disk system forms ripples, the effects of dynamical friction may be important in the later evolution of the system. The inclusion of test particles around both the companion galaxy and the main galaxy might show the development of accretion, mass transfer, and collisional ripples as the simulation progresses. In addition, observational studies of early-type disk galaxies which have both an interacting companion and ripples should also give insight into the mechanisms for the formation of ripples.

V. REFERENCES

Appleton, P. N. and Struck-Marcell, C. (1987) *Ap. J.* **312**, 566.

Binney, J. and Tremaine, S. (1987) *Galactic Dynamics* (Princeton : Princeton University Press).

Hernquist, L., and Quinn, P. (1987) *Ap. J.* **312**, 1.

Johnson, H. L. (1964) *Ap. J.* **142**, 923.

Lynds, R., and Toomre, A. (1976) *Ap. J.* **209**, 382.

Schmidt, M. (1959) *Ap. J.* **129**, 243.

Schweizer, F. and Seitzer, P. (1988). *Ap. J.* **328**, 88.

Struck-Marcell, C. and Appleton, P. N. (1987) *Ap. J.* **323**, 480.

APPENDIX A : THE RESTRICTED THREE-BODY METHOD

I. THE RESTRICTED THREE-BODY METHOD

In order to model the gravitational interaction between two galaxies, it is necessary to make some simplifying assumptions. Given a system of n bodies, the acceleration the i^{th} particle will feel from the other bodies will be given by

$$a_i = \sum_{j=1}^{n} \frac{G M_j (r_i - r_j)}{|r_i - r_j|^3} \qquad (1)$$

Since a galaxy typically contains approximately 10^{11} stars, over 10^{11} calculations would be necessary to calculate the acceleration for each star at each time step. In an N-body approach, the computation time for the entire system increases proportionately to N^2, so approximately 10^{22} calculations would need to be completed for each time step.

The first approximation which used is to consider regions of the galaxy as point masses. By using the masses of regions in a galaxy instead of the masses of individual stars and clouds, the number of points in the simulation can be lowered. Even though the number of particles in the simulation can be greatly reduced, a moderate number is still needed to preserve resolution. The number of particles for a given resolution is given by

$$N = \frac{V}{r n} \qquad (2)$$

where V is the volume of the object to be examined, r is the desired resolution, n is the number of particles in this resolution element, and N is the total number of particle in the object. This can be best illustrated with a simple example.

Assume we have a disk of thickness 1 kpc and radius 10 kpc which we wish to resolve with 10 particles in each 1 kpc^3 region. From equation (2), we would need approximately 3000 particles to achieve this resolution. Using an N-body code, approximately 10^7 calculations would be needed for each time step. Because of the high computational costs, N-body codes are usually impractical for general studies of interacting galaxies where a wide variety of initial conditions must be tested at high resolution.

One alternative to a true N-body calculation is the restricted three-body approximation. Traditionally in this approach, the two galaxies in the interaction are represented with softened point masses and massless test particles are used to represent the disk particles. Computationally this method is much cheaper than the N-body method because the interactions between particles are not calculated. The forces on a particle are from only two sources so the number of calculations for a given time step is directly proportional to the number of particles in the simulation. Figure 1 shows the test particle and its relationship to the masses M_1 and M_2.

If we choose a coordinate system which is fixed with respect to M_1 in Figure 1, the acceleration of a test particle p_i is given by

$$a = \frac{GM_1 r_1}{|r_1|^2 + \varepsilon^2} + \frac{GM_2 r_2}{|r_2|^2 + \varepsilon^2} - \frac{GM_2 R}{|R|^2 + \varepsilon^2} \tag{3}$$

The first term on the right-hand side of equation (3) is caused by the gravitational acceleration on p_1 by M_1, and the second term is from the gravitational acceleration from M_2. The third term is due to the acceleration of M_1 away from p_1 due to the tidal forces from M_2. This term is present in the equations because of the noninertial coordinate system we are using in for the particles and is essential to the formation of tidal tails.

The parameter ε is known as the softening length. It is included to extend the effective density distribution of the point masses and help prevent numerical instabilities from the singularities present when $\varepsilon = 0$. The softening length gives a simple one parameter approximation to the galactic bulge distribution and asymptotically approaches a point mass as ε/r approaches zero.

The use of a softening length introduces a bit of confusion about what to use for the initial orbital velocity of test particles inside or near the softening length. The value of the circular orbital velocity can be calculated by either the virial theorem or by the balance of forces. The virial theorem yields a circular orbital velocity of

$$v = \left\{ \frac{GM}{\varepsilon} \left[\frac{\pi}{2} - \mathrm{am}\left(\frac{r}{\varepsilon}\right) \right] \right\}^{\frac{1}{2}} \tag{4}$$

while the balance of forces gives

$$v = \sqrt{\frac{GMr}{r^2 + \varepsilon^2}} \tag{5}$$

As expected, these values converge as ε/r approaches zero, but for small values of r, there are minor differences in the values from the different methods. In these simulations, the balance of forces is used for circular velocities.

A set of dimensionless units was used in the program to simplify the numerical calculations. In these simulations, the gravitational constant G was defined as one. The mass of the galaxy and companion are expressed in terms of "galactic masses" and the distances are measured in terms of "disk radii". The unit of time used in these simulations results from the application of Kepler's third law. Table 1 has been constructed to convert between the program units and the normal physical units.

A constant time-step 4th order Runge-Kutta routine was used to solve the equations of motion for the test particles and the companion galaxy. The stability of this routine was tested by integrating a set of 1000 test particles ahead by 5 units of time and then reversing the process and moving them back toward their original position. The mean residual displacement was then calculated along with a standard deviation of this mean. Runs were conducted for the disk alone and the disk with a close passage of

the companion for 3 different time steps. The results of these test are summarized in Table 2.

In addition to the consistency tests, the results of the program were compared to those of Toomre and Toomre (1972). Several of the test cases used in this paper were duplicated with this code to check the dynamical equations being used. Although statistical comparisions were impossible, no significant differences were seen in the morphologies produced by the two methods.

The large dispersions present in the displacements are due to the close approach of the companion to a few outer particles. Even with the largest time step used in the disk+companion tests, over 75% of the particles had displacements less than 0.1. The timesteps used in the runs were chosen to be between 0.005 and 0.02 depending somewhat arbitrarily on the qualitative strength of the perturbation in the interaction to be modeled. This strength is based on the velocity, inclination, distance of minimum approach, and the mass of the companion galaxy.

The geometry of the tidal interaction is shown in Figure 2. The companion galaxies orbit is described in terms of an inclination (i), an argument of perigee (ω), and a radius of minimum approach (r_{min}). All orbits in these simulations are assumed to be parabolic with the time of closest approach defined to be t=0. Note the x axis is defined along the line of nodes for the perturbing galaxy. The complete interaction is defined in terms of these quantities, the mass of the companion galaxy and the softening lengths for the

main galaxy and the companion. If the interaction between two disks were being modeled, two additional angles and a radius of the companion disk would be need to describe the system.

To initialize the position and velocity of the companion galaxy, it is initially placed with the position and velocity it will have at t=0. Its position is then integrated backwards to a starting position. The disk particles are distributed in circular orbits around the companion will an adjustable radial distribution profile. The parameters of the radial profile is adjusted to the disk to be modeled.

The viewing angle for the simulation is defined in terms of the angles α and β in Figure 3. Most of the simulations in this manuscript are viewed from directly above the disk with both angles equal to zero.

II. REFERENCES

Toomre, A. and Toomre, J. (1972) *Ap. J.* **178**, 623.

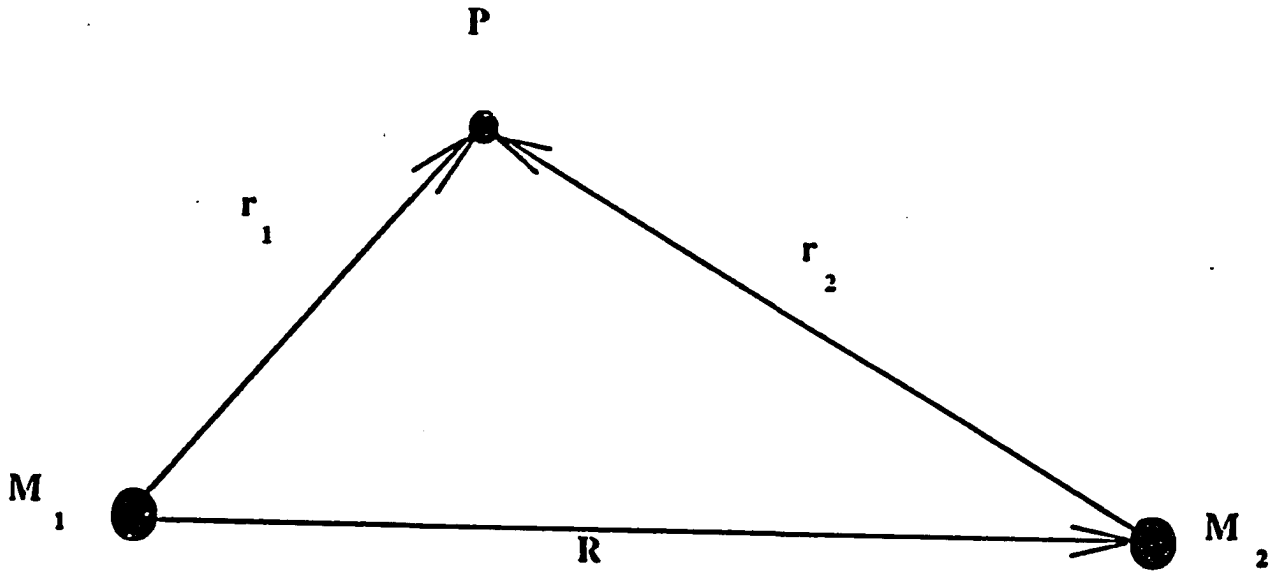

Figure 1. The geometry of the main galaxy, the companion galaxy, and a test particle. The main galaxy is denoted by the point M_1, the companion galaxy is represented by the point M_2, and the test particle is represented by P

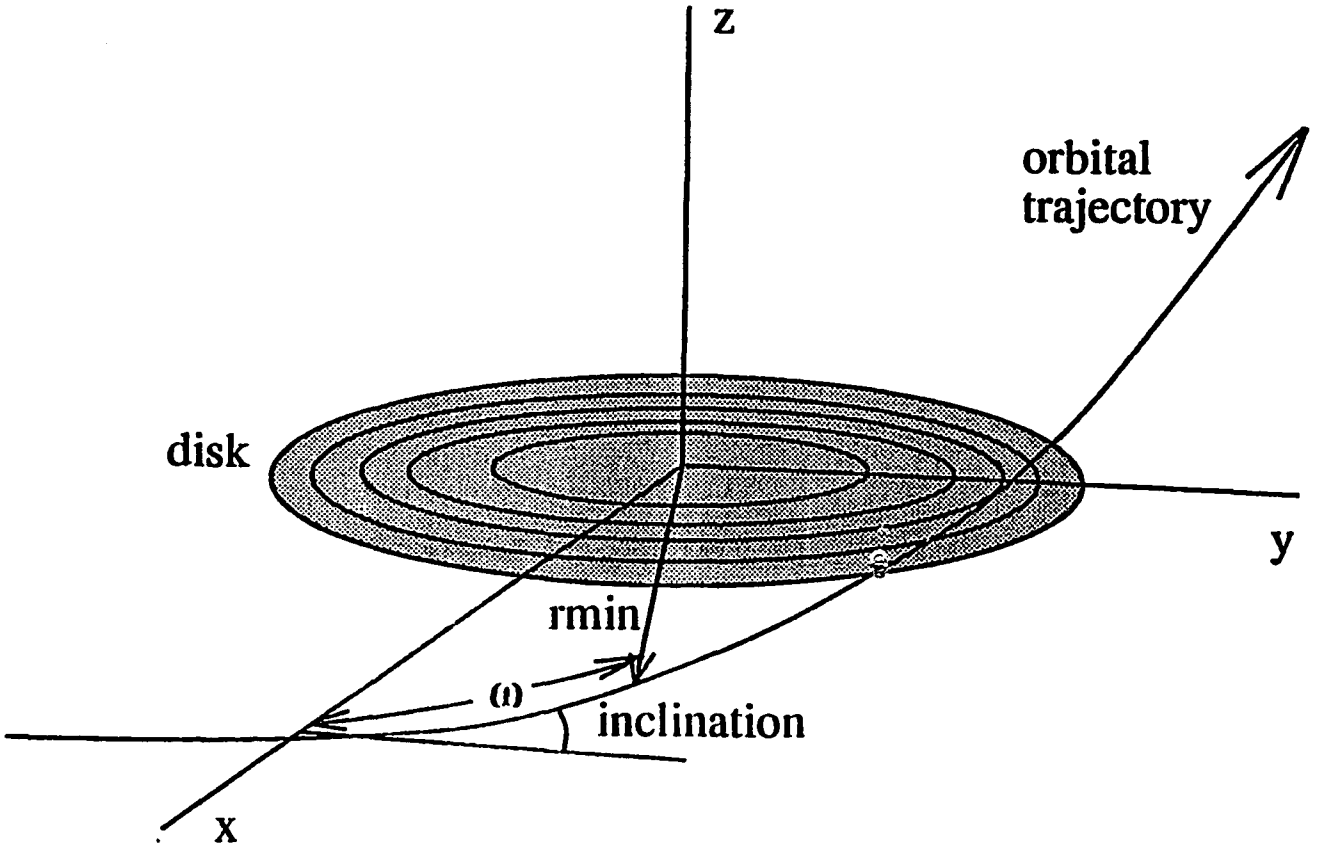

Figure 2. The geometry of the companion galaxy's orbit. The disk of the companion galaxy defines the coordinate system for these simulations. The inclination is measured with respect to the main galaxies orbital plane. The node of the companion's orbit defines the location of the X-axis. The arguement of periapse (ω), the inclination (i), and the radius of minimum approach (r_{min}) are seen in this diagram

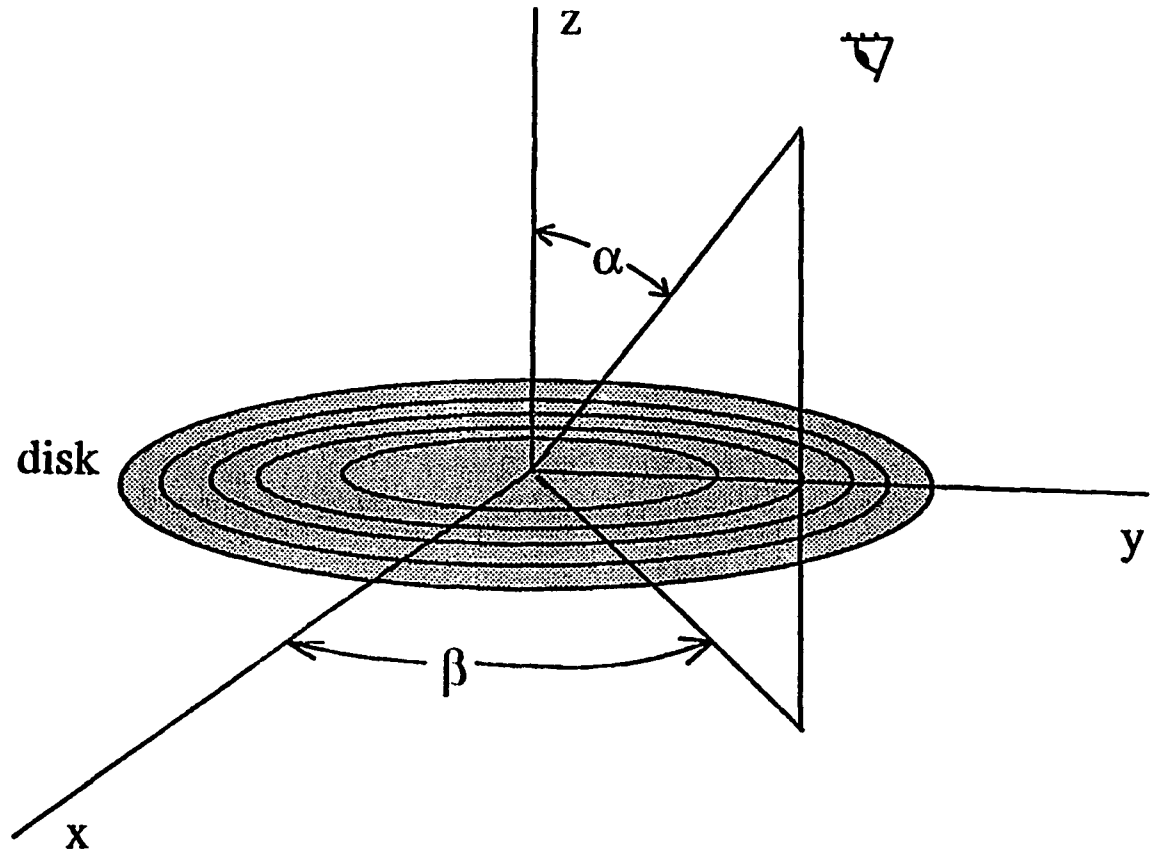

Figure 3. The geometry of the viewing angle for the simulations. The viewing angles α and β are measured with respect to the main galaxy's orbital axis and the node of the companion galaxy's orbit. The angle α measures the tilt angle away from the companion galaxy's disk and the angle β measures the azmuthal angle from the node

Table 1. The relationship between simulation units and physical units in a typical galaxy.

Constant	Program Units	Physical Units
G	1	6.67×10^{-8} dyn cm^2 gm^{-2}
M	1	2.0×10^{44} gm
R	1	15.0 kpc
T	1	82.8 Myr
V	1	172 km s^{-1}

Table 2. The stability of the numerical integration routine. The stability of the numerical integration routine is tested by integrating the system forward in time by 6 units and then integrating back to the initial positions. The average displacement, average velocity change, maximum displacement, maximum velocity change, and the number of particles with a displacement greater than 0.1 units is presented. There were 1000 randomly distributed particles in the disk for these tests

Dynamical tests without the companion time-step[a]	average Δr[b]	average Δv[c]	maximum Δr[d]	maximum Δv[e]	N[f]
0.02 (4.51×10^{-1})	3.47×10^{-1} (7.02×10^{0})	2.65×10^{0}	2.05×10^{-1}	4.45×10^{0}	41
0.005 (7.39×10^{-2})	7.15×10^{-2} (6.34×10^{-1})	3.83×10^{-1}	1.14×10^{-1}	2.47×10^{-1}	0

Dynamical tests with the companion time-step[a]	average Δr[b]	average Δv[c]	maximum Δr[d]	maximum Δv[e]	N[f]
0.02 (1.042×10^{0})	3.57×10^{0} (1.038×10^{0})	4.52×10^{0}	1.0743×10^{1}	5.598×10^{0}	233
0.005 (2.78×10^{-1})	4.40×10^{-2} (3.13×10^{-1})	8.08×10^{-1}	3.99×10^{0}	4.43×10^{0}	33
0.0025 (7.61×10^{-2})	9.08×10^{-3} (1.13×10^{-2})	2.75×10^{-2}	1.851×10^{0}	2.055×10^{0}	8

[a]The time-step for the Runge-Kutta routine in dimensionless units.

[b]The average displacement and its standard deviation for particles in the simulation after they are integrated back to their initial conditions.

[c]The average velocity change and the standard deviation for particles after they are integrated back to their initial conditions.

[d]The maximum displacement for the particles in the simulation after they are integrated to their initial conditions.

[e]The maximum velocity change caused by integrating the particles back to their initial condition.

[f]The number of particles which are displaced by more than 0.1 units from their initial position.

APPENDIX B

PHOTOMETRIC EVOLUTIONARY MODELS

I. THE INITIAL MASS FUNCTION

To model the photometric evolution of galaxies, a number of different physical inputs are needed, including the initial mass function, the star formation rate and stellar evolutionary tracks. In this section, I will give a brief summary of the methods to determine the form of the IMF and a survey of commonly used analytical forms. Scalo (1986) gives a comprehensive review of the initial mass function, and much of the discussion here will be derived from this source.

The initial mass function is defined to be "the frequency distribution of stellar masses at birth" (ibid.). Mathematically, it is defined such that f(m)dm is the number of stars with masses between m and m+dm.

Before the initial mass function can be found, the present day mass function (PDMF) must be determined. The PDMF is determined using data from star counts, the mass-luminosity relationship and a spectral class to mass conversion derived from binary stars. Careful attention must be made to observational selection effects including the scale height as a function of spectral type, evolutionary effects, and dust obscuration of young stars.

Using the present day mass function, the lifetime of stars as a function of mass, and the star formation rate, it is possible to derive the initial mass function. For individual clusters, the method of finding the initial mass function is considerably simplified since the star formation rate is assumed to be a delta function. The initial

mass function of field stars is much more difficult to derive since the form of the star formation rate in the galaxy is not accurately known.

The form of the derived field star initial mass function as derived by Scalo is shown in Figure 1. At higher masses, the number of stars decreases drastically. In the field stars, there is more than a two order of magnitude drop in abundance between the stars at one solar mass and those at 10 solar masses.

A number of semi-analytical approximations are used to model the initial mass function. The simplest was given by Salpeter (1955). The Salpeter or power law IMF has the form

$$f(m) = A\, m^{-\gamma} \tag{1}$$

where γ is the initial mass function index, m is the mass, f is the initial mass function, and A is a normalization factor. The constant A is derived from the normalization

$$\int_{m_l}^{m_u} f(m)\, dm = 1 \tag{2}$$

where m_l is the lower mass limit and m_u is the upper mass limit for the mass function.

Typically γ is set equal to about -2.3. One variation of the power law initial mass function was proposed by Tinsley (1980). This form of the IMF uses a piecewise continuous power law function which has the form

$$f(m) = \begin{cases} 1.00\, m^{-1.25} & 0.4 < m \leq 1.0 \\ 1.00\, m^{-2.0} & 1.0 < m \leq 2.0 \\ 1.23\, m^{-2.3} & 2.0 < m \leq 10.0 \\ 12.3\, m^{-3.3} & 10.0 < m \leq 50.0 \end{cases} \quad (3)$$

The normalization constants in the equation have been chosen so the conditions of equation (2) are met and the function is continuous.

Another commonly used analytic form of the IMF was given by Miller and Scalo (1979). In this form, a power law mass function is used with the index of the mass function given by-

$$\gamma = -\log m \quad (4)$$

The normalization factor for this form is given by the conditions of equation (2).

Figure 2 illustrates the different analytic initial mass functions presented here. The simplest one presented is clearly the Salpeter IMF, however the Tinsley and Miller-Scalo IMFs are quite similar to

each other and to the observed field star initial mass function. All four of these IMF are allowed options in the photometric evolutionary code used in this paper. Because of the similar nature of the curves and similar results from different IMFs for photometric evolutionary studies (cf. Tinsley 1980), the Tinsley initial mass function was used for all the runs presented here. Figure 3 illustrates the B-V evolution of a simple burst using different initial mass functions. The agreement in colors between populations synthesized with different IMFs in Figure 3 illustrates the weak dependence the broadband photometric colors have on the form of the IMF. Because the light of a stellar population is normally dominated giants and bright main sequence stars (Tinsley 1980), the slope of the initial mass function at high masses affects the stellar populations colors more than the behavior of the IMF at low masses.

II. THE STAR FORMATION RATE

The normal units for measuring the star formation rate (SFR) for a galaxy or a region are given by the number of solar masses per year per cubic parsec ($M_O/yr/pc^3$). The form for a star formation rate is then constructed so that M solar masses per cubic parsec of material are formed between time zero and infinity, that is-

$$\int_0^\infty \psi(t)\,dt = M \qquad (M_O/pc^3) \tag{5}$$

There are several different analytical forms of the star formation rate which are used for photometric evolutionary models. The simplest model is that of a single burst. In a simple burst model, all stars are assumed to be a constant nonzero value between a time of 0 and dt and zero in times greater than dt. The simple burst type model is most similar to open clusters, globular clusters, and elliptical galaxies. Analytically, this function is given by

$$\begin{aligned} \psi(t) &= A \qquad 0<t\leq dt \\ &\quad 0 \qquad t>dt \end{aligned} \tag{6}$$

Another model that is commonly used is a exponential decay in the SFR of the form-

$$\psi(t) = R\, e^{-t/t_o}\ (M_o/yr/pc^3) \qquad (7)$$

where R is a constant multiplying factor and t_o is the time constant. The value of this time constant determines the behavior of the system's relative SFR and the constant R determines the absolute brightness of the system. It is interesting to note that the multiplying factor R does not affect the colors of a stellar population, only the absolute magnitude. The colors of a stellar population are determined by the relative star formation rate history rather than the absolute amount of star formation present.

III. STELLAR EVOLUTIONARY TRACKS

Another input needed for photometric evolutionary models are stellar evolutionary tracks. Numerical models of stellar interiors are normally used for these evolutionary tracks. Because of the difficulty in handling all the stages of stellar evolution in a single program, a number of different models for different evolutionary stages must be combined for the entire evolution of a single star.

One of the primary difficulties in modeling low mass (<3 solar masses) stars is the helium flash. As the core in a red giant builds up, a large highly degenerate core builds up until the pressure and temperature reach a level which helium burning can ignite. When this ignition takes place, the amount of energy produced in the core of the star increases to a level of approximately 10^{11} solar luminosities because of the weak dependence of pressure on temperature in degenerate matter. Eventually this degeneracy is removed because of the large amount of energy production and normal core helium building begins (Clayton 1983). The evolutionary timescale for these changes is on the order of minute, while the typical evolutionary timesteps used in most stellar interior modeling programs are typically 10^5 to 10^7 years (Guzik 1989). Evolutionary codes have been specifically designed to deal with this complicated and rapidly changing phase of stellar evolution, but they are not used for the general modeling of stars on the main sequence.

To combine the calculations for different evolutionary stages, the temperatures and luminosities are joined at equivalent evolutionary points to form a smooth track [1](cf. Bruzual 1981, Renzini and Buzzoni 1986). The resulting track for a solar type star shows the evolution through the main sequence, subgiant branch, first giant branch, helium flash, horizontal giant branch, and asymptotic giant branch. After the asymptotic giant branch, the amount of energy coming from the stages of evolution after the asymptotic giant branch is usually small compared to the other stages of evolution, so they are neglected in this program. Figure 4 shows the relative amount of energy from each evolutionary state as a function of time assuming a single burst of star formation (Renzini and Buzzoni 1986).

It should be noted, however, that the white dwarf and planetary nebula central stars give off a significant amount of the ultraviolet flux in elliptical galaxies and globular clusters because of the lack of high and intermediate mass main sequence stars. For spiral galaxies with on-going star formation, the near ultraviolet flux is dominated by the light from the young massive main sequence stars (Renzini and Buzzoni 1986).

Because tracks are not available for the large number of mass bins needed for photometric evolutionary models, additional tracks

[1]Equivalent evolutionary points are points in a star's evolution where the internal structure of the star is the same. The luminosities and effective temperature are then fitted using a linear smoothing between the points.

must be interpolated from the existing tracks. Once again, equivalent evolutionary points are used to make these additional tracks. The because of the similarity between tracks between of masses which are nearly equal, a simple linear interpolation between equivalent evolutionary points suffices to make additional tracks.

One of the principal problems in photometric evolution is the finding of consistent stellar evolutionary models for stars. The problem of stellar modeling is an extremely complex and uses a number of parameters and inputs to determine the structure a star. The luminosity of most stellar models is fairly well determined since it depends only on the energy generation of the core. The effective temperature is determined by the size of the outer stars photosphere. The outer structure of the star is influenced by a number of factors including the mixing length and opacity.

The mixing length in stellar modeling is a dimensionless ratio involving the convective mixing length and the pressure scale height. As the mixing length is increased, the size of the photosphere is extended as material is mixed to larger radii in the outer convective layers of the star. Since stars more massive than the sun are convective outside the core, the luminosity of the star is not greatly affected by a changing mixing length. Because the luminosity is constant, the star has a lower effective temperature when the radius extends.

The opacity of the models also affects the effective temperature of stellar models by changing the places where convection begins and the amount of heating in the inner layers. When the opacity in a region decreases, the radiation escapes more easily lowering the amount of heat available. With less heat, there is less pressure so the star may contract slightly lowering the effective radius.

Advances in opacity calculations and the comparison of the mixing length to the observational parameters have been used to improve the fit between observation and theory in stellar modeling. One additional input used for stellar model is the luminosity function. The luminosity function is the defined as the amount of energy radiating at a given effective temperature or color for a given mass. The observed shape of the luminosity function (Tinsley and Gunn 1976) has been very useful in testing the shape of the red giant evolutionary tracks. For a large population of stars, the luminosity function is the parameter which determines the spectral colors of a population rather than the exact shape of the stellar evolutionary track. A detailed description of the models used in this code is contained elsewhere in this manuscript.

IV. CONVERSION OF EFFECTIVE TEMPERATURE TO BROAD-BAND SPECTRAL COLORS

The Johnson photometric system was used to compare the modeled spectral colors to observed galaxies. The spectral response for the Johnson photometric system filters is shown in Figure 5. The magnitudes for these filters are normalized so the color in all bands is equal to 0.0 for a star with an effective temperature of 10,000 K. The conversion of effective temperatures from the stellar models to broad-band spectral colors is done by the use of tables by Johnson (1966). In the Johnson paper, a large observational sample of all types of stars was made and the broad-band spectral colors were compared to the spectral types. Bolometric corrections for the spectral classes were also used. The effective temperature of these spectral types was then calculated by examining the radiation temperature from the excitation strength of lines. Figure 6 shows the relationship between the B-V color and the effective temperature for main sequence stars.

Model atmospheres of stars have also been used to generate the broad-band spectral colors for different effective temperatures (cf. Buser and Kurucz 1978). In these models, a stellar atmosphere code is used to create a synthetic spectrum for a star with given effective temperature, luminosity, surface gravity, and composition. The results from this synthetic spectrum are then convolved with the spectral response of the Johnson photometric system including

the atmospheric absorption of the earths atmosphere, the filter response, and the photomultiplier tube spectral sensitivity. The results from these models have not been used in this paper for a number of reasons. First of all, the spectral bands modeled so far have only been in the visual. Second, the agreement between the effective temperature and the color from model atmospheres agrees very closely to the results from the Johnson paper (Buser and Kurucz 1978). The combination of these two facts makes the use of the Johnson results quite acceptable for these models.

V. POPULATION SYNTHESIS

The initial mass function and star formation rate are used to synthesize a population of stars. To synthesize a population, the continuum of masses is divided into discrete bins centered on the masses of the stellar evolutionary tracks. Time is also divided into quantized bins typically with lengths of about one million years. In this and other codes (c.f., Struck-Marcell and Tinsley 1978, Bruzual 1981) the initial mass function is assumed to be constant during the systems history. The number of stars formed with a mass between m and m+dm during a time between t and t+dt is equal to

$$N(m,t) = f(m)\,\psi(t)\,dt\,dm \qquad (8)$$

Once this populations has been constructed, the effective temperature and luminosity is derived for each grid point. The grid N(m,t) is used to calculate the number of stars with a mass of m and an age of T-t where T is the age of the system under investigation. This age and mass of the grid point are then used as pointers in an array of stellar evolutionary tracks to find the effective temperature, luminosity and luminosity class.

Once the effective temperature and luminosity class are know, the broad-band spectral colors can be found from the tables by Johnson (1966). Bolometric corrections are also included to convert the luminosity into the Johnson photometric system. A spectral luminosity is then calculated for each grid point in each

photometric band. The total broad-band spectral luminosity is then found by summing the grid points. The broad band spectral colors are then found for the entire system.

VI. REFERENCES

Bruzual, G. A. (1981) *Spectral Evolution of Galaxies*, Ph. D. Thesis, University of California, Berkeley.

Buser, R. and Kurucz, R. L. (1978) *Astron. Astrophys.* **70**, 555.

Clayton, D. D. 1968, 1983, *Principles of Stellar Evolution and Nucleosynthesis* (Chicago : U. of Chicago Press).

Guzik, J. (1989) Private communication. Los Alamos National Laboratory.

Johnson, H. L. (1964) *Ap. J.* **142**, 923.

Johnson, H. L. (1966) *Ann. Rev. Astron. Astrophys.*, **4**, 193.

Miller, G. E. and Scalo, J. M. (1979) *Ap. J. Suppl.* **41**, 513.

Renzini, A. and Buzzoni, A. (1986) in *The Spectral Evolution of Galaxies*, eds. C. Chiosi and A. Renzini (Dordrecht : D. Reidel), p. 195.

Salpeter, E. E. (1955) *Ap. J.* **121**, 161.

Scalo, J. M. (1986) *Fund. Cosmic Phys.* **11**, 1.

Struck-Marcell, C. and Tinsley, B. M. (1978) *Ap. J.* **221**, 562.

Tinsley, B. M. (1980) *Fund. Cosmic Phys.* **5**, 287.

Tinsley, B. M. and Gunn, J. E. (1976) *Ap. J.* **203**, 52.

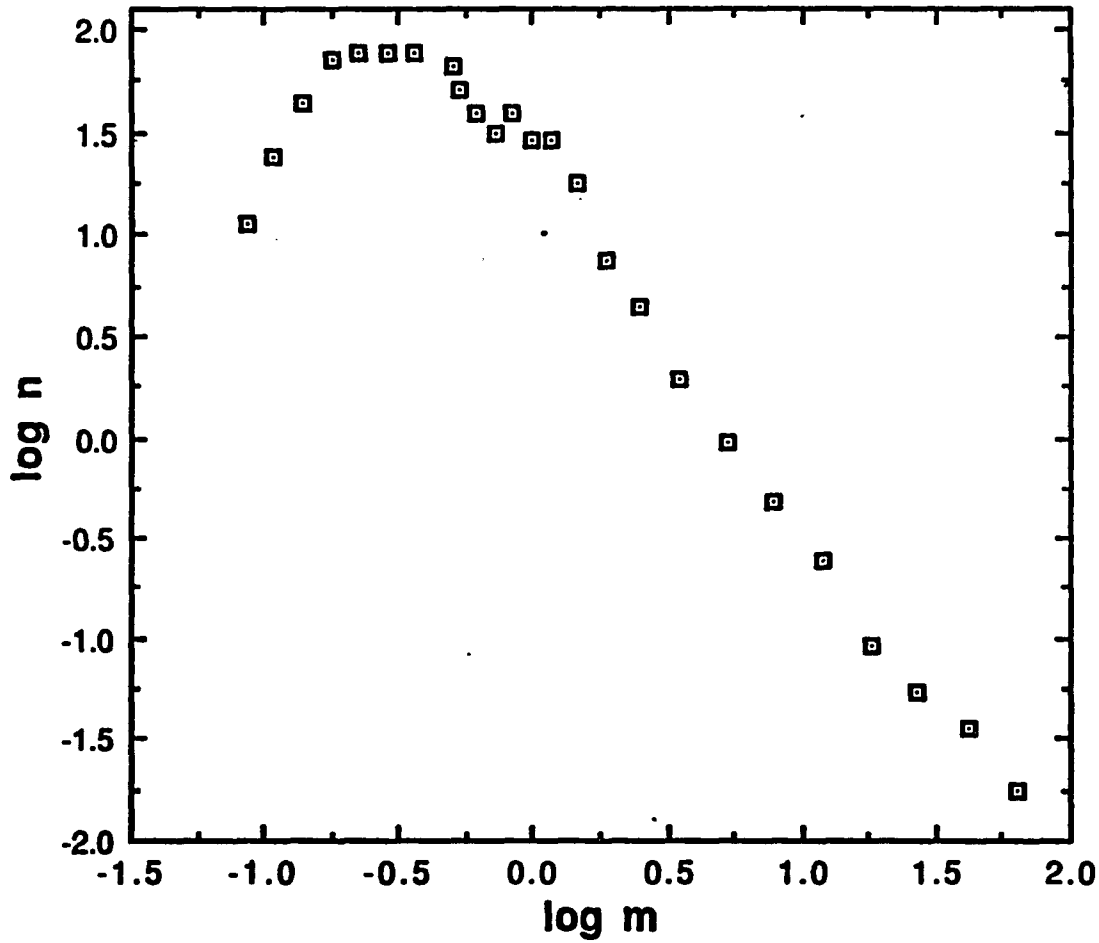

Figure 1. Scalo field star IMF. This figure illustrates the measured field star initial mass function for our galaxy. The data are taken from Scalo (1986)

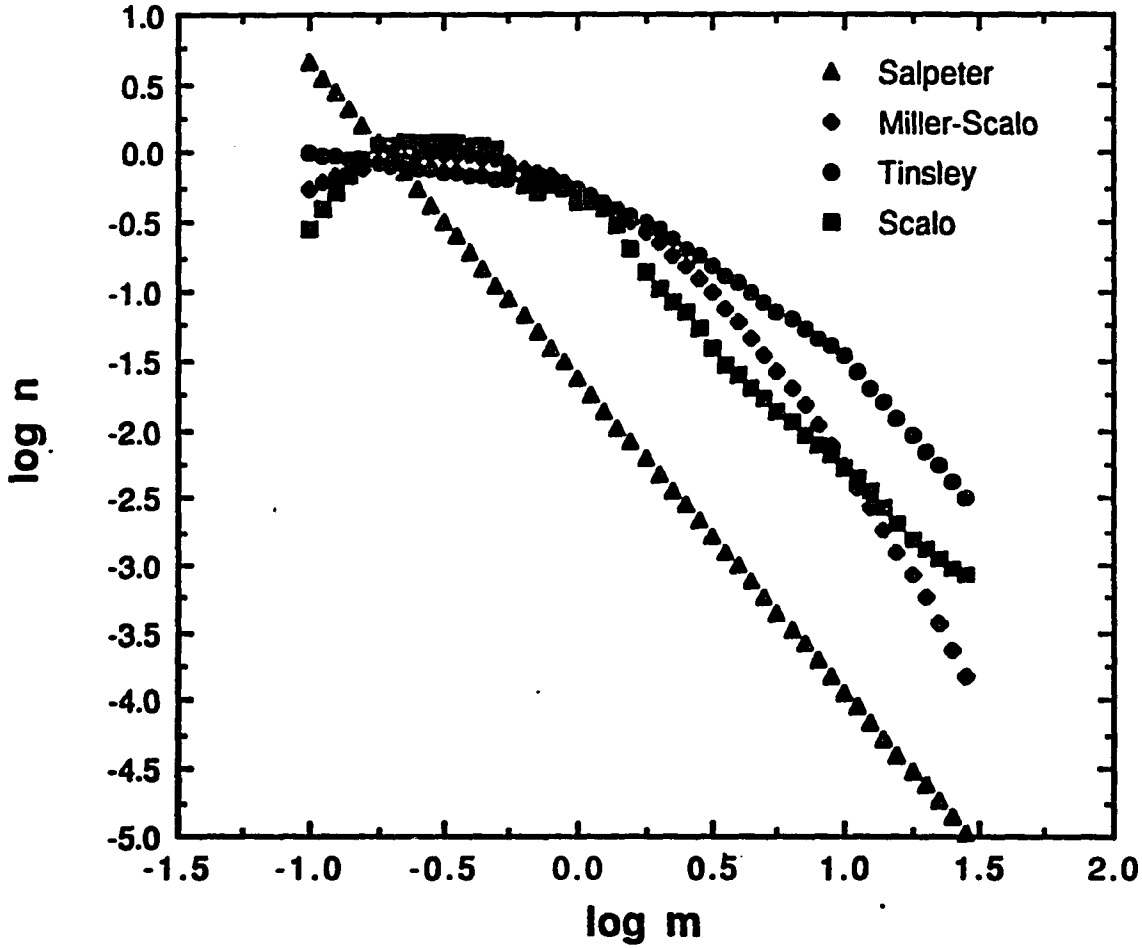

Figure 2. The Salpeter, Miller-Scalo, Tinsley, and Scalo IMFs. The colors of a population depend primarily on the slope of the initial mass function at high masses rather than the absolute number of star formed at a given mass. Notice the slopes of the four IMFs are similar at high masses. The differences between the Scalo IMF and Figure 1 are due to different normalization conditions between the two graphs

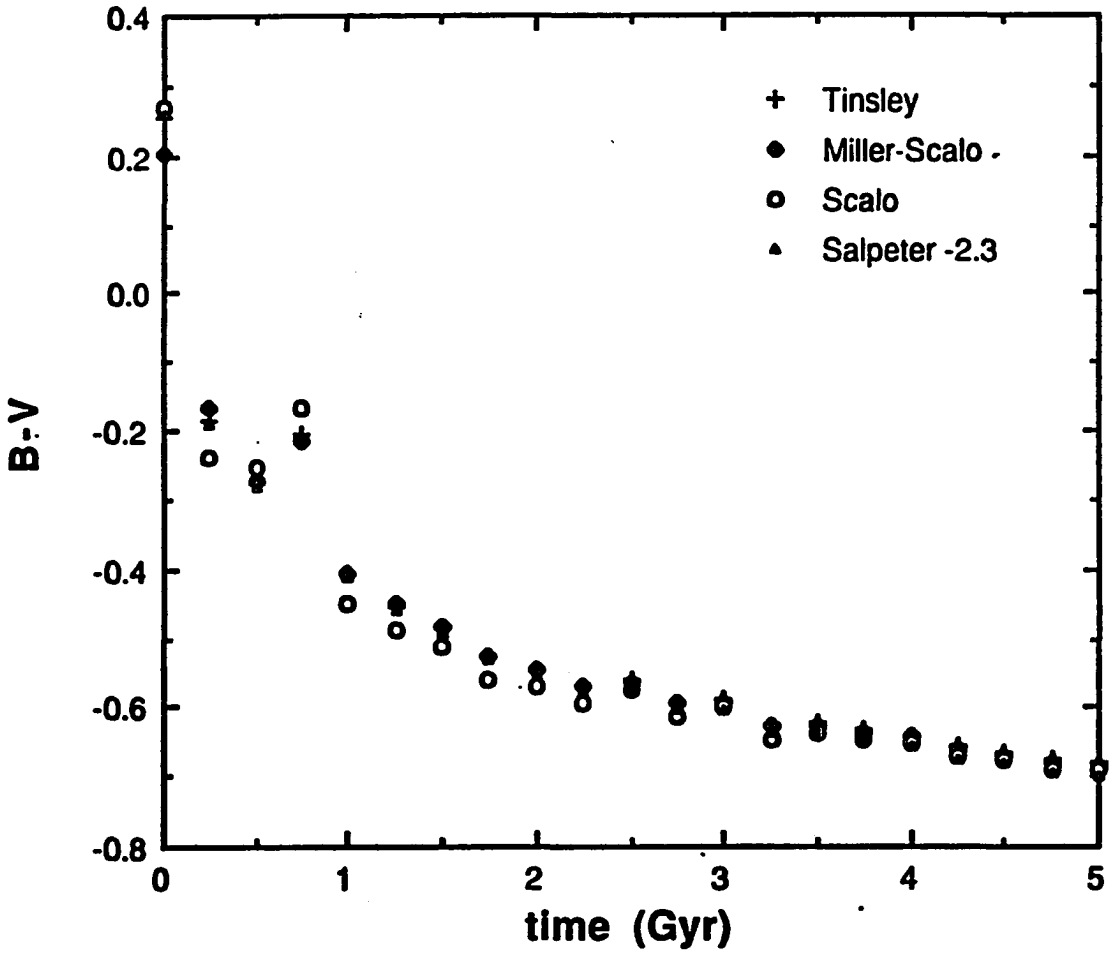

Figure 3. B-V evolution of a simple population with different IMFs. The first 5 Gyr of the evolution for a single burst of star formation is shown in the B-V colors. The discontinuity at t=0.75 is caused by a rounding error in the synthesis program due to the relatively small number of stellar evolutionary tracks. It is caused of the population synthesis method used and can be considered and artifact of the simulations

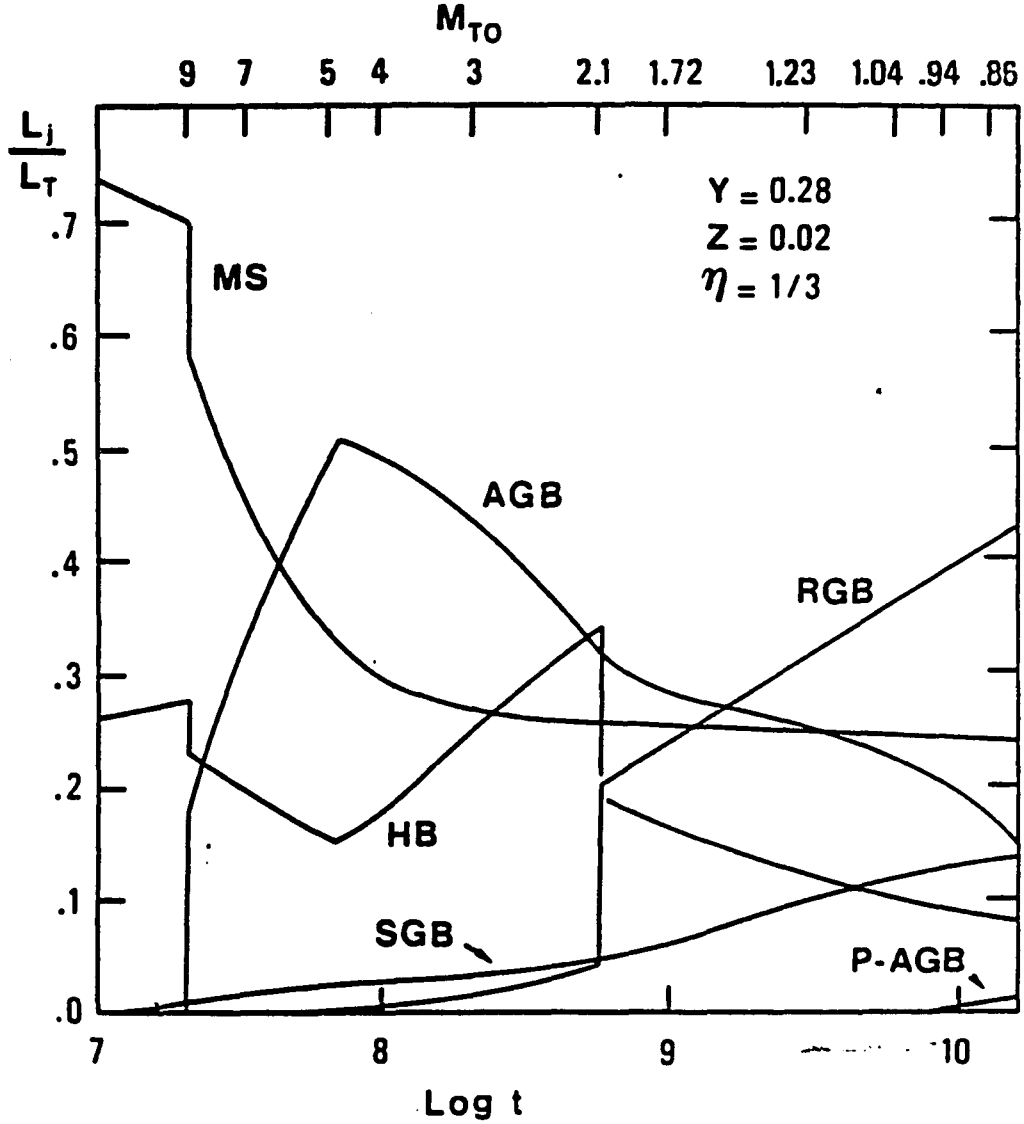

Figure 4. Relative energy output as a function of evolutionary stage for a simple stellar population. This graph shows the relative energy output of the stars in a single burst as a function of time. The graph is taken from Renzini and Buzzoni (1986)

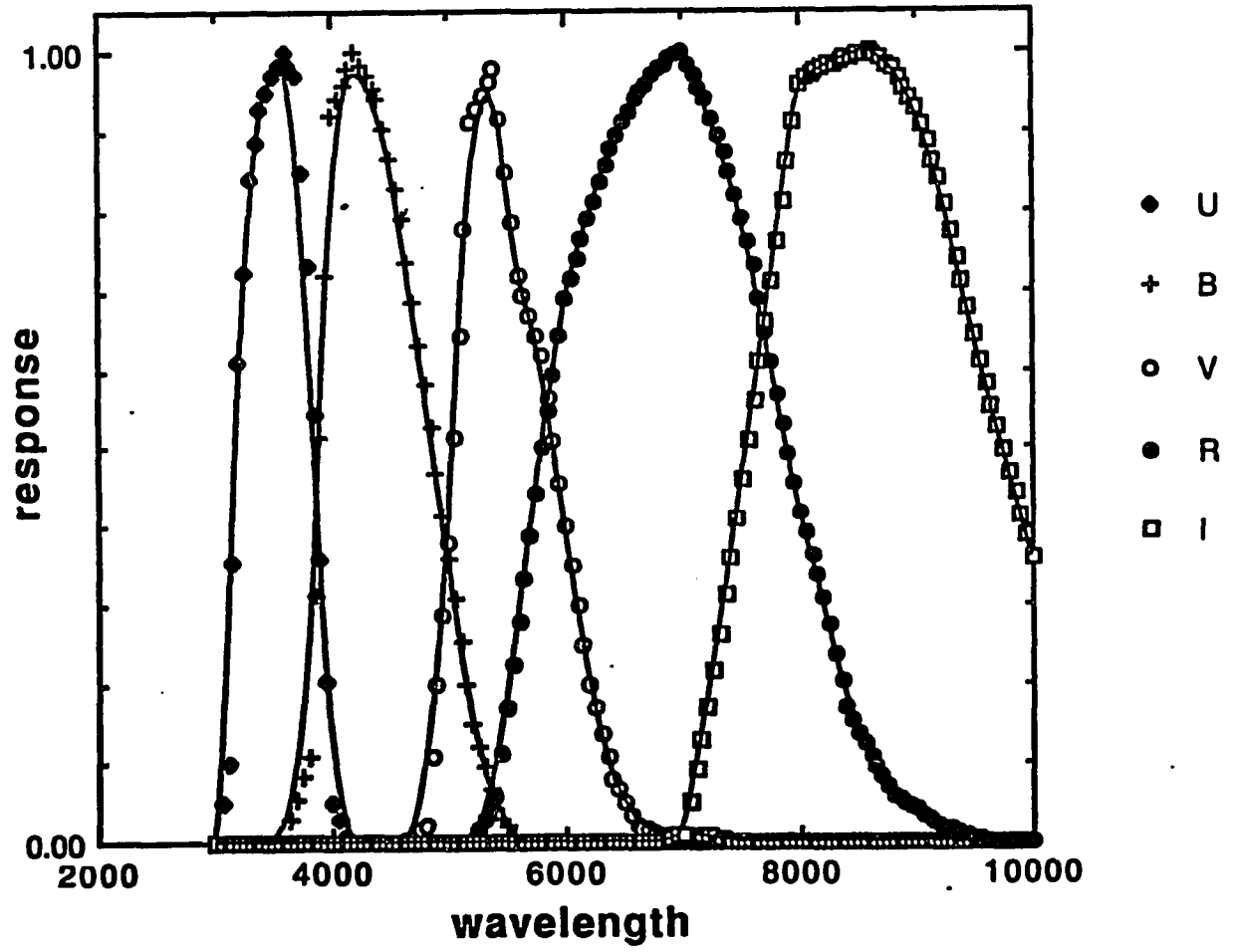

Figure 5. Spectral response of the Johnson photometric filters. The curves show the relative spectral response of different Johnson system filters. The data for this graph are taken from Johnson (1964)

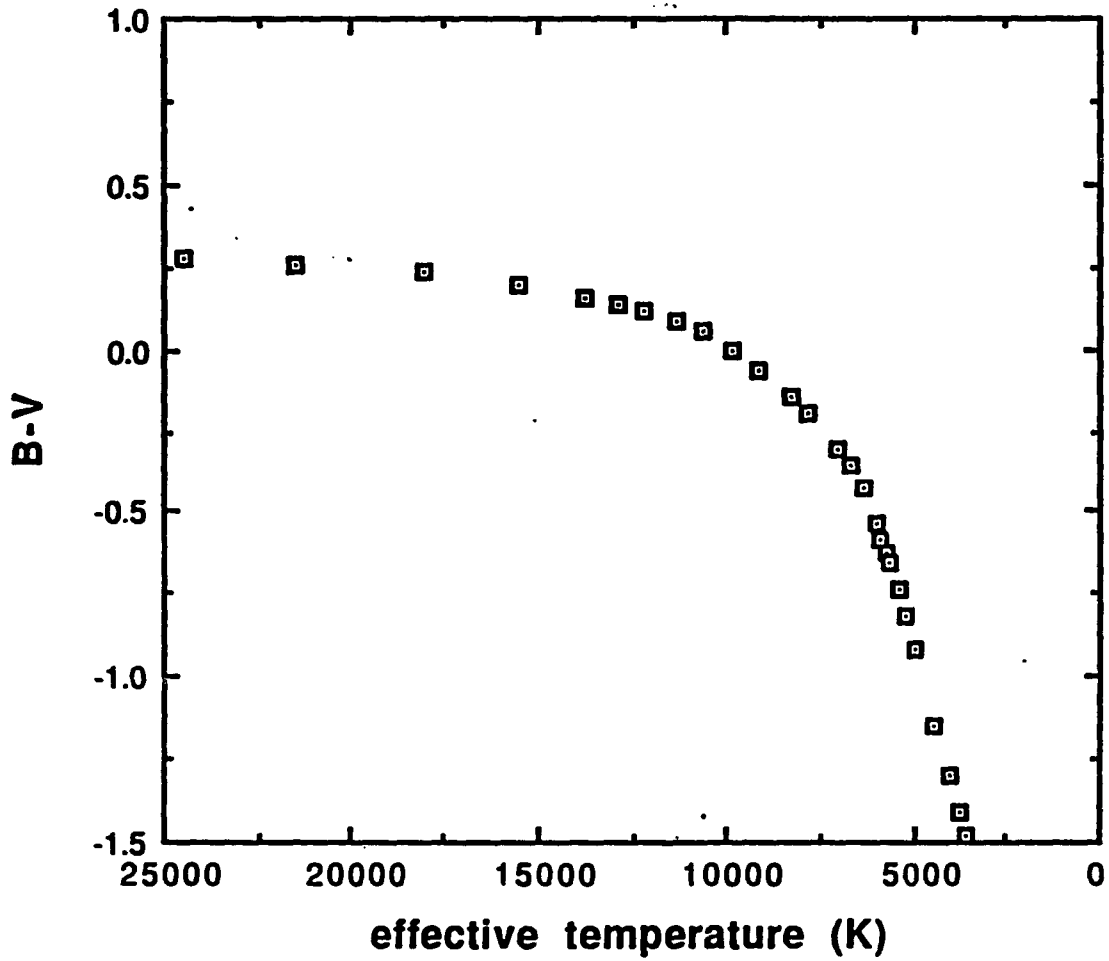

Figure 6. B-V as a function of main sequence effective temperature. The curve shows the dependence of the B-V color on the star's effective temperature

APPENDIX C

RESTRICTED THREE-BODY PROGRAM LISTING

```
//RABBIT JOB
//STEP1 EXEC FORTVCLG,REGION.GO=4000K
//FORT.SYSIN DD *
C
C
C     AUTHOR:  JOHN F. WALLIN
C     COPYRIGHT 1987 STARCHILD SOFTWARE
C
C     THIS PROGRAM SETS UP THE INITIAL  CONDITIONS
C     FOR THE Stellar Program Animation Module (SPAM).
C     THE CURRENT IMPLIMENTATION SETS UP THE PARTICLES
C     FOR A SINGLE DISK AND POSITIONS THE COMPANION
C     AT THE INITIAL CONDITION.
C
C     PARAMETERS USED TO DESCRIBE THE ORBITS OF THE
C     COMPANION AND THE GEOMETRY OF THE DISK ARE DESCRIBED
C     IN APPENDIX C OF WALLIN'S 1989 DISSERTATION.
C
C     THIS PROGRAM IS FREE FOR USE BY ALL INTERESTED PARTIES
C     AS LONG AS AN ACKNOWLEDGEMENT TO THE PROGRAM AND ITS
C     AUTHOR APPEARS SOMEWHERE IN THE PAPER.
C
C     THE AUTHOR TAKES NO RESPONSIBILITY FOR THE ACCURACY OF THE
C     PROGRAM OR THE DAMAGE TO GALAXIES WHICH MAY RESULT FROM
C     ITS USAGE.
C
C
C     THE PROGRAM HAS EVOLVED FROM THE NAS TO THE APOLLO
C     BACK TO THE NAS, SO LOTS OF FORTRAN BAGGAGE HAS NOT
C     BEEN PROPERLY ELIMINATED.  THE AUTHOR APOLOGIZES FOR THE
C     CONFUSION.
C
C
      REAL H,T0,A,VT,THETA,M,SL,PI,X,Y,Z,TF,DT,
     1  VX,VY,VZ,RMIN,OMEGA,INCL,E,V1,CP(6),CM(6)
      REAL X0(10001,7),XXE(7),XX0(7),ALPHA,BETA
      REAL IRING1,ORING1,XE(10001,7)
      REAL GAMX,GAMY,GAM,ALPH,FACT,HEAT1
      REAL R(10001),V(10001),ANGLE(10001)
      INTEGER N,NTOT1,NF,NN,OPT
      INTEGER SEED
      INTEGER N1,N2
      CHARACTER TEX*17,TEX1*10
      REAL RSCALE1(3),THETA1,PHI1
      REAL DX,DY,DZ
C
      COMMON /POS/ X0,XE,N,CM,CP
      COMMON /RAD/ R,V,ANGLE
      COMMON /INP/ N1,N2,H,ALPHA,BETA
C
C
      PI=3.1415926
      DO 3 I=1,10
3     PRINT*,''
      PRINT*,'SPAM VERSION 4.0.0   89.03.01'
      PRINT*,''
      PRINT*,''
      PRINT*,'COPYRIGHT 1989 STARCHILD SOFTWARE'
      PRINT*,'     ALL RIGHTS RESERVED'
C
*
*
*THIS VERSION SETS UP THE FIRST 50 PARTICLES IN A RING AT RADIUS
*R1 AND THE REST OF THE PARTICLES IN A RANDOM-EXPONENTIAL DISK.
*
C       OPEN(10,FILE='FISH1',FORM='UNFORMATTED')
      PRINT*,''
      PRINT*,''
```

```
      PRINT*,'MAIN GALAXY'
      PRINT*,'TOTAL NUMBER OF PARTICLE - DISK 1?'
      READ*,NTOT1
      PRINT*,'OPT?'
      READ*,OPT
      PRINT*,'RSCALE 1,2,3?'
      READ*,RSCALE1(1),RSCALE1(2),RSCALE1(3)
      PRINT*,'INNER RING DIAMETER?'
      READ*,IRING1
      PRINT*,'OUTER RING DIAMETER?'
      READ*,ORING1
      PRINT*,'SOFTENING LENGTH?'
      READ*,CM(4)
      PRINT*,'HEAT OF DISK (VRANDOM/VORBIT)?'
      READ*,HEAT1
C
      THETA1=0
      PHI1=0
C
999   PRINT*,'PERTURBER GALAXY'
99    PRINT*,'PERTURBER TRAJECTORY-'
      PRINT*,''
      PRINT*,'PERTURBER MASS?'
      READ*,CP(1)
C     NEED TO HAVE THE SOFTENING LENGTH ALWAYS
C     FOR CALCULATIONS
      PRINT*,'SOFTENING LENGTH?'
      READ*,CP(4)
      PRINT*,'INCLINATION?'
      READ*,INCL
      PRINT*,'OMEGA?'
      READ*,OMEGA
      PRINT*,'MINIMUM RADIUS?'
      READ*,RMIN
      PRINT*,'V/VESC ?'
      READ*,FACT
      PRINT*,'INITIAL TIME (USUALLY ~-10.)?'
      READ*,T0
      PRINT*,'STEP SIZE H ?'
      READ*,H
      PRINT*,'PICK A SEED, ANY SEED?'
      READ*,SEED
C
C
      PRINT*,''
      PRINT*,'DISPLAY DATA-'
      PRINT*,''
      PRINT*,'ALPHA?'
      READ*,ALPHA
      PRINT*,'BETA? '
      READ*,BETA
C
C
C     SET UP COLLISION PARAMETERS
C
      CP(2)=0.0
      CP(3)=0.01
      CP(5)=0.0
      CP(6)=0.0
      DO 20 I=2,3
20      CM(I)=CP(I)
      DO 21 I=5,6
21      CM(I)=CP(I)
C
      CM(1)=1.0
C
C     RMIN= CLOSEST APPROACH DISTANCE
C     CP1=MASS INSIDE CAUSTIC
```

```
C     CP2=NOT USED
C     CP3=NOT USED
C     CP4=SOFTENING LENGTH
C     CP5,CP6 ARE NOT USED
C     CP=PERTURBING POTENTIAL, CM=MAIN POTENTIAL
C
C
C
C     THE HEAT PARAMETER INCLUDED USES THE CHARACTERISTIC
C     VELOCITY FOR THE SYSTEM TIMES THE HEAT PARAMETER
C     TIMES A RANDOM NUMBER.  VCHAR IS DEFINED HERE AS
C     THE ORBITAL VEL AT R=SL/2.  WHY?  BECAUSE, THAT'S
C     WHY.
C
      DO 610 I=1,7
      XX0(I)=0.
610     CONTINUE
      XX0(1)=T0
      N = NTOT1
      N1 = NTOT1
      N2 = 0
C
      CALL PROFILE(IRING1,ORING1,RSCALE1,NTOT1,HEAT1,CM(1),
     + THETA1,PHI1,CM(4),XX0,SEED,T0,OPT)
C
C
*
**********************************************************
*
C     NOW FIND THE PERTURBER POSTION XX0(1-7)
C
      INCL=INCL*PI/180.0
      OMEGA=OMEGA*PI/180.0
      THETA=ASIN(SIN(INCL)*SIN(OMEGA))
C
      XX0(1)=0.0
      XX0(2)=0.0
      XX0(4)=RMIN*COS(THETA)
      XX0(6)=RMIN*SIN(THETA)
*
*     NOW FIND V FOR RMIN
*     E=SYSTEM ENERGY  0 FOR PARABOLA
*     1/SL*(PI/2.0-ATN(A/SL))*M FOR OTHERS
*     WHERE A=SEMIMAJOR AXIS.
*
C     THE SOFTENING LENGTH FOR THE MAIN GALAXY IS ASSUMED
C     FOR THE VELOCITY CALCULATIONS
      V1=SQRT(2.0*(CM(1)+CM(2)+CP(1)+CP(2))
     +       *(PI/2.0-ATAN(RMIN/CM(4)))/CM(4))
      V1=V1*FACT
C
C     SET THE CHARACTERISTIC VELOCITY FOR THE
C     REDSHIFT ANALYSIS
C
C     NOW POINT VEL VECTOR IN CORRECT DIRECTION
C
      IF (OMEGA.LT.1E-6) THEN
      GAM=PI/2.0-INCL
C
      ELSE
231       ALPH=ASIN(SIN(OMEGA)*COS(INCL)/COS(THETA))
      GAMX=COS(INCL)/COS(THETA)
      GAMY=(COS(ALPH)-COS(OMEGA)*COS(THETA))/(SIN(OMEGA)
     +  *SIN(THETA))
C
      GAM=ATAN(GAMY/GAMX)
C
      IF (GAMY.LT.0.0) THEN
      GAM=GAM+PI
```

```
      ELSEIF (GAMX.LT.0.0) THEN
      GAM=GAM+2.0*PI
      ENDIF
     ENDIF
C
      XX0(3)=-V1*SIN(GAM)
      XX0(5)=-V1*COS(GAM)*SIN(THETA)
      XX0(7)= V1*COS(GAM)*COS(THETA)
C
*
*     NOT MOVE POSITION BACK TO T0 FROM T=0.0
*
92      IF (T0.GT.XX0(1)) GOTO 13
      CALL RK41(XXE,XX0,-H)
C
      DO 34 I=1,7
34      XX0(I)=XXE(I)
      GOTO 92
C
C     SET THE TIME TO T0
13      XX0(1)=T0
C
C     NEW CHARACTERISTIC VELOCITY
C
      VCHAR=SQRT(CP(1)/(5.0*CP(4)))
* INCLUDE THE PERTURBING GALAXY
      N=N+1
C
      X0(N,2)=XX0(2)
      X0(N,4)=XX0(4)
      X0(N,6)=XX0(6)
      X0(N,3)=XX0(3)



C
C     NEW CHARACTERISTIC VELOCITY
C
      VCHAR=SQRT(CP(1)/(5.0*CP(4)))
* INCLUDE THE PERTURBING GALAXY
C
      X0(N,2)=XX0(2)
      X0(N,4)=XX0(4)
      X0(N,6)=XX0(6)
      X0(N,3)=XX0(3)
      X0(N,5)=XX0(5)
      X0(N,7)=XX0(7)
      X0(N,1)=T0
C
*****************************************************************
*
*
      CALL OUTPT2
      CLOSE(10)
      WRITE(*,201)
201     FORMAT(1X,'SIMULATION DATA')
      WRITE(*,17) CP(1)
      WRITE(*,110)INCL*180./PI
      WRITE(*,111) OMEGA*180./PI
      WRITE(*,112) RMIN
      WRITE(*,311) FACT
C
17    FORMAT(1X,'MASS = ',F10.3)
110     FORMAT(1X,'INCL = ',F10.3)
111     FORMAT(1X,'OMEGA= ',F10.3)
112     FORMAT(1X,'RMIN = ',F10.3)
311     FORMAT(1X,'V/VESC =',F10.5)
      WRITE(*,313) T0
```

```
313   FORMAT(1X,'T0    =',F10.5)
      WRITE(*,326) TF
326   FORMAT(1X,'TF    =',F10.5)
      WRITE(*,327) DT
327   FORMAT(1X,'DT    =',F10.5)
      WRITE(*,312) H
312   FORMAT(1X,'STEP SIZE=',F10.5)
      WRITE(*,314)
314   FORMAT(1X)
      WRITE(*,315 ) ALPHA
315   FORMAT(1X,'ALPHA  =',F10.5)
      WRITE(*,316) BETA
316   FORMAT(1X,'BETA   =',F10.5)
      WRITE(*,314)
      WRITE(*,317)
317   FORMAT(1X,'MAIN GALAXY'/)
      WRITE(*,318) NRING1,NPART1
318   FORMAT(1X,'NRING  =',I4/,2X,'NPART =',I4)
      WRITE(*,337) NTOT1,RSCALE1(1),RSCALE1(2),RSCALE1(3)
337   FORMAT(1X,'NTOT = ',I6/,2X,'RSCALE =',3F10.5)
      WRITE(*,319) IRING1,ORING1
319   FORMAT(1X,'INNER RING  =',F10.5/,2X,'OUTER RING =',F10.5)
      WRITE(*,322) CM(4)
      WRITE(*,325) HEAT1
325   FORMAT(1X,'HEAT =',F10.7)
      WRITE(*,314)
322   FORMAT(1X,'SL =',F7.4)
      WRITE(*,321) THETA2,PHI2
321   FORMAT(1X,'THETA =',F10.5/'PHI   =',F10.5)
      STOP
      END
C
C
C-------------------------------------------------------
      SUBROUTINE RK41(XXE,XX0,H)
       DIMENSION XXE(7),XX0(7),CP(6),CM(6),X(7),F(7)
       REAL X0(10001,7),XE(10001,7)
       REAL XX0,XXE,X,CP,CM,H,F
       INTEGER J
       COMMON /POS/ X0,XE,N,CM,CP
C
      DO 20 J=1,7
20     X(J)=XX0(J)
C
      CALL DIFFQ1(F,X)
C
     DO 30 J=1,7
      XXE(J)=XX0(J)+H*F(J)/6.0
 30    X(J)=XX0(J)+H*F(J)/2.0
      CALL DIFFQ1(F,X)
C
      DO 40 J=1,7
       XXE(J)=XXE(J)+H*F(J)/3.0
 40     X(J)=XX0(J)+H*F(J)/2.0
      CALL DIFFQ1(F,X)
C
       DO 50 J=1,7
        XXE(J)=XXE(J)+H*F(J)/3.0
 50       X(J)=XX0(J)+H*F(J)
      CALL DIFFQ1(F,X)
C
       DO 60 J=1,7
60       XXE(J)=XXE(J)+H*F(J)/6.0
C
     RETURN
     END
C
C
```

```
C-------------------------------------------------------
      SUBROUTINE DIFFQ1(F,X)
       DIMENSION F(7),X(7),CP(6),CM(6)
       REAL CP,CM,F,R1,R21,M1,A1
       REAL X0(10001,7),XE(10001,7)
       INTEGER N
       INTEGER K
       COMMON /POS/ X0,XE,N,CM,CP
C
C
       R21=X(2)*X(2)+X(4)*X(4)+X(6)*X(6)
      R1=SQRT(R21)
C
C
       M1=CM(1)+CP(1)
C
C
C
 40    A1=-M1/(R21+CM(4)*CM(4))
C
C
 55    F(1)=1.0
       F(2)=X(3)
       F(3)=A1*X(2)/R1
       F(4)=X(5)
       F(5)=A1*X(4)/R1
       F(6)=X(7)
       F(7)=A1*X(6)/R1
C
C
 50    RETURN
      END
*-------------------------------------------------
*
*
       SUBROUTINE PROFILE(RIN,ROUT,RSCALE,NTOT,HEAT,M,
     + THETA,PHI,SL,X1,SEED,T0,OPT)
C
       REAL RIN,ROUT,RSCALE(3),HEAT,M,X0(10001,7),THETA,PHI
       REAL XE(10001,7),CP(6),CM(6)
       REAL T0,X1(7)
       INTEGER OPT,NTOT,NRING,NPART
       INTEGER SEED
C
       REAL STHETA,CTHETA,SPHI,CPHI,PI
       INTEGER I,PARTY,N
       REAL NORM,R(10001),V(10001),ANGLE(10001),ST
       REAL CT,X3,Y3,Z3,XV3,YV3,ZV3,X2,Y2,Z2,XV2,YV2,ZV2
       REAL X,Y,Z,XV,YV,ZV
*
       REAL RNORM,DR,RP(1000),R1,RAN
       INTEGER NPROF
*
       COMMON /POS/ X0,XE,N,CM,CP
       COMMON /RAD/ R,V,ANGLE
*
*
*      VARIABLES-
*      OPT - OPTION FOR THE DISTRIBUTION
*      RIN - INNER RADIUS
*      ROUT - OUTER RADIUS
*      RSCALE - SCALE OF BRIGHTNESS DROP
*      NTOT - NUMBER OF PARTICLES
*      HEAT - HEAT PARAMETER
*      M - MASS OF GALAXY
*      SL - SOFTENING LENGTH
*      NRING - NUMBER OF RINGS
*      NPART - NUMBER OF PARTICLE PER RING (OPT)
*      X0 - POSITION OF CENTER OF MASS
```

```
*     X1 - ARRAY OF POSITION
*
      PI = 3.1415926
C
C     THE FOLLOWING IS NOT AN ERROR-
C
C     THE SIN AND COS WERE CHANGE TO MAKE THETA
C     ROTATE PROPERLY
C
      CTHET=SIN(THETA*PI/180.0)
      STHET=COS(THETA*PI/180.0)
      SPHI=SIN(PHI*PI/180.0)
      CPHI=COS(PHI*PI/180.0)
*
*     SET UP THE PROBABLITY DISTRIBUTION FOR THE DISK
      NP = 50
      NPROF = 250
      RNORM = 0.
      DO 60 I=1,NP
       ANGLE(I)= (2.*PI*FLOAT(I))/FLOAT(NP)
      R(I) = 1.
60     CONTINUE
*
      DR = (ROUT - RIN)/FLOAT(NPROF)
      DO 10 I=1,NPROF
      R1 = FLOAT(I)*DR + RIN
      RP(I) =  DISTRB(R1,OPT,RSCALE ) * R1 * DR * 2. * PI
      RNORM = RNORM + RP(I)
      RP(I) = RNORM
10     CONTINUE
*
*SET UP RADIAL AND ANGULAR POSITIONS
*
      DO 50 I=NP+1,N
       RAN = RANDOM(SEED)
       DO 20 J=1,NPROF
        IF (RAN.LT.RP(J)/RNORM) GOTO 30
20      CONTINUE
30      CONTINUE
       R(I) = FLOAT(J)*DR + RIN
       ANGLE(I) = 2.*PI*RANDOM(SEED)
50     CONTINUE
*
      DO 100 I=1,N
C       V(I) = SQRT(M/R(I))
       V(I) = SQRT( M*R(I)/ ( R(I)*R(I) + SL*SL ) )
C       V(I) = SQRT( M * (PI/2.0 - ATAN( R(I)/SL ) )/SL)
*
*     SET UP PARAMETERS
*
       ST=SIN(ANGLE(I))
       CT=COS(ANGLE(I))
C
       X3=CT*R(I)
       Y3=ST*R(I)
      Z3=0.0
C
       XV3=-V(I)*ST
       YV3=V(I)*CT
      ZV3=0.0
C
C     NOW ROTATE ABOUT Y PRIME AXIS
C
       X2=X3*CPHI+Z3*SPHI
      Y2=Y3
       Z2=-X3*SPHI+Z3*CPHI
C
       XV2=XV3*CPHI+ZV3*SPHI
```

```
      YV2=YV3
       ZV2=-XV3*SPHI+ZV3*CPHI
C
C      ROTATE ABOUT Z AXIS
C
       X=X2*CTHET-Y2*STHET
       Y=X2*STHET+Y2*CTHET
      Z=Z2
C
       VX=XV2*CTHET-YV2*STHET
       VY=XV2*STHET+YV2*CTHET
      VZ=ZV2
C
C
       X0(I,2)=X+X1(2)
       X0(I,4)=Y+X1(4)
       X0(I,6)=Z+X1(6)
       X0(I,3)=VX+X1(3)+RANDOM(SEED)*HEAT
       X0(I,5)=VY+X1(5)+RANDOM(SEED)*HEAT
       X0(I,7)=VZ+X1(7)+RANDOM(SEED)*HEAT
      X0(I,1)=T0
*
*
100    CONTINUE
*
*
1000    RETURN
      END
*
*
*
*
C-------------------------------------------------------------
C
       FUNCTION RANDOM(SEED)
      REAL RANDOM
      INTEGER SEED
       REAL X0(10001,7),XE(10001,7),CP(6),CM(6)
      INTEGER N
      COMMON /POS/ X0,XE,N,CM,CP
      COMMON /RAD/ R,V,ANGLE
      SEED = MOD(16807*SEED,2147483647)
       RANDOM=FLOAT(SEED)*4.6566128752458E-10
      RANDOM= (RANDOM+1.)/2.
      RETURN
      END
C
C
C-------------------------------------------------------------
       SUBROUTINE OUTPT2
      DIMENSION X0(10001,7),XE(10001,7),CP(6),CM(6)
       REAL X0,XE,CP,CM,ALPHA,BETA,H
       INTEGER N,I,N1,N2
       CHARACTER NAME*10
      COMMON /POS/ X0,XE,N,CM,CP
       COMMON /INP/ N1,N2,H,ALPHA,BETA
      WRITE(10,2) N,N1,N2
      WRITE(10,4) 0,0
      WRITE(10,4) 0,0
      WRITE(10,1) ALPHA,BETA,H,X0(1,1)
C
      DO 10 I=1,N
      WRITE(10,3) X0(I,2),X0(I,4),X0(I,6),X0(I,3),X0(I,5),X0(I,7)
C       WRITE(*,3)X0(I,2),X0(I,4),X0(I,6),X0(I,3),X0(I,5),X0(I,7)
10     CONTINUE
      WRITE(10,3) CP(1),CP(2),CP(3),CP(4),CP(5),CP(6)
      WRITE(10,3) CM(1),CM(2),CM(3),CM(4),CM(5),CM(6)
      WRITE(10,5)
```

```
C
C
 1    FORMAT(4E16.8)
 2    FORMAT(3I5)
 3    FORMAT(6E16.8)
 4    FORMAT(2I5)
 5    FORMAT('END')
      RETURN
      END
C
C
C---------------------------------------------------------------
*
*
      FUNCTION DISTRB(R1,OPT,RSCALE)
      REAL R1,RSCALE(3),DISTRB
      INTEGER OPT
*
      IF (OPT.EQ.1) THEN
      DISTRB = 1./R1
      ELSEIF (OPT.EQ.2) THEN
       DISTRB = EXP(-R1/RSCALE(1))
      ELSEIF (OPT.EQ.3) THEN
       DISTRB = EXP(-R1*R1*RSCALE(1) - RSCALE(2)*R1 - RSCALE(3) )
      ENDIF
*
      RETURN
      END
//GO.FT10F001 DD UNIT=DISK,DISP=(NEW,CATLG),
//  DCB=(RECFM=FB,LRECL=96,BLKSIZE=6160),
//  SPACE=(6160,(10,10),RLSE),DSN=J.I4304.IN13
//GO.SYSIN DD *
10000
1
0,0,0
.1
1.1
.1
0
1.00
.1
0
0
2.5
1.
-3.0
.005
12345
0
0
/*
```

```
//SPAM  JOB
/*JOBPARM BLOCK=NIGHT
//STEP1 EXEC FORTVCLG,TIME.GO=90,PARM='OPT(2)',
//  REGION.GO=4096K
//FORT.SYSIN DD *
      PROGRAM SPAM
C%INCLUDE '/SYS/INS/BASE.INS.FTN'
C%INCLUDE '/SYS/INS/GPR.INS.FTN'
C%INCLUDE '/SYS/INS/TIME.INS.FTN'
C%INCLUDE '/SYS/INS/CAL.INS.FTN'
C%INCLUDE '/SYS/INS/FIO.INS.FTN'
C     LAST UPDATE  10/18/88
C
C     SPAM V4.0.0
C
C
C
C       WRITTEN BY JOHN F. WALLIN
C
C
C     COPYRIGHT 1987 STARCHILD SOFTWARE
C
C
C
C
C   Stellar Particle Animation Module (SPAM)
C
C     THIS PROGRAM IS WRITTEN TO NUMERICALLY INTERGRATE
C     THE EQUATIONS OF MOTION OF TEST PARTICLES DURING A
C     SIMULATED GALACTIC INTERACTION.  THE RESTRICTED
C     THREE-BODY APPROXIMATION IS USED FOR THE PARTICLES IN
C     THIS PROGRAM WITH THE FORCES SET FROM A SOFTENED
C     POINT MASS.  OTHER FORCELAWS CAN BE SIMPLY ADAPTED
C     BY CHANGING THE DIFFEQ SUBROUTINE.
C
C     THE INPUT FILE FROM THIS PROGRAM IS FROM THE COMPANION PROGRAM.
C     THE FORMAT OF THE FILE IS DESCRIBED IN THE CODE BELOW.
C
C     THERE ARE TWO OUTPUT FILES IN THIS CODE.  THE FIRST
C     FOLLOWS THE SAME FORMAT AS THAT PRODUCED BYRABBIT
C     DIFFERENT TIME STEPS ARE SAVED FOR FURTHER ANALYSIS
C     BY THE PROGRAM.  THE INTERVALS AND ENDING TIMES FOR THE
C     SIMULATIONS ARE CHANGED INTERNALLY.
C     THE SECOND FILE IS A DENSITY HISTORY FOR SELECTED PARTICLES.
C     DETAILS ARE LISTED BELOW IN THE CODE.
C
C
C     THIS PROGRAM IS FREE FOR USE BY ALL INTERESTED PARTIES
C     AS LONG AS AN ACKNOWLEDGEMENT TO THE PROGRAM AND ITS
C     AUTHOR APPEARS SOMEWHERE IN THE PAPER.
C
C     THE AUTHOR TAKES NO RESPONSIBILITY FOR THE ACCURACY OF THE
C     PROGRAM OR THE DAMAGE TO GALAXIES WHICH MAY RESULT FROM
C     ITS USAGE.
C
C     THIS CODE HAS BEEN THROUGH A GREAT NUMBER OF REVISIONS
C     AND SYSTEM ADAPTATIONS WHICH MAY NOT SEEM TO HAVE MUCH
C     USE IN THE CURRENT IMPLIMENTATION.  IN SIMPLE TERMS, IT
C     IS A MESS.  THE AUTHOR APOLOGIZES FOR THE PROBLEMS THIS
C     MAY CAUSE.
C
C     THIS PROGRAM READS IN A FILE WITH THE INITIAL
C     TEST POINT POSITIONS AND VELOCITIES ALONG WITH THE
C     GALAXY POTENTIAL CHARACTERISTICS AND EVOLVES THEM.
C     THE DATA FILE REQUIRED IS OF THE FORM-
C     T0 = INITIAL TIME
C     N = NUMBER OF TEST POINTS + 1
C     X(I),VX(I),Y(I),VY(I),Z(I),VZ(I)
```

```
C     POSITIONS AND VELOCITIES OF THE N-1 TEST PARTICLES
C     AND POSITIONS AND VELOCITIES OF THE INTERSECTING
C     GALAXY.  THE MAIN GALAXY IS AT (0,0,0) WITH V=0.
C     CP(1-6)
C     CM(1-6)
C     THE CP AND CM PARAMETERS ARE USED TO CHARACTERIZE
C     THE POTENTIALS OF THE PERTURBING AND MAIN  GALAXIES.
C     THEY ARE USED IN THE ROUTINE DIFFEQ TO FIND THE
C     GRAVITATIONAL ACC.
C     THE OUTPUT FILES ARE STORED IN THE SAME FORMAT AS
C     THE INPUT FILE.
C     FOR SPECIFIC FORMATS USED, SEE OUTPUT AND INPUT SUBROUTINES.
C
C
      DIMENSION X0(10001,7),XE(10001,7),CP(6),CM(6),FRICTN(6)
      DIMENSION XPOS(10001),YPOS(10001)
      REAL*8 X0,XE,CP,CM,TF,DT,P0,H,ALPHA,BETA
      REAL*8 INCL,OMEGA,RMIN,VCAR
      REAL*8 DX,DY,DZ,T1(10),T2(2)
       REAL*8 RSCALE,XSIZE,YSIZE
       INTEGER NF,III
       INTEGER I,J,N
       INTEGER XPOS,YPOS,GRID(200,200),NN
       CHARACTER*10 NAME
       INTEGER N1,N2,NPTS,PT(60),NUM(60)
C
      COMMON /POS/ X0,XE,CM,CP,N
       COMMON /PROJ/ XPOS,YPOS,RSCALE,XSIZE,YSIZE
       COMMON /INP/ N1,N2,H,ALPHA,BETA
      COMMON /FISH/ GRID
C
      NAME='FISH2'
C       OPEN(10,FILE=NAME,FORM='UNFORMATTED')
      NAME='FISH1'
C       OPEN(11,FILE=NAME,FORM='UNFORMATTED')
C
C
C     READ IN DATA FILE
C
      CALL INPUT(TF,DT,T1,NF,T2,NN,NPTS,PT,DX,DY,DZ)
C
C
C     END OF PROGRAM ?
40     IF (TF.LT.X0(1,1)) GOTO 10
C
C       PRINT OUTPUT ??
      P0=X0(1,1)
      P0=ABS(P0) + ABS(H/2.)
      P0 = DMOD(P0,DT)
       IF (P0.LT.H) THEN
      CALL OUTPT2
      PRINT*,X0(1,1),DT,P0,H
      PRINT*,'OUT'
       ENDIF
.
.
.
       IF (NPTS.EQ.0) GOTO 80
       DO 70 III=1,NPTS
        CALL LDENSITY(PT(III),NUM(III),DX,DY,DZ)
70      CONTINUE
      CALL OUT3(NUM,NPTS,X0(1,1))
C
C     MOVE STUFF
80     CALL RK4(H)
C
C     REDEFINE X0
      DO 30 I=1,N
```

```
      DO 30 J=1,7
30      X0(I,J)=XE(I,J)
C
C     REPEAT PROCEDURE
      GOTO 40
C
C
10    CONTINUE
      CALL OUTPT2
      CLOSE(10)
      CLOSE(11)
      CLOSE(12)
      PRINT*,'END'
      STOP
      END

C-----------------------------------------------------------------
C
      SUBROUTINE OUTPUT
*
      DIMENSION X0(10001,7),CP(6),CM(6)
      DIMENSION XE(10001,7),XPOS(10001),YPOS(10001)
      REAL*8 CP,CM,XE,X0,H,ALPHA,SALPHA,CALPHA,PI,XT,YT
      REAL*8 SBETA,CBETA,BETA
      REAL*8 RSCALE,XSIZE,YSIZE
      INTEGER N,I
      INTEGER XPOS,YPOS
      INTEGER N1,N2
      COMMON /POS/ X0,XE,CM,CP,N
      COMMON /PROJ/ XPOS,YPOS,RSCALE,XSIZE,YSIZE
      COMMON /INP/ N1,N2,H,ALPHA,BETA
C
      PI=3.1415926
C
       SALPHA=SIN(ALPHA*PI/180.)
       CALPHA=COS(ALPHA*PI/180.)
       SBETA=SIN(BETA*PI/180.)
       CBETA=COS(BETA*PI/180.)
C
C
      DO 10 I=1,N
       XT=X0(I,2)*CBETA-X0(I,4)*SBETA
       YT=X0(I,2)*SBETA+X0(I,4)*CBETA
       XPOS(I)=INT(XT*RSCALE+XSIZE/2.)
       YPOS(I)=INT((YT*CALPHA-X0(I,6)*SALPHA)*RSCALE+YSIZE/2.)
10     CONTINUE
C
C
      RETURN
      END
C
C*
C-----------------------------------------------------------------
       SUBROUTINE INPUT(TF,DT,T1,NF,T2,NN,NPTS,PT,DX,DY,DZ)
       DIMENSION X0(10001,7),XE(10001,7),CP(6),CM(6)
       REAL*8 X0,XE,CP,CM,ALPHA,BETA,H
      REAL*8 DX,DY,DZ
       INTEGER N,I,N1,N2,NN
       INTEGER NNX,NN1,NN2
       INTEGER PT(60),NPTS,NF
       REAL*8 T1(10),T2(2),DT,TF
       CHARACTER TMP*10
      COMMON /POS/ X0,XE,CM,CP,N
      COMMON /INP/ N1,N2,H,ALPHA,BETA
C
*     LOCAL DENSITY PARAMETERS
      DX=0.1
      DY=0.1
      DZ=0.1
```

```
      NPTS = 50
      DO 20 I=1,NPTS
       PT(I) = I
20     CONTINUE
*
*
*      LOCAL GRID SIZE
      NN = 100
*
*      OUTPUT INTERVAL AND FINISH TIME
      DT = 0.2
      TF = 3.0
*
      READ(11,2) NNX,NN1,NN2
      N=NNX
      N1= NN1
      N2= NN2
       PRINT*,'N = ',N
      READ(11,4) NN1,NN2
      READ(11,4) NN1,NN2
      READ(11,1) ALPHA,BETA,H,X0(1,1)
C
     DO 10 I=1,N
      READ(11,3) X0(I,2),X0(I,4),X0(I,6),X0(I,3),X0(I,5),X0(I,7)
10     CONTINUE
      READ(11,3) CP(1),CP(2),CP(3),CP(4),CP(5),CP(6)
      READ(11,3) CM(1),CM(2),CM(3),CM(4),CM(5),CM(6)
      READ(11,5) TMP
C
C
 1     FORMAT(4E16.8)
 2     FORMAT(3I5)
 3     FORMAT(6E16.8)
 4     FORMAT(2I5)
 5     FORMAT(A10)
*
*
      RETURN
      END
C
C
C-----------------------------------------------------------------
       SUBROUTINE OUTPT2
      DIMENSION X0(10001,7),XE(10001,7),CP(6),CM(6)
       REAL*8 X0,XE,CP,CM,ALPHA,BETA,H
       INTEGER N,I,N1,N2
       CHARACTER NAME*10
      COMMON /POS/ X0,XE,CM,CP,N
      COMMON /INP/ N1,N2,H,ALPHA,BETA
C
      WRITE(10,2) N,N1,N2
      WRITE(10,4) 0,0
      WRITE(10,4) 0,0
      WRITE(10,1) ALPHA,BETA,H,X0(1,1)
      PRINT*,' H = ',H
C
      DO 10 I=1,N
      WRITE(10,3) X0(I,2),X0(I,4),X0(I,6),X0(I,3),X0(I,5),X0(I,7)
10     CONTINUE
      WRITE(10,3) CP(1),CP(2),CP(3),CP(4),CP(5),CP(6)
      WRITE(10,3) CM(1),CM(2),CM(3),CM(4),CM(5),CM(6)
      WRITE(10,5)
C
C
 1     FORMAT(4E16.8)
 2     FORMAT(3I5)
 3     FORMAT(6E16.8)
 4     FORMAT(2I5)
```

```
 5    FORMAT(1X,'END')
      RETURN
      END
C
C
C-----------------------------------------------------------------
C
      SUBROUTINE RK4(H)
      DIMENSION XE(10001,7),X0(10001,7),CP(6),CM(6),
     + X(7),F(7),XN(7),XN1(4,7)
      REAL*8 X0,XE,X,CP,CM,H,F,XN,XN1
      INTEGER I,J,N
      COMMON /POS/ X0,XE,CM,CP,N
C
C
C       THIS IS A TRICKY THING- FIRST SOLVE
C       THE MOTION OF THE MASSIVE PARTICLE FOR
C       THE FOUR CALLS, THEN SOLVE FOR EVERYTHING
C       ELSE.
C
C       THE PROBLEM EXISTS BECAUSE WE ARE SOLVING A
C       SET OF SIMULTANIOUS DIFF. EQ. WHICH ARE LINKED
C       TOGETHER.  DOING EACH PARTICLE SEPARATELY WILL
C       NOT WORK, SINCE THE PERTURBING MASS IS CHANGING
C       POSITIONS AT EACH STEP.
C
      DO 100 J=1,7
      X(J) = X0(N,J)
      XN1(1,J)=X0(N,J)
100     XN(J) =X0(N,J)
C
      CALL DIFFEQ(F,X,XN,N)
      DO 101 J=1,7
       XE(N,J)=X0(N,J)+H*F(J)/6.0
       X(J)=X0(N,J)+H*F(J)/2.0
       XN(J)=X(J)
       XN1(2,J)=XN(J)
101     CONTINUE
C
      CALL DIFFEQ(F,X,XN,N)
      DO 102 J=1,7
       XE(N,J)=XE(N,J)+H*F(J)/3.0
       X(J)=X0(N,J)+H*F(J)/2.0
       XN(J)=X(J)
       XN1(3,J)=XN(J)
102     CONTINUE
C
      CALL DIFFEQ(F,X,XN,N)
      DO 103 J=1,7
       XE(N,J)=XE(N,J)+H*F(J)/3.0
       X(J)=X0(N,J)+H*F(J)
       XN(J)=X(J)
       XN1(4,J)=XN(J)
103     CONTINUE
C
      CALL DIFFEQ(F,X,XN,N)
      DO 104 J=1,7
       XE(N,J)=XE(N,J)+H*F(J)/6.0
104     CONTINUE
C
C
      DO 120 I=1,N
      DO 20 J=1,7
       XN(J)=XN1(1,J)
20      X(J)=X0(I,J)
C
      CALL DIFFEQ(F,X,XN,I)
      DO 30 J=1,7
```

```
      XE(I,J)=X0(I,J)+H*F(J)/6.0
      XN(J)=XN1(2,J)
30      X(J)=X0(I,J)+H*F(J)/2.0
C
      CALL DIFFEQ(F,X,XN,I)
      DO 40 J=1,7
       XE(I,J)=XE(I,J)+H*F(J)/3.0
       XN(J)=XN1(3,J)
40      X(J)=X0(I,J)+H*F(J)/2.0
C
      CALL DIFFEQ(F,X,XN,I)
      DO 50 J=1,7
        XE(I,J)=XE(I,J)+H*F(J)/3.0
        XN(J)=XN1(4,J)
50      X(J)=X0(I,J)+H*F(J)
C
      CALL DIFFEQ(F,X,XN,I)
      DO 60 J=1,7
60      XE(I,J)=XE(I,J)+H*F(J)/6.0
C
120   CONTINUE
C
      RETURN
      END
C
C
C-----------------------------------------------------------------
      SUBROUTINE DIFFEQ(F,X,XN,I)
      DIMENSION F(7),X(7),CP(6),CM(6),XN(7)
      REAL*8 CP,CM,F,X,R1,R21,R2,R22,M1,M2,A1,A2,A3,XN
      REAL*8 X0(10001,7),XE(10001,7)
      INTEGER I,N,K
      COMMON /POS/ X0,XE,CM,CP,N
C
C
      R22=(X(2)-XN(2))*(X(2)-XN(2))+(X(4)-XN(4))*
     1 (X(4)-XN(4))+(X(6)-XN(6))*(X(6)-XN(6))
      R21=X(2)*X(2)+X(4)*X(4)+X(6)*X(6)
      R2N=XN(2)*XN(2)+XN(4)*XN(4)+XN(6)*XN(6)
C
CC
C
      R2=SQRT(R22)
      R1=SQRT(R21)
      RN=SQRT(R2N)
C
C
      M1=CM(1)
      M2=CP(1)
C
C
      A1=-M1/(R21+CM(4)*CM(4))
C
C
40    A2=-M2/(R22+CP(4)*CP(4))
C
C
C       REMOVE ACCELERATION FOR PERTURBING GALAXY-
C       FROM PERTURBING GALAXY
C
      IF (I.EQ.N) THEN
      A2=0.0
      R2=1.0
      ENDIF
C
      A3=-M2/(R2N+CP(4)*CP(4))
C
C
      F(1)=1.0
```

```
      F(2)=X(3)
      F(3)=A1*X(2)/R1+A2*(X(2)-XN(2))/R2+A3*XN(2)/RN
      F(4)=X(5)
      F(5)=A1*X(4)/R1+A2*(X(4)-XN(4))/R2+A3*XN(4)/RN
      F(6)=X(7)
      F(7)=A1*X(6)/R1+A2*(X(6)-XN(6))/R2+A3*XN(6)/RN
C
C
50    RETURN
      END
*
*****************************************************************
*
*
      SUBROUTINE LDENSITY(I,K,DX,DY,DZ)
*
      REAL*8 DX,DY,DZ
      REAL*8 X0(10001,7),XE(10001,7),CP(6),CM(6)
      INTEGER N,I,K
*
      REAL*8 X,Y,Z
      INTEGER J,II
      COMMON /POS/ X0,XE,CM,CP,N
*
*     I - PARTICLE NUMBER
*     N - TOTAL NUMBER OF PARTICLES
*     K - NUMBER OF PARTICLES IN THE BOX
*     DX,DY,DZ - BOX DIMENSIONS
*     X0 - POSITIONS OF THE PARTICLES
*
      X=X0(I,2)
      Y=X0(I,4)
      Z=X0(I,6)
      K=0
*
      DO 10 J=1,N
      IF ((X0(J,2).LT.X-DX/2.).OR.(X0(J,2).GT.X+DX/2.)) GOTO 10
      IF ((X0(J,4).LT.Y-DY/2.).OR.(X0(J,4).GT.Y+DY/2.)) GOTO 10
      IF ((X0(J,6).LT.Z-DZ/2.).OR.(X0(J,6).GT.Z+DZ/2.)) GOTO 10
      K=K+1
10    CONTINUE
*
*
      RETURN
      END
*---------------------------------------------------------
*
      SUBROUTINE OUT3(NUM,NPTS,T0)
*
      INTEGER NPTS,NUM(60)
      REAL*8 T0
      INTEGER I
      WRITE(12,1) T0,(NUM(I),I=1,NPTS)
1     FORMAT(F15.7/,5( 10( (I10) )/) )
      RETURN
      END
//GO.FT11F001 DD UNIT=DISK,DISP=SHR,
// DSN=J.I4304.IN13
//GO.FT10F001 DD UNIT=DISK,DISP=(NEW,CATLG),
// DCB=(RECFM=FB,LRECL=96,BLKSIZE=6160),
// SPACE=(6160,(4000,500),RLSE),DSN=J.I4304.OU13,
// VOL=SER=UCC008
//GO.FT12F001 DD UNIT=DISK,DISP=(NEW,CATLG),
// DCB=(RECFM=FB,LRECL=100,BLKSIZE=6160),
// SPACE=(6160,(20,25),RLSE),DSN=J.I4304.DEN13
//GO.SYSIN DD *
/*
```

ACKNOWLEDGMENTS

I would like to thank Curt Struck-Marcell for his aid and assistance with my dissertation. His encouragement, help, and understanding have made my time at Iowa State both pleasant and productive. I would also like to thank Dr. James Schombert for his help in learning observational techniques and access to his data. The observational data on tidal tails and shell galaxies provided much of the motivation for this project.

The professors of the astronomy group at Iowa State have been extremely helpful in my graduate studies, my research, and my teaching. I would like to thank Dr. Lee Ann Willson, Dr. George Bowen, and Dr. Richard Lamb for their support and encouragement. Special thanks to Dr. Phil Appleton for his help with the IRAS project and access to the Apollo workstation. Additional thanks to Dr. David Lewis for aid in moving data between machines.

A number of graduate students have been very supportive during my time at Iowa State. I would like to thank Tom Beach and Joyce Guzik for their encouragement, their help, and especially their friendship. Additional thanks go to Deanna Snyder, Cindy Neyer and Heather Preston for their friendship and support. The late night grad-cokes provided hours of needed relaxation and relief from the pressures of school. Pnina Luban deserves a special thanks for putting up with my idiosyncrasies during her time as my office-mate. Thanks to Sara

Thiemann for her help in editing and revising portions of this manuscript.

The decision to become an astrophysicist was not made in a vacuum. I was greatly encouraged by Dale Gibbs, Don Penn, Larry Mascotti and Jim Pierce during high school and undergraduate school. I would also like to thank my mother for her patience and her encouragement for me to achieve my goals.

In addition, I would like to thank the members of the Silent Knights glider club for giving me wings, the ISU SCUBA club for giving me fins, the Big Creek Triathalon for giving me endurance, and the woods of northern Minnesota for giving me silence.